

# Thermal, electric and spin transport in superconductor/ferromagnetic-insulator structures

Tero T Heikkilä<sup>a</sup>, Mikhail Silaev<sup>a</sup>, Pauli Virtanen<sup>a,b</sup>, F. Sebastian Bergeret<sup>c,d</sup>

<sup>a</sup>*University of Jyväskylä, Department of Physics and Nanoscience Center, P.O. Box 35 (YFL), FI-40014 University of Jyväskylä, Finland*

<sup>b</sup>*NEST, Istituto Nanoscienze-CNR and Scuola Normale Superiore, I-56127 Pisa, Italy*

<sup>c</sup>*Centro de Fisica de Materiales (CFM-MPC), Centro Mixto CSIC-UPV/EHU, Manuel de Lardizabal 5, E-20018 San Sebastian, Spain*

<sup>d</sup>*Donostia International Physics Center (DIPC), Manuel de Lardizabal 4, E-20018 San Sebastian, Spain*

---

## Abstract

A ferromagnetic insulator (FI) attached to a conventional superconductor (S) changes drastically the properties of the latter. Specifically, the exchange field at the FI/S interface leads to a splitting of the superconducting density of states. If S is a superconducting film, thinner than the superconducting coherence length, the modification of the density of states occurs over the whole sample. The coexistence of the exchange splitting and superconducting correlations in S/FI structures leads to striking transport phenomena that are of interest for applications in thermoelectricity, superconducting spintronics and radiation sensors. Here we review the most recent progress in understanding the transport properties of FI/S structures by presenting a complete theoretical framework based on the quasiclassical kinetic equations. We discuss the coupling between the electronic degrees of freedom, charge, spin and energy, under non-equilibrium conditions and its manifestation in thermoelectricity and spin-dependent transport.

---

## Contents

<b>1</b>	<b>Introduction</b>	<b>4</b>
<b>2</b>	<b>Ferromagnetic insulator–superconductor structures</b>	<b>6</b>
2.1	Induced spin splitting in a superconductor–ferromagnetic insulator structure . . . . .	7
2.2	Spin-split density of states in a superconductor . . . . .	9
2.3	Paramagnetic depairing mechanisms and the FFLO state . . . . .	11
2.4	Static spin susceptibility of conventional superconductors . . . . .	14

---

*Email addresses:* Tero.T.Heikkila@jyu.fi (Tero T Heikkilä), fs.bergeret@csic.es (F. Sebastian Bergeret)

2.5	Other effects related to the Zeeman and exchange fields . . . . .	15
2.5.1	Fermi liquid effects . . . . .	15
2.5.2	Long-range triplet correlations . . . . .	16
2.5.3	Cryptoferrromagnetic state . . . . .	17
<b>3</b>	<b>Quasiclassical theory of diffusive FI/S structures</b>	<b>18</b>
3.1	Nonequilibrium quasiparticles . . . . .	21
3.1.1	Kinetic equations . . . . .	22
3.1.2	Observables . . . . .	23
3.2	Elastic relaxation mechanisms . . . . .	24
3.2.1	Nonequilibrium spin relaxation . . . . .	26
3.3	Inelastic relaxation mechanisms . . . . .	28
3.3.1	Electron-phonon coupling . . . . .	28
3.3.2	Particle-particle collisions . . . . .	31
3.4	Description of hybrid interfaces . . . . .	31
3.5	Free energy . . . . .	33
3.6	Linear response and generalized Onsager relations . . . . .	34
3.7	Nonequilibrium effects on the superconducting order parameter .	36
3.8	Overall strategy to explore the transport and spectral properties of hybrid superconducting systems . . . . .	38
<b>4</b>	<b>Transport properties of ferromagnetic insulator–superconductor heterostructures</b>	<b>39</b>
4.1	Detection of spin and charge imbalance: non-local transport mea- surements . . . . .	40
4.2	Nonequilibrium properties of a superconductor with spin splitting	42
4.2.1	Relaxation of the nonequilibrium modes . . . . .	45
4.2.2	Kinetic equations with supercurrent . . . . .	49
4.2.3	Non-local conductance measurements . . . . .	50
4.3	Spin Hanle effect in normal metals and superconductors . . . . .	53
4.3.1	Normal-metal non-local spin valve . . . . .	53
4.3.2	Hanle effect in spin-split superconductors . . . . .	54
4.4	Linear response of a spin-split superconductor to a rf field . . . .	62
4.5	Nonlinear spin imbalance of a spin-split superconductor in a rf field	65
4.6	S/F tunnel junction dynamics . . . . .	67
<b>5</b>	<b>Thermoelectric effects in superconducting structures</b>	<b>69</b>
5.1	Thermoelectric effects and heat engines . . . . .	70
5.2	Thermoelectric effects in superconductors . . . . .	72
5.3	Thermoelectric effects at a spin-polarized interface to a spin-split superconductor . . . . .	75
5.4	Linear response and a heat engine . . . . .	80
5.4.1	Effect of spin mixing . . . . .	83
5.4.2	Nonlinear response heat engine . . . . .	85
5.4.3	Effect of non-collinear magnetizations . . . . .	85
5.5	Thermally induced spin currents . . . . .	86

<b>6 Summary</b>	<b>87</b>
<b>Appendix A Conservation of spin and charge by the electron-phonon scattering</b>	<b>115</b>
<b>Appendix B Pauli matrices in Nambu–spin space</b>	<b>116</b>

## 1. Introduction

The study of the interaction between ferromagnetism and conventional superconductivity in hybrid systems has attracted a great attention during the past decades [1, 2, 3]. In principle, these two states of matter are antagonistic: whereas the ferromagnetic correlations try to align the spins of electrons, a conventional singlet Bardeen-Cooper-Schrieffer (BCS) [4] superconductor exhibits a condensate with electron pairs (Cooper pairs) with opposite spins. This simple argument explains why usual ferromagnetic metals do not show transition to a conventional superconducting state at any temperature.

Superconductivity and magnetism can coexist though in hybrid systems consisting of superconductor (S) and ferromagnet (F) layers, where the two states couple through mutual proximity effects. The interplay between them leads to striking novel phenomena not present in either system alone. For example the spatial oscillation of the superconducting correlations induced in F via the proximity effect leads to the  $\pi$ -junctions in S/F/S Josephson systems [5, 6]. The exchange field in F also leads to a triplet component of the superconducting condensate [1, 2, 7].

The effects discussed above are caused by the leakage of the superconducting condensate into the ferromagnet. There is also a reciprocal effect, caused by the interaction of the condensate with the exchange field that can leak back into the S region over distances of the order of the superconducting coherence length  $\xi_s$ . These triplet correlations induced in the superconductor lead to a finite magnetization and a drastic change of the local density of states [8, 9, 10, 11]. If the superconductor is a thin film with thickness smaller than  $\xi_s$ , this magnetic proximity effect may cause an almost homogeneous spin splitting of the BCS density of states (DOS) [12]. Such spin splitting plays a central role in this review.

In an all-metallic S/F system however it is difficult to achieve such a homogeneous spin splitting. The reason for this is the leakage of Cooper pairs from S to F. Usual metallic ferromagnets such as Fe, Co or Ni, have intrinsic exchange fields much larger than the characteristic superconducting energy ( $\sim \Delta$ , the BCS pair potential). For thin S-films such strong exchange fields in F lead eventually to a full suppression of the superconducting state. Indeed, the first observation of the  $0-\pi$ -transition in S/F/S Josephson could be achieved thanks to the use of ferromagnetic alloys with small exchange fields [6, 13]. However, a sharp splitting of the DOS in a superconductor in all-metallic systems has not been observed.

A quite different situation emerges when instead of a metallic ferromagnet one uses a ferromagnetic insulator (FI) adjacent to a thin S layer. The band gap of the FI prevents the penetration of the superconducting condensate into the FI. Electrons are reflected at the S/FI interface. Because the FI is magnetic, this reflection is spin-dependent and leads to the creation of an effective exchange field in the superconductor [14]. Superconductivity with a spin-splitting field has been observed in several spectroscopy experiments on Al films attached to europium chalcogenides, such as EuO, EuS and EuSe [15, 16, 12].

Interestingly, the spin splitting in the DOS observed in those experiments resembles the spin splitting created by a strong in-plane field applied to a thin superconducting film. This is caused by the fact that when a magnetic field is applied parallel to a thin S film, the orbital diamagnetic effect is weak [17] and the field mainly induces a paramagnetic response [18, 19, 20, 21]. This effect was explored experimentally already in the 1970s [22, 23]. The spin-split DOS has been utilized to determine the spin polarization of ferromagnets in S/F structures [24, 25, 26, 27, 12].

Even though spectral properties of S/FI have been intensively studied for a long time, only recently it has been realized that spin-split superconductors may find applications in spintronics, thermoelectricity, and sensors [3, 28, 29, 30, 31, 32, 33, 34]. To understand the physics underlying these applications one needs to consider nonequilibrium phenomena. Nonequilibrium effects can extend over distances larger than the coherence length and they are related to the deviation of the electron distribution function from its equilibrium form. Such a deviation leads to an imbalance of the electron degrees of freedom: charge, energy and spin. From recent studies it has turned out that non-equilibrium effects in spin-split superconductors is a very rich field of research [35, 36, 37, 38, 31, 39].

In this work we review the non-equilibrium properties of spin-split superconductors, focusing on thermal, electric and spin transport. We have recently published a Colloquium on this topic [3] in which we gave a qualitative overview of the field and the experimental activity. Our main purpose here is different: We mainly focus on the theoretical aspects of the transport properties of S/FI structures and elaborate deeper on the thermoelectricity in superconducting systems. We provide all the necessary theoretical tools for those readers interested in exploring non-equilibrium effects in novel setups combining superconductors and magnetic materials. Those readers seeking more phenomenological approach are referred to the Colloquium mentioned above.

The review is organized as follows: In Sec. 2 we summarize the main properties of S/FI structures and discuss the coexistence between superconductivity and ferromagnetism in these systems. The main focus is on the spin-splitting induced in the S layer and its manifestation on the spectrum. We also analyze the magnetic susceptibility of superconductors and briefly discuss other effects related to spin-splitting fields, including the Fulde-Ferrel-Larkin-Ovchinnikov (FFLO) state, triplet superconducting correlations and the cryptoferromagnetic state in the FI layer.

In Sec. 3 we present the quasiclassical Green's function formalism, with a special focus on the description of non-equilibrium properties of diffusive S/FI systems, the role of inelastic scattering and transport through hybrid interfaces. In this section we introduce the concept of nonequilibrium modes which is essential for understanding the different ways of exciting a spin-split superconductor out of equilibrium. Especially the charge, spin and heat transport properties are determined by these modes and their coupling.

On the basis of the quasiclassical formalism we analyze in Sec. 4 the transport properties of different FI/S structures. We focus in particular on spin injection, diffusion and relaxation, in different setups.

In Sec. 4.3.2 we study the non-equilibrium quasiparticle dynamics of a spin-split superconductor in an alternating radio frequency field, both in the linear and the non-linear regime. For this we make use of time-dependent quasiclassical equations.

Spin splitting the BCS spectrum leads to a strongly electron-hole asymmetric spin-resolved density of states. The symmetry is recovered by averaging over spin, but the electron-hole asymmetry shows up in the case of spin-polarized tunneling into spin-split superconductors. Section 5 discusses the transport properties of such spin-polarized contacts to spin-split superconductors, with a special emphasis on the thermoelectric response of such systems. We also review thermoelectricity in superconducting systems in general to set this finding into historical context.

Finally, Sec. 6 summarizes the main phenomena discussed in the review.

## 2. Ferromagnetic insulator–superconductor structures

At interfaces between a superconductor (S) and a magnetic material (F) both states of matter may coexist, however with certain modifications. Such modifications extend over the characteristic correlation lengths in each material. In S this length is the coherence length, which in diffusive systems and at low temperatures is of the order of  $\sqrt{D/\Delta_0}$ , where  $D$  is the diffusion coefficient and  $\Delta_0$  the superconducting gap at zero temperature. If the ferromagnet is a metal, the superconducting condensate (Cooper pairs) can penetrate into it. The superconducting correlation length in usual ferromagnets as Ni, Co or Fe, is approximately given by  $\sqrt{D/h}$ , where  $h$  is the intrinsic exchange field of the ferromagnet. Usually this length is very short (a few nanometers or even less) and therefore one speaks about a short-range proximity effect. Interestingly, the interaction of singlet electron pairs stemming from the S layer with the local exchange field leads to pairs in a triplet state that can get back into superconductor [2]. Such leakage of pairs and the suppression of the density of Cooper pairs in singlet state leads to a suppression of superconductivity [1].

If instead of a metal, a ferromagnetic insulator (FI) is placed adjacent to a superconductor, no leakage of pairs is possible. Conduction electrons are reflected at the FI/S interface and during this process their spin interacts via exchange interaction with the localized magnetic moment of the FI material. If the latter is not too strong and the superconducting layer is thin enough, both magnetic and superconducting orders can coexist. In this case the superconductor behaves as a ferromagnetic superconductor with a density of states showing a spin splitting, similar to the one that an external in-plane magnetic field would induce in a thin S layer [12].

In this section we describe the main features of superconductors with a spin-split density of states due to the proximity of a FI. Such artificial ferromagnetic superconductors are the main focus of this review. They have been fabricated and measured in several experiments along the past decades [15, 16, 40, 41].

### 2.1. Induced spin splitting in a superconductor–ferromagnetic insulator structure

As mentioned above, a way of creating a superconductor with a spin-split density of states is via the exchange field induced by an adjacent ferromagnetic insulator. This may lead to a spin splitting of the order of the superconducting gap, even without an externally applied magnetic field. The first evidence of an exchange field induced in a superconductor via the magnetic proximity effect was observed in a thin Al film in contact with an EuO film [15] and with EuS [16, 42, 40]. The equivalent internal field of the Zeeman splitting in Al-EuS systems has been reported to be as large as 5 T [43]. Another S-FI combination explored so far is GdN-NbN [44, 45]. This system shows, however, a weaker and less clear spin splitting than the Al-europium chalcogenide combination, due to the influence of the sizable spin-orbit interaction in Nb compared to the Al-based devices.

Because the electrons of the superconductor cannot penetrate into the insulating FI, the superconducting properties are only modified by the induced spin-splitting field at the S/FI interface, and not by the leakage of Cooper pairs into the FI. Moreover, FIs can also be used as spin-filter barriers [43], in some cases with a very high spin-filtering efficiency, and therefore they will play a crucial role for several of the applications discussed in subsequent sections which require strong spin filtering.

The amplitude of the spin splitting in a FI/S structure depends on both the intrinsic properties of the superconductor, such as the amount of magnetic impurities and the strength of spin-orbit coupling, and on the quality of the S/FI interface. The latter is crucial for obtaining a large splitting, as shown for example in Ref. [16].

Large splitting and spin-filter efficiencies have been achieved in different FI/S combinations, such as in EuO/Al/AlO<sub>3</sub>/Al [15], Au/EuS/Al [46], Al/EuS/Al [16], Ag/EuSe/Al [16], EuSe/Al/AlO<sub>3</sub>/Ag, NbN/GdN/NbN [44], NbN/GdN/TiN [47]. A summary of these parameters in different FI-S structure is presented in Table I of Ref. [3].

The spin splitting caused by a ferromagnetic insulator on an adjacent superconductor can be understood with the help of the following model [48, 49]. The effective Hamiltonian describing a FI/S bilayer consists of the ferromagnetic coupling within the FI layer,

$$H_{\text{FI}} = - \sum_{\mathbf{r}, \mathbf{r}'} J_{\mathbf{r}, \mathbf{r}'} \mathbf{S}_{\mathbf{r}} \mathbf{S}_{\mathbf{r}'} + H_{\text{an}}, \quad (1)$$

where  $J_{\mathbf{r}, \mathbf{r}'}$  is the exchange coupling between the localized spins  $\mathbf{S}_{\mathbf{r}}$ . The term  $H_{\text{an}}$  describes the magnetic anisotropy whose specific form does not need to be fixed here.

The S layer is described by the usual BCS Hamiltonian [4, 17], whereas for the FI/S interface we consider a model of an ensemble of localized magnetic moments that interact with the spin of the conduction electrons of the super-

conductor via exchange interaction,

$$H_{ex} = -J_{ex} \sum_{\mathbf{r}} \Psi_{\alpha}^{\dagger}(\mathbf{r}) (\mathbf{S}_{\mathbf{r}} \sigma)_{\alpha\beta} \Psi_{\beta}(\mathbf{r}). \quad (2)$$

Here, the symbol  $\tilde{\Sigma}$  means that we consider only the magnetic moments  $\mathbf{S}_{\mathbf{r}}$  localized at the interface.  $J_{ex}$  is an effective parameter which for example describes the s-d or s-f exchange interaction. We consider a ferromagnetic insulator with a Curie temperature much larger than the superconducting transition temperature. Thus we can assume that the magnetization of the FI is only determined by the Hamiltonian in Eq. (1) and not affected by the superconducting state [50, 51]. With this assumption Hamiltonian (2) describes conduction electrons interacting with an effective exchange field proportional to the local spin average  $\langle \mathbf{S}_{\mathbf{r}} \rangle$  at the FI/S interface. This average can be computed by solving independently the magnetic Hamiltonian (1) [41].

In the superconducting state the localized exchange field leads to a modified density of states characterized by the splitting of the coherent BCS peaks. This modification of the spectral properties of the superconductor is non-local and survives over distances away from the FI/S interface of the order of the coherence length  $\xi_s$  [14, 8]. If the thickness  $d$  of the S film is much smaller than  $\xi_s$ , the spin splitting can be assumed to be homogeneous across the film. Thus the density of states is given by Eq. (4) with an effective exchange field  $\mathbf{h}_{eff} \approx J_{ex} \langle \mathbf{S}_{\mathbf{r}} \rangle a/d$  [52, 48, 14], where  $a$  is the characteristic distance between the localized spins.

In this review we mainly focus on thin S films and hence we adopt this approximation for the description of the uniform magnetic proximity effect when the film is adjacent to a FI layer. For an inhomogeneous magnetic configuration of the FI layer the spatial scale that determines the effective splitting is the superconducting coherence length. Thus the splitting becomes observable if the ferromagnet consists of magnetic domains with sizes larger than the superconducting coherence length. This is for example the case of EuS films with magnetic domains of micrometer size [53] that explain the spin splitting observed in experiments [16] on Al-EuS structures, where the Al layers are a few nanometers thick and with a coherence length of the order of 100 nm. In contrast, a spatially fast changing magnetization averages to zero and results in a vanishing effective splitting [41, 54].

It also follows from this description that the strength of the spin splitting depends crucially on the quality of the FI/S interface. The growth of any non-magnetic oxide between the FI and S layers drastically suppresses the effective exchange interaction  $J_{ex}$  and hence reduces the spin splitting [16]. In addition to the quality of the interfaces, the spin splitting also depends on the intrinsic properties of the superconducting film. For example, magnetic disorder may lead to a strong suppression of superconductivity in the S film [55]. But even in the absence of magnetic disorder and magnetic impurities, spin-orbit coupling may lead to a modification in the DOS. In particular, large spin-orbit scattering rates lead to a rounding of the BCS peaks and to a less sharp spin splitting. This explains why splitting has been observed in materials with relative small atomic number  $Z$ , such as Al, Be, V, but not in heavier materials such as Pb.



For a detailed description of the intrinsic properties of different superconductors in this respect, we refer the reader to the excellent review in Ref. [12].

Spin splitting in a superconductor can also be achieved by applying an external magnetic field [22, 24, 26, 27, 16, 40]. In this case, however, the magnetic field also couples to the orbital motion of the electrons and creates circulating currents, the Meissner effect, [56] that try to expel the field from the bulk (diamagnetic response). By increasing the amplitude of the applied field superconductivity is gradually reduced. We denote below this mechanism of suppression of superconductivity by the *orbital depairing* effect. This mechanism dominates in bulk samples or in thin films with the field applied perpendicular to the plane of the film. If the amplitude of the applied field reaches a critical value  $H_c$ , the created currents increase the free energy such that the system undergoes a transition into the normal state [17]. However, in superconducting films with thickness smaller than the London penetration length, the critical value  $H_{c\parallel}$  for a magnetic field applied in-plane largely exceeds the critical value  $H_{c\perp}$  of a perpendicular field [17, 57]. In such a case the spin paramagnetic effect (due to Zeeman effect) dominates with respect to the orbital one. The magnetic field penetrates uniformly the film, screening currents are relatively small and therefore  $H_{c\parallel}$  is limited by the spin paramagnetic effect that tries to align the spin of the original singlet Cooper pairs, as demonstrated in Refs. [19, 18]. At  $T = 0$ , and in the absence of spin-orbit coupling and magnetic impurities, the critical field due to the paramagnetic effect is given by  $H_{cP} = \Delta_0/(\sqrt{2}\mu_B)$ , where  $\Delta_0$  is the superconducting gap at zero field and temperature and  $\mu_B$  is the Bohr magneton. For conventional BCS superconductors with critical temperature ranging from 1 to 10 K,  $H_{cP}$  can be of the order of several Tesla and hence superconductivity exists within a large range of field strengths. In short, the paramagnetic effect in thin superconducting films leads to a Zeeman splitting of the density of states (DOS) [22, 24, 26, 27, 16, 40], similar to the spin-splitting induced in S-FI structures.

## 2.2. Spin-split density of states in a superconductor

The splitting discussed in the previous section can be detected by measuring the tunneling conductance of the superconductor with a normal or a superconducting probe. For example, if one uses a normal metal (N) tunnel coupled to a superconducting film S, the current through the normal-insulator-superconductor (NIS) junction is determined by the tunneling expression [58]

$$I(V) = \frac{G_T}{e} \int_{-\infty}^{\infty} N(\varepsilon - V) N_s(\varepsilon) [n_F(\varepsilon - V) - n_F(\varepsilon)] d\varepsilon, \quad (3)$$

where  $N$  and  $N_s$  are the reduced density of states of the normal metal and the superconductor, respectively,  $n_F$  the Fermi distribution function and  $G_T$  is the conductance of the insulating tunneling barrier I. We first assume  $G_T$  to have no spin polarization. Electronic transport occurs mainly at energies close to the Fermi level where the density of states of the normal probe  $N(\varepsilon)$  can be accurately approximated by a function independent of the energy. In such a

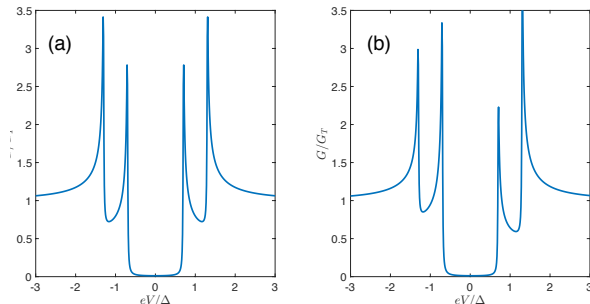


Figure 1: Differential conductance of a FI-S-I-N obtained from Eq. (3) (a) when N is a non-magnetic metal; (b) and for a spin-polarized N.

case, and at low temperatures the measured differential conductance  $G = dI/dV$  is proportional to the density of states of the superconductor. If the normal metal probe is non-magnetic, i.e., electrons are not spin-polarized, the measured  $G$  shows the spin-split peaks and is symmetric with respect to the voltage as sketched in Fig. 1(a).

If the tunneling barrier has a spin-dependent transmission, i.e., a spin filter, or a ferromagnetic electrode with a non-vanishing spin polarization, the observed peaks are asymmetric [26] [see Fig. 1 (b)]. The asymmetry is proportional to the spin polarization of the conduction electrons of the electrode or the spin-filter efficiency of the barrier. Indeed spin-split superconductor-ferromagnet bilayers have been used for determining the spin polarization of magnetic metals [26, 27, 24].

The normalized total density of states of the spin-split superconductor, sketched in Fig. 1 (a), can be written as the sum of the DOS  $N_{\uparrow/\downarrow}$  of each spin species,<sup>1</sup>

$$N = \frac{1}{2} \text{Re} \frac{\varepsilon + h_{\text{eff}}}{\sqrt{(\varepsilon + h_{\text{eff}})^2 - \Delta^2}} + \frac{1}{2} \text{Re} \frac{\varepsilon - h_{\text{eff}}}{\sqrt{(\varepsilon - h_{\text{eff}})^2 - \Delta^2}}, \quad (4)$$

where  $\pm h_{\text{eff}}$  is the effective spin-splitting field.

Equation (4) for the DOS is a simplified description of spin-split superconductors, which is accurate, as we see below, only in certain limiting cases. The expression does not take into account the effect of magnetic impurities or spin-orbit coupling (SOC). For example, magnetic impurities suppress superconductivity and eventually lead to a gap-less situation [55]. On the other hand the SOC counteracts the magnetic impurities but it may also lead to a broadening of the coherence peaks in the spectrum [59, 60, 61, 23]. Moreover, if the

<sup>1</sup> As conventional, here and below  $\sqrt{\varepsilon^2 - |\Delta|^2}$  means  $\text{sgn}(\text{Re } \varepsilon) \sqrt{\varepsilon^2 - |\Delta|^2}$  in terms of the principal branch  $\text{Re } \sqrt{\cdot} \geq 0$  of the square root.

spin-splitting field  $h_{\text{eff}}$  in Eq. (4) is due to an external magnetic field, also orbital depairing contributes to the pair breaking. We present a more quantitative analysis of these effects in the next section.

### 2.3. Paramagnetic depairing mechanisms and the FFLO state

When writing the DOS of a superconductor in an exchange field, Eq. (4), we assume that the ground state of the S layer corresponds to a spatially homogeneous order parameter  $\Delta$ . The value of the order parameter is determined from the self-consistency equation, written in terms of the Matsubara frequencies  $\omega_n = (2n + 1)\pi T$ ,<sup>2</sup>

$$\Delta \ln(T_{c0}/T) = 2\pi T \sum_{\omega_n > 0}^{\infty} \left( g_{01} - \frac{\Delta}{\omega_n} \right) \quad (5)$$

and a free-energy functional discussed in Sec. 3.5. Here  $g_{01}$  is a singlet anomalous part of the Green's function described in more detail in Sec. 3. In the following we describe the behavior of  $\Delta$  as a function of the exchange field  $h$ . For this, we denote  $\Delta_0 = 1.76T_{c0}$  the order parameter at  $T = h = 0$  without depairing effects.  $T_{c0}$  is the corresponding critical temperature. In the absence of spin relaxation the results coincide with those of Ref. [62]: For large values of  $h$ , the paramagnetic depairing drives the superconductor to the normal state. There is a critical value of temperature,  $T_0 \approx 0.556T_{c0}$ , above which the transition between the normal and superconducting states is of the second order. For  $T < T_0$ , the transition is of the first order, and the self-consistency equation has three solutions, of which one is unstable. The stable solutions correspond to superconducting ( $\Delta \neq 0$ ) and normal ( $\Delta = 0$ ) states. Below the critical field  $h_c$ , known as the Chandrasekhar-Clogston limit [18, 19], the superconducting state is preferred, and above it the normal state. At  $T = 0$  this critical field is  $h_c = \Delta_0/\sqrt{2}$ . Finally, for  $h > \Delta_0$ , the superconducting solution does not exist at all.

A non-zero spin relaxation rate leads to a quantitative modification of this behavior [63]. In Fig. 2 we show the computed  $\Delta$  as a function of temperature and exchange field for a normal-state spin relaxation rate  $1/T_{c0}\tau_{sn} = 0.96$ . Panels (a) and (b) in Fig. 2 show the effects of spin-flip ( $\beta = 1$ ) and spin-orbit ( $\beta = -1$ ) scattering, respectively. The phase-transition line,  $\Delta(T, h) = 0$ , is shown in Fig. 2 by the solid curve in the  $(T, h)$  plane. The red part on this curve corresponds to the second-order transition where  $\Delta(h)$  continuously goes to zero with increasing  $h$ . This behavior changes to the abrupt first-order transition at  $T < T_0$ . The first-order transition line is shown by circles in the  $(T, h)$  plane and it is different from the  $\Delta(T, h) = 0$  curve shown by the green line at  $T < T_0$ . Both relaxation mechanisms reduce the range of temperatures for which the first-order transition takes place. In other words, the threshold

<sup>2</sup>In this review we set  $\hbar = k_B = 1$  and hence the temperature, frequencies and inverse times have dimensions of energy, whereas the momentum has a dimension of inverse length.

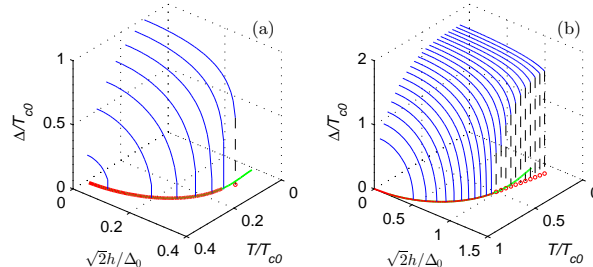


Figure 2: Order parameter  $\Delta$  as a function of the temperature  $T$  and the exchange field  $h$ . Spin relaxation rate  $\tau_{sn} = 1/(\tau_{sf}^{-1} + \tau_{so}^{-1})$  is  $1/(T_{c0}\tau_{sn}) = 0.96$ . (a) Spin-flip relaxation  $\beta = (\tau_{so} - \tau_{sf})/(\tau_{so} + \tau_{sf}) = 1$ . (b) Spin-orbit relaxation  $\beta = -1$ . The transition line  $\Delta(h, T) = 0$  is shown by the solid curve in the  $(h, T)$  plane. Its thick red part at  $T > T_0$  shows the second-order transition line. Its thin green part at  $T < T_0$  shows the points on  $T, h$  plane where the unstable branch starts (not shown). The first-order transition is shown by the circles in the  $(h, T)$  plane.

temperature  $T_0$  between first- and second-order phase transitions is reduced as compared to the case without relaxation.

In other respects the modification of the superconducting state strongly depends on the spin relaxation mechanism. Spin-flip scattering breaks the time-reversal symmetry and therefore leads to a strong suppression of the superconducting gap and  $T_c$ . On the other hand, spin-orbit interaction is time-reversal invariant and keeps the  $T_c$  intact.

A striking effect of the spin-orbit scattering is that it increases the critical field of the Chandrasekhar-Clogston limit [63]. This tendency is shown in Fig. 3, where we compare the dependencies of the superconducting gap on  $h$  and relaxation rates  $1/\tau_{sn}$  for (a) spin-flip and (b) spin-orbit relaxation, respectively. These two cases are characterized by the opposite behaviors of the critical field  $h_c$  as a function of  $1/\tau_{sn}$  — it is suppressed by spin-flip scattering and enhanced by the spin-orbit one. This effect can be understood from the comparison to the changes in the density of states caused by the two spin-relaxation mechanisms (see Fig. 4): spin-flip scattering primarily lifts the gap in the density of states, whereas spin-orbit scattering acts to nullify the spin splitting without affecting the gap. In both cases there is a threshold value of the scattering rate  $\tau_0^{-1}$  when the superconducting phase transition changes from the second order at  $\tau_{sn}^{-1} > \tau_0^{-1}$  to the first order at  $\tau_{sn}^{-1} < \tau_0^{-1}$ .

The assumption of a homogeneous order parameter does, however, not always correspond to the lowest-energy state of the system. In Refs. [20, 21] it was predicted that the exchange or Zeeman field can cause a transition to an inhomogeneous superconducting state, with a spatial periodical modulation of the order parameter at the scale of the coherence length. Such an FFLO state exists for temperatures below  $T_0$  and only for exchange fields that satisfy  $0.71\Delta_0 < h < 0.755\Delta_0$  when  $T \rightarrow 0$ .

The FFLO state has not been observed in conventional superconductors.

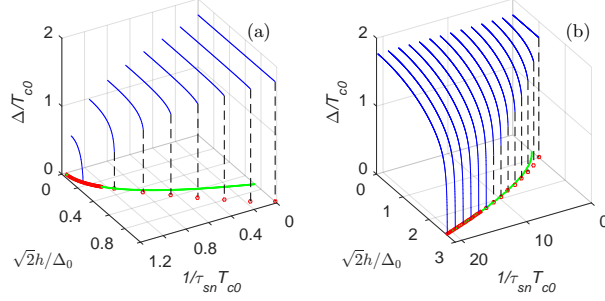


Figure 3: Order parameter  $\Delta$  as a function of the exchange field  $h$  and the normal-state spin relaxation rate  $1/\tau_{sn}$ . The temperature is  $T = 0.1T_{c0}$ . (a) Spin-flip relaxation  $\beta = 1$ . (b) Spin-orbit relaxation  $\beta = -1$ . The line of critical relaxation rates given by  $\Delta(h, \tau_{sn}^{-1}) = 0$  is shown by the solid curve in the  $(\tau_{sn}^{-1}, h)$  plane. Its thick red part at  $\tau_{sn}^{-1} > \tau_0^{-1}$  shows the second-order phase transition line. Its thin green part at  $\tau_{sn}^{-1} < \tau_0^{-1}$  corresponds to the points where the unstable branch starts (not shown). The first-order transition is shown by the circles in the  $(\tau_{sn}^{-1}, h)$  plane.

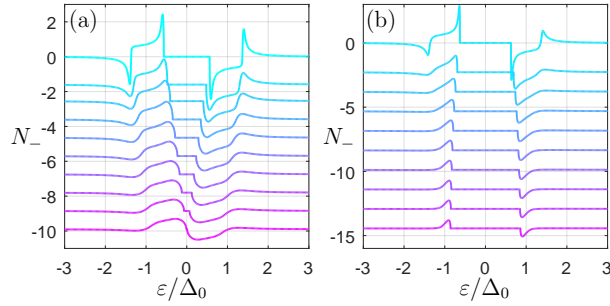


Figure 4: Calculated difference between spin-up and spin-down density of states  $N_- = N_\uparrow - N_\downarrow$  of a thin superconducting film at  $T = 0.1T_c$ ,  $h = 0.4\Delta_0$  and different spin relaxation rates  $\tau_{sn}$ . (a) Spin-flip relaxation  $\beta = 1$ , curves from top to bottom correspond to an increasing  $(\tau_{sn}T_{c0})^{-1}$ , varying equidistantly from 0.03 by 0.07 steps. (b) Spin-orbit relaxation  $\beta = -1$ , curves from top to bottom correspond to an increasing  $(\tau_{sn}T_{c0})^{-1}$ , varying equidistantly from 1 by steps of 2. For clarity the curves are shifted along the vertical axis.

One of the main reasons for this is that it is very sensitive to disorder [64] and spin-orbit coupling and hence it is expected to occur only in extremely clean samples. In the present review we mainly focus on diffusive systems and therefore we do not pay further attention to the FFLO state. Moreover, the effective exchange fields we mostly consider are far below the range for the FFLO state to occur.

The FFLO state has been also studied in the context of heavy-fermion superconductors [65] and ultra-cold Fermi gases [66, 67, 68] especially in the context of the BCS-BEC crossover [69, 70].

#### 2.4. Static spin susceptibility of conventional superconductors

The spin splitting has a direct consequence on the paramagnetic spin susceptibility of the superconductor. In general, the spin susceptibility  $\chi$  can be found by calculating the spin polarization  $\mathbf{S} = -\chi\mathbf{h}$  generated by a small spin-splitting field  $\mathbf{h}$ . In the superconducting state the susceptibility normalized with respect to that of the normal state  $\chi_n$  can be expressed in terms of the difference between spin-up and spin-down DOS  $N_- = N_\uparrow - N_\downarrow$  and the equilibrium distribution function  $f_{\text{eq}} = \tanh(\varepsilon/2T)$  [71, 2],

$$\chi/\chi_n = 1 + \frac{1}{4h} \int_{-\infty}^{\infty} \tanh\left(\frac{\varepsilon}{2T}\right) N_- d\varepsilon. \quad (6)$$

Using Eq. (4) for the spin-split DOS in the absence of magnetic depairing processes one can see that  $\int_{-\infty}^{\infty} N_- d\varepsilon = -4h$ . Therefore for  $T \rightarrow 0$  and in the absence of spin-dependent scattering  $\chi(T=0) = 0$ . This is a consequence of the lack of polarizability of the condensate consisting of spin-singlet Cooper pairs.

However, if spin-dependent scattering is present, in the form of spin-orbit and/or magnetic impurities causing spin flips, the superconducting condensate may exhibit a nonzero paramagnetic susceptibility for  $T \rightarrow 0$  [71, 72].

A generalization of this result can be obtained by using the microscopic equations introduced in Sec. 3 below. Here we are interested in the final results for the susceptibility shown in Fig. 5. In particular, we show the low-temperature dependence of the spin susceptibility as a function of the normal-state spin scattering rate  $1/\tau_{sn} = 1/\tau_{so} + 1/\tau_{sf}$  and the parameter  $\beta = (\tau_{so} - \tau_{sf})/(\tau_{so} + \tau_{sf})$  determining the relative strength of spin-flip and spin-orbit scattering. From these plots one can see that both scattering mechanisms result in a nonzero susceptibility at low temperatures. Notice that only the spin-flip scattering generates a strong suppression of the order parameter (see Fig. 2). Therefore, at  $T \ll T_{c0}$  the growth of  $\chi$  as a function of the rate  $1/\tau_{sn}$  towards the normal-state value is much faster when the spin-flip scattering dominates the spin-relaxation in the normal state, *i.e.* when  $\beta > 0$ . The non-zero susceptibility explains the observed Knight shifts in ordinary superconductors [73].

The static spin susceptibility (6) characterizes the paramagnetic response of the superconductor to the external magnetic field. This expression cannot be used for calculating the non-equilibrium spin accumulation induced by the

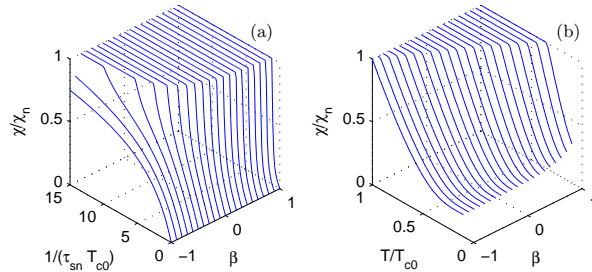


Figure 5: Paramagnetic susceptibility of a thin superconducting film for different values of  $\beta$  as a function of (a) the normal-state spin scattering rate  $1/\tau_{sn}T_{c0}$  and (b) the temperature. In (a)  $T = 0.1T_{c0}$  and in (b)  $1/\tau_{sn} = 0.5T_{c0}$ , where  $T_{c0}$  is the critical temperature in the absence of spin scattering.

spin-dependent chemical potential shift  $\pm\delta\mu$  when the distribution functions in different spin subbands are given by  $f_{\uparrow}(E) = f_0(E+\delta\mu)$  and  $f_{\downarrow}(E) = f_0(E-\delta\mu)$ . The theory of non-equilibrium spin states in superconductors is explained in detail in Secs. 3 and 4. In particular, there we explicitly show [see the discussion after Eqs. (25,26)] that the non-equilibrium spin accumulation generated by  $\delta\mu$  is always exponentially suppressed at low temperatures provided that there is a non-zero gap in the quasiparticle spectrum. This is the case even in the presence of the strong spin-orbit interaction [*cf.* Fig. 4(b)] although the static spin susceptibility (6) is non-zero at  $T = 0$ .

## 2.5. Other effects related to the Zeeman and exchange fields

In the next sections we discuss effects related to non-equilibrium properties of spin-split superconductors in FI-S structures. It is however important to mention other effects that we are not considering but that may appear in the presence of Zeeman and exchange fields.

### 2.5.1. Fermi liquid effects

The analysis in the previous subsections assumes noninteracting electrons, which is a rather good approximation in metals. Corrections due to interactions can be incorporated by renormalizing certain parameters of the theory with the help of the powerful Landau's Fermi-liquid theory [74]. In the context of the quasiclassical theory such effects have been studied in Ref. [75]. In particular, and importantly for our work, the spin-splitting field amplitude  $h \equiv |\mathbf{h}|$  entering Eq. (8) is renormalized. According to the Fermi liquid theory it is given by [76, 40]:

$$h = 2\mu_B \frac{H_{\text{ext}} + H_{FI}}{1 + G^0}, \quad (7)$$

where  $H_{\text{ext}}$  is the external magnetic field,  $H_{FI}$  is the field induced by a FI, and  $G^0$  is the effective antisymmetric Fermi-liquid parameter of Landau's theory. The value of  $G^0$  in the superconducting state depends on temperature, is negligibly small at low temperatures ( $T \ll T_c$ ), and nonzero for temperatures

close to the superconducting critical temperature  $T_c$  and above it. In what follows we neglect the Fermi-liquid corrections by assuming that  $G^0 \ll 1$ . This is justified at the low temperatures where majority of our work concentrates. However, when describing equilibrium properties of spin-split superconductors at temperatures close to  $T_c$ , the Fermi-liquid corrections to the field  $h$  in Eq. (8) should also be included for some superconductors. For example, for Al films  $G^0 \sim 0.16 - 0.3$  [77, 76] close to  $T_c$  and above, whereas in V it is negligibly small at all temperatures [78].

### 2.5.2. Long-range triplet correlations

In this review we mainly focus on the transport properties of the superconductor in S/F structures. For completeness, however, we briefly discuss in this section the appearance of triplet correlations in ferromagnetic metals induced by the superconducting proximity effect [79, 2]. Such correlations may induce non-dissipative spin-polarized currents that could be particularly useful to lower the energy consumption in spintronic devices [80, 81, 7].

Superconducting correlations can be induced in non-superconducting (N) metals by means of the proximity effect [82]. This can be seen as the "leakage" of Cooper pairs from the superconductor into the normal region. The microscopic origin of this "leakage" is the Andreev reflection [83], where an incident electron from N is retro-reflected as a hole, resulting in the formation of a Cooper pair in S. An important consequence of the Andreev reflection is that the correlation between the electron and the hole leads to a formation of a non-vanishing pair amplitude in N, within a characteristic distance  $\xi_N$  away from the S-N interface. This distance depends on the intrinsic properties of N, such as the degree of disorder, spin-dependent fields, etc. For example, in a diffusive normal metal without magnetic impurities this length is of the order of the thermal length  $\sqrt{D/T}$ , where  $D$  is the diffusion coefficient.

In a superconductor-ferromagnet (S-F) junction the situation is very different. In usual ferromagnets the intrinsic exchange field  $h$  is much larger than the superconducting characteristic energies. The proximity-induced superconducting correlations decay and oscillate on the length scale  $\xi_F = \text{Re}\sqrt{D/h}$ . The oscillation of the condensate leads to the well-established  $0-\pi$  transition in S-F-S Josephson junctions predicted in Ref. [5] and observed much later in experiments [6, 84] on SFS structures with ferromagnetic alloys with a weak exchange field. In conventional ferromagnets, such as Fe, Ni or Co, the effective exchange field is large ( $\sim 0.1 - 1$  eV) and hence  $\xi_F$  is very short [85]. This explains why the Josephson effect in S-F-S junctions with transition metals has been only observed for thickness of the F layer smaller than 10 nm [86, 87].

The situation is very different if the exchange field is spatially non-homogeneous, as for example in a magnetic domain wall. In such a case, as shown in Ref. [79], triplet components with equal spin components can be generated. These are insensitive to the local exchange field and hence can penetrate the F metal over the thermal length. Such long-range triplet component of the superconducting condensate explains the long-range Josephson currents observed in S-F-S junctions made for example of half-metal [88, 89], ferromagnetic multilayers [90],



and ferromagnets with intrinsic inhomogeneous magnetization [91].

We emphasize that the physics of the triplet component addressed in this section describes the equilibrium state of ferromagnets in contact with superconducting electrodes. The main focus of the present review is however the non-equilibrium properties of superconductors in spin-splitting fields, either generated by an adjacent FI or by an external field. As discussed in Sec. 2.3, in order to preserve the superconducting state, those fields have to be smaller than the superconducting gap, and hence all components of the condensate, singlet and triplets, vary over similar length scales. This in particular means that no distinction between short- and long-range has to be made.

### 2.5.3. *Cryptoferromagnetic state*

The way we model the exchange field generated in a thin superconducting film by an adjacent ferromagnetic-insulating layer, see Sec. 2.1, is based on the assumption that the magnetic ordering of the FI is the same in both the normal and superconducting states of the S layer. This requires that the effective exchange constants  $J$  and  $J_{ex}$  in Eqs. (1) and (2), respectively, satisfy  $J \gg J_{ex}$ . In this case the ferromagnetic order is robust against the exchange interaction with the conduction electrons and the superconducting condensate. Roughly speaking, this corresponds to the case when the Curie temperature  $T_{\text{Curie}}$  of the FI layer is larger than the effective exchange field, whose maximum value in the superconducting state is smaller than the superconducting order parameter  $\Delta$ . For example, in EuS/Al junctions  $T_{\text{Curie}} \sim 16.6$  K and  $\Delta_0 \sim 0.25$  meV, thus  $k_B T_{\text{Curie}}/\Delta_0 \sim 5.3$ . In other FIs such as EuO or NbN, the Curie temperature is even larger and hence this ratio increases. Thus the approximation made in Sec. 2.1 is well justified.

In the case of a weak magnetic stiffness of the FI compared to the characteristic superconducting energy  $\Delta$ , one should take into account the effect of the superconducting condensate on the magnetic ordering mediated by the Hamiltonian in Eq. (2). The competition between superconducting and magnetic ordering in such a case has been first considered in Ref. [92]. They considered a ferromagnetic state mediated via the Ruderman-Kittel-Kasuya-Yosida (RKKY) indirect exchange interaction. Above the superconducting critical temperature  $T_c$  the ground state of the system is a homogeneous magnetic state. When the temperature is lowered below  $T_c$  the ground state of the system corresponds to a spatially inhomogeneous magnetic structure characterized by a modulation with a wave vector of the order of  $(\lambda_F^2 \xi_s)^{1/3}$ , where  $\lambda_F$  is the Fermi wavelength and  $\xi_s$  is the superconducting coherence length. This state was called by Anderson and Suhl the cryptoferromagnetic state and may describe the situation of certain ternary rare earth compounds [93]. Such a magnetic modulation was also predicted for thin metallic [50, 51] and insulating [49] ferromagnetic films on top of bulk superconductors.

Although in this review we assume that the condition  $k_B T_{\text{Curie}}/\Delta_0 \gg 1$  is satisfied, and hence no cryptoferromagnetic state is induced, it is important to keep in mind that such a state may exist in the case of FIs with weak magnetic stiffness.

### 3. Quasiclassical theory of diffusive FI/S structures

In this section, we outline a microscopic theory useful for describing nonequilibrium effects in spin-split superconductors. We concentrate on diffusive superconductors where scattering by non-magnetic impurities results to a mean free path that is small compared to other lengths involved in the problem, with the exception of the Fermi wavelength  $\lambda_F$ . This condition is equivalent to the assumption that the inverse of the elastic relaxation time  $1/\tau$  is much larger than all characteristic energies apart from the Fermi energy.

Within a quasiclassical theory framework, which operates on length scales large compared to the Fermi wavelength, the superconducting properties can be described by a diffusion-like equation [94], now called the Usadel equation, which describes the behavior of the Keldysh Green's function (GF),

$$D\nabla \cdot (\check{g}\nabla\check{g}) + [i\varepsilon\tau_3 - i\mathbf{h} \cdot \boldsymbol{\sigma}\tau_3 - \check{\Delta} - \check{\Sigma}, \check{g}] = 0. \quad (8)$$

Here  $D$  is the diffusion coefficient,  $\check{\Sigma} = \check{\Sigma}(\mathbf{r}, \varepsilon)$  is the general self-energy term and  $\check{g}(\mathbf{r}, \varepsilon)$  is the (momentum isotropic part of the) quasiclassical Green's function, obtained by integrating the microscopic Green's functions over the quasiparticle energy. In addition to (8), the GF satisfies the quasiclassical normalization condition

$$\check{g}^2 = \check{1}. \quad (9)$$

The derivation of the Usadel equation (8) is discussed in several previous works [95, 94, 96, 2], and we do not present it here. For the readers not familiar with the quasiclassical method it is sufficient to understand that the knowledge of the structure of the GF sheds light on the spectral and transport properties of superconductors. In particular, the self-energies  $\check{\Sigma}$  generate the collision integrals for the different scattering processes of the kinetic transport theory, as described in more detail in Sec. 3.1.

In Eq. (8), the matrices  $\tau_j$ ,  $j = 1, 2, 3$  are Pauli matrices in the Nambu (or electron-hole) space.<sup>3</sup> The matrices  $\sigma_j$  ( $j = 0, 1, 2, 3$ ), are the Pauli matrices in spin space, with  $\sigma_0$  denoting the unit matrix. The vector  $\mathbf{h}$  denotes the spin-splitting field generated either by an external field or the magnetic proximity effect in a FI/S junction, and  $\check{\Delta} = \Delta\tau_\uparrow + \Delta^*\tau_\downarrow$  is the singlet superconducting order parameter.

The Green functions and self-energies are functions of the spatial coordinate and the energy. They are also matrices in the Keldysh $\otimes$ Nambu $\otimes$ spin space. The  $4 \times 4$  Nambu $\otimes$ spin matrix structure corresponds to the Nambu bi-spinor, which we in this review choose as

$$\Psi = \begin{pmatrix} \psi_\uparrow(\mathbf{r}, t) & \psi_\downarrow(\mathbf{r}, t) & -\psi_\downarrow^\dagger(\mathbf{r}, t) & \psi_\uparrow^\dagger(\mathbf{r}, t) \end{pmatrix}. \quad (10)$$

---

<sup>3</sup>In this review, when the matrices  $\tau_i$  or  $\sigma_i$ ,  $i = 1, 2, 3$  show up alone, if required by the context, this should be understood in terms of an outer product of the  $2 \times 2$  Pauli matrix in one (Nambu or spin) space and the  $2 \times 2$  identity matrix in the other space. See also Appendix B.

The structure in the Keldysh space can be represented via three independent components. Here we use the representation

$$\check{g} = \begin{pmatrix} \hat{g}^R & \hat{g}^K \\ 0 & \hat{g}^A \end{pmatrix}, \quad (11)$$

where the retarded (R), advanced (A) and Keldysh (K) components are  $4 \times 4$  matrices in the Nambu  $\otimes$  spin space.

The set of equations is completed by expressions for the self-energy  $\check{\Sigma}$  and a self-consistency relation for  $\Delta$ . The former is discussed in subsequent sections, and the latter for conventional superconductors can be written as

$$\Delta = \frac{\lambda}{16i} \int_{-\Omega_D}^{\Omega_D} d\varepsilon \text{Tr}[(\tau_1 - i\tau_2)\hat{g}^K(\varepsilon)]. \quad (12)$$

Here,  $\lambda$  is the effective coupling constant and  $\Omega_D$  is the Debye cutoff frequency.

Quite generally, the R/A components of the Green function are related to spectral properties of the superconductors whereas K also contains information about the quasiparticle kinetics. Indeed, it can be related to the electron distribution function  $\hat{f}$ ,

$$\hat{g}^K = \hat{g}^R \hat{f} - \hat{f} \hat{g}^A. \quad (13)$$

In the most general case, the  $4 \times 4$  matrix distribution function  $\hat{f}$  can be written as

$$\hat{f} = f_L \hat{1} + f_T \tau_3 + \sum_j (f_{Tj} \sigma_j + f_{Lj} \sigma_j \tau_3). \quad (14)$$

where  $f_{T/L,j}$  are real-valued. Here, we generalize the notation introduced in Ref. [97] to the spin-dependent case. The different components of  $\hat{f}$  carry specific information of the nonequilibrium state of the electron system. In equilibrium at temperature  $T$  the distribution function is  $\hat{f} = \hat{1} \tanh(E/2T)$ . We discuss the physical interpretation of each component in the following section.

For a homogeneous bulk superconductor, with no spatial dependence in the quantities, we can write the general form of R and A functions as

$$\hat{g}^{R(A)} = \sum_{j=0}^3 \left( \tau_1 g_{j1}^{R(A)} + \tau_3 g_{j3}^{R(A)} \right) \sigma_j. \quad (15)$$

The off-diagonal components, i.e., those proportional to  $\tau_1$ , are characteristic of the superconducting state and describe the anomalous GFs. The component of the anomalous GFs proportional to  $\sigma_0$  describes the usual singlet correlations in the BCS theory. On the other hand, the terms proportional to the Pauli matrices  $\sigma_j$ ,  $j = 1, 2, 3$ , describe the three triplet components of the condensate that appear in the presence of spin-dependent fields [79, 2]. The density of states, normalized by its normal state value, can also be written in terms of them:

$$N_+(\varepsilon) = \frac{1}{2} (g_{03}^R - g_{03}^A) = N_\uparrow + N_\downarrow, \quad (16)$$

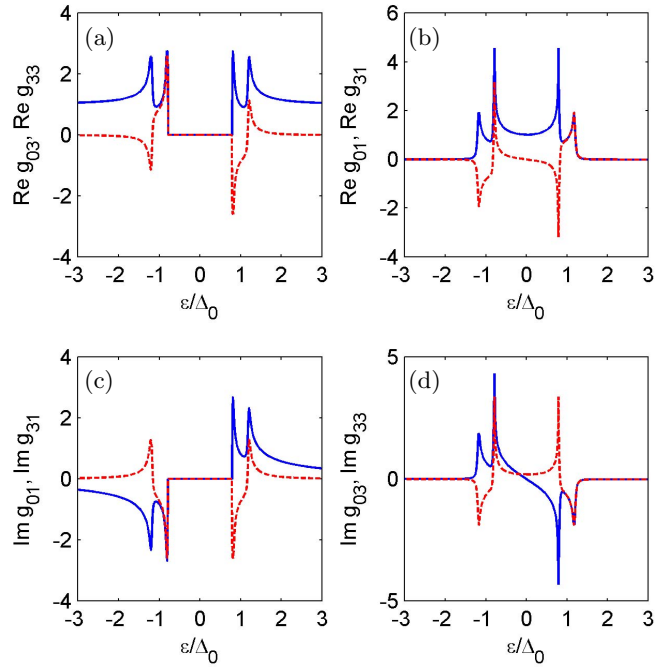


Figure 6: Nonzero components of the retarded Green's function  $g^R$  in a homogeneous spin-split superconductor. In all panels the blue solid curves show the spin-singlet amplitudes  $g_{01}$ ,  $g_{03}$  and the red dashed lines show the spin-triplet ones  $g_{31}$ ,  $g_{33}$ . The curves are calculated for  $h = 0.2\Delta_0$ ,  $\tau_{sn}^{-1} = 0.25T_{c0}$  and  $\beta = -0.9$ .

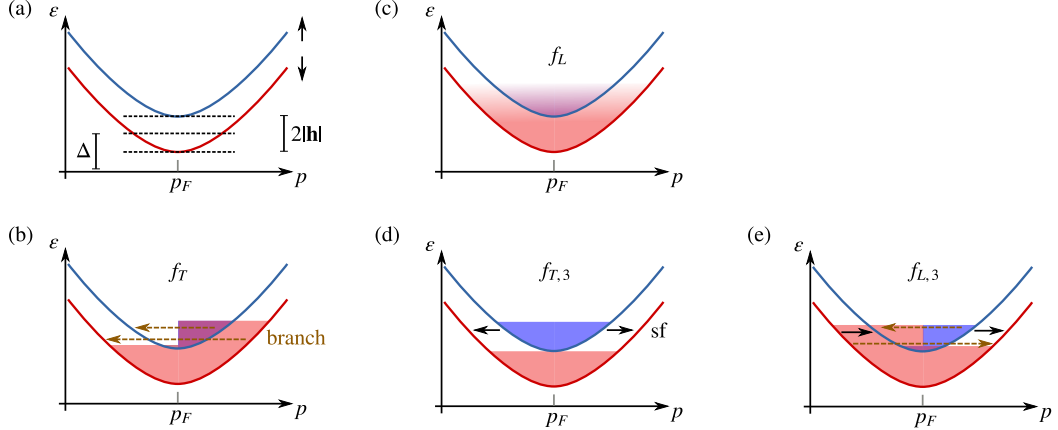


Figure 7: Schematic excitation spectrum for a spin-split superconductor, and illustration of the different nonequilibrium modes. (a) Schematic excitation spectrum. (b-e) Nonequilibrium population modes of the different branches. Relevant *elastic* relaxation processes are also shown (spin-flip: black arrows, branch-imbalance relaxation: brown dashed arrows).

which for a bulk spin-split superconductor reduces to Eq. (4). Accordingly, the difference of the DOS of the spin split bands is determined by

$$N_-(\epsilon) = \frac{1}{2} (g_{33}^R - g_{33}^A) = N_\uparrow - N_\downarrow. \quad (17)$$

The latter quantity is shown in Fig. 4. The real and imaginary parts of the different components of the retarded Green's function are plotted in Fig. 6 in the case of a homogeneous magnetization pointing in the  $z$  direction. In that case, the GF components proportional to  $\sigma_{1,2}$  vanish.

In what follows, we discuss the nonequilibrium quasiparticle physics in more detail.

### 3.1. Nonequilibrium quasiparticles

We call the different components  $f_{T/Lj}(\epsilon)$ ,  $j = 0, 1, 2, 3$  of the distribution function the *nonequilibrium modes*. They provide a description of the different ways in which the electron distribution in the quasiclassical limit can deviate from equilibrium.

The excitation spectrum of a spin-split superconductor has distinct electron- and hole-like branches, each with spin either up or down. The exchange field  $h$  splits the energies of the spin branches, as illustrated in Fig. 7(a). In a collinear situation with a single spin quantization axis, the electron population can be described with the four distribution function components  $f_T$ ,  $f_L$ ,  $f_{T3}$ , and  $f_{L3}$ .

The mode  $f_T \equiv f_{T0}$  [Fig. 7(b)] is well-known in superconductor physics: it is the *charge imbalance* (or “branch imbalance”) mode [98, 99, 100], which corresponds to an imbalance in the number of quasiparticles above and below the Fermi surface. This mode can be generated by charge injection into the

superconductor for example from a normal-state electrode, and measured by observing the local potential  $\mu$  of the quasiparticles. The mode  $f_L$  is associated with the energy content of the superconductor, and reflects local changes in the effective temperature. It can generally be induced by any heating mechanism.

The spin imbalance mode  $f_{T3}$  [Fig. 7(d)] is related to a spin accumulation  $\mu_z$ , which can be nonzero also in the absence of spin splitting of the spectrum. It can be induced for example by a spin-polarized injection from a ferromagnetic electrode, even in the normal state [101]. Finally, the spin-energy mode  $f_{L3}$  encodes a nonequilibrium state with antisymmetric differences in the electron-hole and spin-up/down distributions. We are not aware of existing experiments probing  $f_{L3}$  nonequilibrium.

The spin splitting of the superconductor spectrum also modifies how the modes contribute to observables, which generally depend on the amount of quasiparticles on the different spectral branches. The charge imbalance potential  $\mu$  then acquires contributions from both electron-hole antisymmetric modes  $f_T$  and  $f_{L3}$ . The other two modes,  $f_L$  and  $f_{T3}$ , contribute to the spin accumulation  $\mu_z$ .

To excite the modes  $f_T$ ,  $f_{T3}$  and  $f_{L3}$ , one only needs to transfer quasiparticles between the different spectral branches in an elastic process, i.e., between equal-energy states (horizontally in Fig. 7). They can also relax back to equilibrium due to elastic scattering processes (horizontal arrows in Fig. 7). These relaxation mechanisms depend on properties of the material, and also on the superconducting spectrum, and are discussed in subsequent sections.

In contrast, relaxation of the  $f_L$  mode generally requires inelastic processes, which often are slow compared to elastic processes at low temperatures. As a consequence, perturbations in  $f_L$  can survive up to longer times and propagate longer distances than those in the other modes. Because the  $f_L$  mode also contributes to the spin accumulation, this is crucial in understanding long-range spin signals observed in spin-split superconductors, for example in Ref. [31], which is discussed in Sec. 4.

### 3.1.1. Kinetic equations

The different parts of the matrix distribution function  $\hat{f}$  are determined by a kinetic equation that describes the balance of different transport and relaxation processes. In a diffusive conductor in the steady-state limit, the kinetic equation can be obtained by inserting Eq. (13) in the Usadel equation (8) and evaluating its different matrix components. This results into a set of diffusion-type equations of the generic tensor form

$$\nabla_k j_{kb}^a = H^{ab} + R^{ab} + I_{\text{coll}}^{ab}, \quad (18)$$

$$j_{kb}^a = \frac{1}{8} \text{Tr} \tau_b \sigma_a (\check{g} \nabla_k \check{g})^K. \quad (19)$$

Here,  $I_{\text{coll}}^{ab} = \text{Tr} \tau_b \sigma_a [\check{\Sigma}, \check{g}]^K / 8$  is the collision integral describing scattering processes with self-energy  $\check{\Sigma}$ . The term  $H^{ab} = \text{Tr} \tau_b \sigma_a [-i\mathbf{h} \cdot \sigma \tau_3, \hat{g}^K] / 8$  describes the Hanle spin precession due to the exchange field, and  $R^{ab} = \text{Tr} \tau_b \sigma_a [\hat{\Delta}, \hat{g}^K] / 8$  the

quasiparticle branch conversion processes involving the superconducting condensate. The detailed forms of the different components of the kinetic equations in spin-split superconductors are discussed in Sec. 4.1. Note that the definition of the collision integrals here depends on the form of the diffusion equation adopted; another definition is discussed in Sec. 4.4.

The above equations are formulated for a stationary situation where  $\Delta$  is time-independent, and here and below, we quite generally only consider this case. The equations are written in a gauge where the zero of the electric potential is taken to be the potential of the superconducting condensate. We also consider only length scales where the metal can be assumed locally charge neutral. The formulation still allows describing normal-state electrodes at nonzero electrochemical potential, by including distribution functions of the form [96]

$$f_{\text{eq},L(T)}(\varepsilon) = \frac{1}{2} \left[ \tanh\left(\frac{\varepsilon + eV}{2T}\right) + (-) \tanh\left(\frac{\varepsilon - eV}{2T}\right) \right], \quad (20)$$

as boundary conditions. Superconducting electrodes however have  $V = 0$  as the quasiparticle and condensate potentials coincide at equilibrium.

### 3.1.2. Observables

Local densities of charge, and excess spin and energy can be obtained from the Keldysh Green function. These equations in the quasiclassical framework read for the charge imbalance and spin accumulation

$$\mu(\mathbf{r}, t) = - \int_{-\infty}^{\infty} \frac{d\varepsilon}{16} \text{Tr} \hat{g}^K(\varepsilon, \mathbf{r}, t) \quad (21)$$

$$\mu_{sa}(\mathbf{r}, t) = \int_{-\infty}^{\infty} \frac{d\varepsilon}{16} \text{Tr} \tau_3 \sigma_a [\hat{g}_{\text{eq}}^K(\varepsilon, \mathbf{r}, t) - \hat{g}^K(\varepsilon, \mathbf{r}, t)], \quad (22)$$

and for the local energy and spin-energy accumulations:

$$q(\mathbf{r}, t) = \int_{-\infty}^{\infty} \frac{d\varepsilon}{16} \varepsilon \text{Tr} \tau_3 [\hat{g}_{\text{eq}}^K(\varepsilon, \mathbf{r}, t) - \hat{g}^K(\varepsilon, \mathbf{r}, t)] \quad (23)$$

$$q_{sa}(\mathbf{r}, t) = \int_{-\infty}^{\infty} \frac{d\varepsilon}{16} \varepsilon \text{Tr} \sigma_a [\hat{g}_{\text{eq}}^K(\varepsilon, \mathbf{r}, t) - \hat{g}^K(\varepsilon, \mathbf{r}, t)]. \quad (24)$$

Here, polarization direction of the spin is encoded in the direction components  $a = 1, 2, 3$ . The energy content is written relative to a system at equilibrium at the chemical potential  $\mu_S = 0$  of the superconducting condensate.

The charge imbalance is related to the local charge density by  $\rho = -\nu_F e^2 \phi - e\nu_F \mu$ , where  $\phi$  is the electrostatic potential. In the locally charge-neutral limit considered here,  $\rho \approx 0$  so that  $-e\phi \approx \mu$  and  $\mu$  corresponds directly to the local electric potential [102, 103].

By using Eqs. (13-17) one can express the charge and spin accumulations in

terms of the distribution functions and the density of states,

$$\mu = -\frac{1}{2} \int_{-\infty}^{\infty} d\varepsilon (N_+ f_T + N_- f_{L3}), \quad (25)$$

$$\mu_z = -\frac{1}{2} \int_{-\infty}^{\infty} d\varepsilon [N_+ f_{T3} + N_- (f_L - f_{eq})]. \quad (26)$$

Similarly for the local energy and spin-energy content:

$$q = \frac{1}{2} \int_{-\infty}^{\infty} d\varepsilon \varepsilon [N_+ (f_L - f_{eq}) + N_- f_{T3}], \quad (27)$$

$$q_{sa} = \frac{1}{2} \int_{-\infty}^{\infty} d\varepsilon \varepsilon [N_- (f_L - f_{eq}) + N_+ f_{T3}]. \quad (28)$$

The above equations apply to the collinear situation with a single spin quantization axis.

The observable current densities of charge, energy, spin, and spin-energy can be obtained from the spectral current (19). Explicitly, they read, (i) the charge current:

$$J_k = \frac{\sigma_N}{2e} \int_{-\infty}^{\infty} d\varepsilon j_{k3}^0, \quad (29)$$

(ii) the spin current density polarized in  $a$ -direction

$$J_k^a = \frac{\sigma_N}{2e^2} \int_{-\infty}^{\infty} d\varepsilon j_{k0}^a, \quad (30)$$

(iii) the energy current density

$$J_{e,k} = \frac{\sigma_N}{2e^2} \int_{-\infty}^{\infty} d\varepsilon \varepsilon j_{k0}^0, \quad (31)$$

and (iv) the spin energy current density

$$J_{e,k}^a = \frac{\sigma_N}{2e^2} \int_{-\infty}^{\infty} d\varepsilon \varepsilon j_{k3}^a. \quad (32)$$

Here,  $\sigma_N = e^2 D \nu_F$  is the normal-state conductivity and  $\nu_F$  is the normal-state density of states at the Fermi level.

### 3.2. Elastic relaxation mechanisms

In addition to the impurity scattering that results in the momentum relaxation, there are also other elastic scattering processes that, while preserving the energy of the excitations, change their other quantum numbers such as the spin. For example, in metals and semiconductors there are two main types of mechanisms that relax the spin: scattering from magnetic impurities and spin-orbit coupling. As discussed in Sec. 2, these processes can modify substantially the



spectral properties of a superconductor. In addition, the superconducting properties are modified by the orbital effect due to external magnetic fields, which for the quasiparticles can result to an electron-hole branch-mixing process.

Within Born approximation, the self-energies for these elastic processes obtain the forms

$$\check{\Sigma}_{so} = \frac{\boldsymbol{\sigma} \cdot \check{g}\boldsymbol{\sigma}}{8\tau_{so}}, \quad (33)$$

$$\check{\Sigma}_{sf} = \frac{\boldsymbol{\sigma} \cdot \tau_3 \check{g} \tau_3 \boldsymbol{\sigma}}{8\tau_{sf}}, \quad (34)$$

$$\check{\Sigma}_{orb} = \frac{\tau_3 \check{g} \tau_3}{\tau_{orb}}. \quad (35)$$

Here,  $\tau_{so}$  and  $\tau_{sf}$  are the two scattering times for impurity spin-orbit and spin-flip scattering. We parametrize these scattering rates in terms of the total spin relaxation time,  $\tau_{sn}^{-1} = \tau_{so}^{-1} + \tau_{sf}^{-1}$  and the relative strength of the two scattering mechanisms  $\beta = (\tau_{so} - \tau_{sf}) / (\tau_{so} + \tau_{sf})$ . Values with  $\beta \approx 1$  correspond to dominant spin-flip scattering, whereas  $\beta \approx -1$  to dominant spin-orbit scattering.

The orbital self-energy above can be used to describe the orbital depairing effect of (Meissner) screening currents induced by an in-plane magnetic field in a thin film, leading to the suppression of superconductivity [104]. It does not enter explicitly the kinetic equation for the distribution function, but modifies indirectly its energy dependence by affecting the spectral properties of the superconductor, contributing to the relaxation of charge imbalance [97, 105]. In the case of a thin magnetic film with thickness  $d$  and an in-plane applied magnetic field, the orbital depairing relaxation time is given by [106]  $1/\tau_{orb} = De^2 B^2 d^2 / 6$ .

In the case of spin-orbit coupling we can distinguish two types of relaxation mechanisms according to the origin, intrinsic or extrinsic. Intrinsic spin-orbit coupling occurs in systems without inversion symmetry, either due to geometry constraints or the crystal potential associated with the electronic band structure. Momentum-dependent spin precession together with random momentum relaxation due to impurities leads to the Dyakonov-Perel relaxation [107]. For example, for a diffusive 2D system with a Rashba spin-orbit coupling  $\alpha_R$ , the Dyakonov-Perel relaxation time is  $\tau_{\parallel} = 1/D(2m\alpha_R)^2$  for an in-plane spin-polarization, and  $\tau_{\perp} = \tau_{\parallel}/2$  for spins perpendicular to the 2D system.

In contrast, the extrinsic spin-orbit effect originates from a random impurity potential and hence leads to an isotropic spin relaxation known as the Elliott-Yafet relaxation mechanism. It is this component that is described by the self-energy Eq. (33). A detailed discussion of spin relaxation mechanisms originating from the spin-orbit coupling can be found in the review [108] and references therein. Because we here focus on centrosymmetric materials, we only consider the extrinsic relaxation mechanism. Moreover, we do not consider effects related to the spin-charge coupling, such as the spin Hall effect [109] and the spin galvanic effects [110]. Such effects enter the kinetic equations in a higher order of the gradient expansion and can be neglected in the leading order. The spin-charge coupling in diffusive superconductors leads to non-dissipative

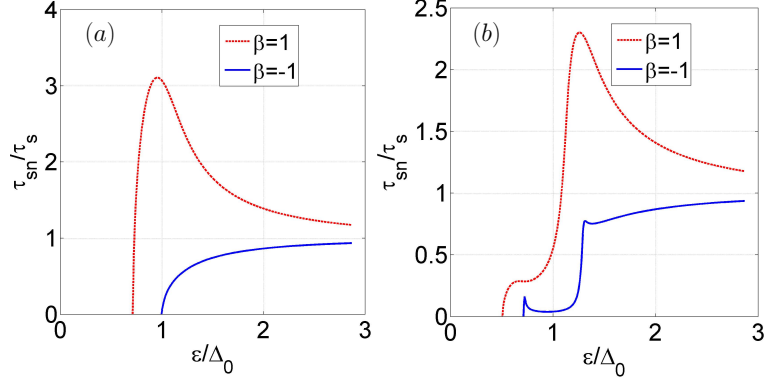


Figure 8: Spin relaxation rates for (a)  $h = 0$  and (b)  $h = 0.3\Delta_0$  and for spin-orbit ( $\beta = -1$ ) and spin-flip ( $\beta = 1$ ) relaxation mechanisms. We assume that the normal-state spin relaxation rate is  $\tau_{sn}^{-1} = 0.2T_{c0}$ .

magnetolectric effects and the appearance of an anomalous phase in Josephson junctions, [111, 112, 113].

The parameters  $\tau_{sf}$ ,  $\beta$  of the spin-dependent scattering are material specific. In Refs. [114, 115], using spin injection experiments, the values  $\tau_{sn} \approx 100$  ps and  $\beta \approx 0.5$  were found for Al for which then  $\tau_{sf} < \tau_{so}$ . According to Refs. [116, 73], the spin-orbit scattering rate is the momentum relaxation rate times  $(Z\alpha)^4$ , where  $Z$  is the atomic number and  $\alpha$  is the fine-structure constant. Therefore, the spin-orbit scattering rate grows rapidly as the atomic number grows. Indeed, in Nb  $\tau_{sn}$  is only 0.2 ps and spin-orbit scattering dominates [117].

### 3.2.1. Nonequilibrium spin relaxation

In this review we only consider centro-symmetric metals, and therefore we only consider spin-relaxation caused by impurities. In this case, the collision integrals entering the kinetic equation due to spin-dependent scattering are given by

$$S_{ab} = \frac{1}{8} \text{Tr} \left\{ \tau_b \sigma_a [\check{\Sigma}_{so} + \check{\Sigma}_{sf}, \check{g}]^K \right\}, \quad (36)$$

where the components  $a, b$  refer to the different nonequilibrium modes and spin projections. The self-energies are defined in Eqs. (33) and (34). In the superconducting state, the form of the spin-flip and spin-orbit contributions to the collision integrals differ due to their different properties under time reversal.

We now discuss the relaxation of the nonequilibrium modes related with the spin and the spin energy imbalances, i.e., the components  $f_{T3}$  [Fig. 7(d)] and  $f_{L3}$  [Fig. 7(e)]. The relaxation of these modes is described by the components ( $b = 0, a = 3$ ) and ( $b = 3, a = 3$ ) of Eq. (36), respectively.

Specifically, the spin relaxation, shown schematically by the arrows in Fig. 7(d), is described by the collision integral  $S_{03}^s = S_{T3} f_{T3}$ , where

$$\tau_{sn} S_{T3} = (\text{Re}g_{03})^2 - (\text{Re}g_{33})^2 + \beta [(\text{Im}g_{01})^2 - (\text{Im}g_{31})^2]. \quad (37)$$

In the normal state these processes are energy independent (within the quasi-classical approximation), and have the rate  $\tau_{sn}^{-1}$ . In the superconducting state, the spin-relaxation is described by Eq. (37), with the energy-dependent rate  $\tau_s^{-1} = S_{T3}(\varepsilon)/N_+$ . Here the collision integral is normalized with the spin-averaged density of states  $N_+$  to counterbalance effects due to the mere changes of the quasiparticle spectrum in the superconducting state. The typical behavior of  $\tau_s^{-1}(\varepsilon)$  is shown in Fig. 8 for dominating spin-flip and spin-orbit mechanisms for (a) zero and (b) nonzero spin splitting.

In the presence of strong spin-orbit scattering ( $\beta < 0$ ), superconductivity results to reduction of the spin relaxation rate  $\tau_s^{-1}$ . Still, there is no significant change in the spin relaxation length  $\lambda_{so}$ : [118] Qualitatively  $\lambda_{so} \sim v_g \tau_s$ , and the reduction in the quasiparticle momentum scattering cross section is mostly canceled by the decrease in the group velocity  $v_g \sim v_F \sqrt{1 - |\Delta|^2/\varepsilon^2}$ . In contrast, the increase in  $\tau_s^{-1}$  due to spin-flip scattering does result to a reduced spin relaxation length: [118] this mechanism is not related to the momentum scattering as the interaction with magnetic impurities does not depend on the propagation direction and the quasiparticle spin does not depend on energy.

In the presence of a Zeeman or exchange field,  $h \neq 0$ , this situation changes drastically. In this case the nonequilibrium spin accumulation couples to the energy mode,  $f_L$ . This mode is robust with respect to elastic spin relaxation processes, resulting to a qualitative change in the observed spin relaxation. This effect, as well as the detailed energy dependence of the spin relaxation lengths, are discussed in detail in Sec. 4.2.

For the relaxation of the spin-energy mode  $f_{L3}$ , the situation is more complicated. As sketched in Fig. 7(e), the relaxation of this mode involves transitions between electron and hole branches of the quasiparticle spectrum. As in the case of charge imbalance relaxation, such inter-branch transitions involve the formation of Cooper pairs via Andreev reflection. This results in two contributions to the relaxation of the spin-energy mode: One stems from the ( $j = 3, k = 3$ ) component of the collision integral (36) that describes transitions between spin-up and spin-down subbands  $S_{33}^s = S_{L3} f_{L3}$ , where

$$\begin{aligned} \tau_{sn} S_{L3} = \\ (\text{Re}g_{03})^2 - (\text{Re}g_{33})^2 + \beta [(\text{Re}g_{31})^2 - (\text{Re}g_{01})^2]. \end{aligned} \quad (38)$$

The second contribution originates from the particle-hole relaxation described by the non-diagonal self-energy in the Keldysh-Usadel equation (8),

$$R_T f_{L3} = \frac{1}{8} \text{Tr}(\tau_3 \sigma_3 [\check{\Delta}, \check{g}^K]) \quad (39)$$

$$R_T = 2\Delta \text{Re}g_{01}. \quad (40)$$

The relaxation of the spin-energy mode in the superconductor is given by the sum  $R_T + S_{L3}$ .

Note that the particle-hole conversion processes responsible for the spin energy relaxation also lead to the generation of charge imbalance producing a

coupling between spin and charge degrees of freedom. These mechanisms are discussed in more detail in Sec. 4.2. At large energies  $\varepsilon \gg \Delta$  the charge and spin energy nonequilibrium modes are decoupled. In this limit the charge relaxation length tends to infinity because the coherence factor  $\text{Re}g_{01} \rightarrow 0$ . At the same time, the spin-energy relaxation length approaches its normal-state value equal to that of the spin relaxation length  $\Lambda_{sn} = \sqrt{D\tau_{sn}}$ .

### 3.3. Inelastic relaxation mechanisms

The inelastic processes that are typically relevant in metallic systems, the particle-phonon and particle-particle collisions, are described by an inelastic self-energy  $\check{\Sigma}_{in} = \check{\Sigma}_{\text{eph}} + \check{\Sigma}_{\text{ee}}$ . These processes do not conserve the energies of colliding quasiparticles, but conserve the total spin. A model self-energy for inelastic relaxation due to electron-phonon scattering is given by [119]

$$\begin{aligned} \check{\Sigma}_{\text{eph}}^{R/A/K}(\varepsilon) &= -ig_{\text{eph}} \int_{-\infty}^{\infty} d\omega \check{\Sigma}_{\text{eph}}^{R/A/K}(\omega, \varepsilon + \omega) \\ \check{\Sigma}_{\text{eph}}^{R(A)} &= D^K(\omega) \hat{g}^{R(A)}(\varepsilon + \omega) - D^{R(A)}(\omega) \hat{g}^K(\varepsilon + \omega) \\ \check{\Sigma}_{\text{eph}}^K &= D^K(\omega) \hat{g}^K(\varepsilon + \omega) - D^{RA}(\omega) \hat{g}^{RA}(\varepsilon + \omega), \end{aligned} \quad (41)$$

where  $D^{R,A} = \pm i\omega|\omega|$ ,  $D^{RA} = D^R - D^A$ ,  $D^K(\omega) = D^{RA}(\omega) \coth(\omega/2T_{ph})$  are parts of Fermi surface averages of the free phonon propagators,  $T_{ph}$  is the phonon temperature and we denote  $X^{RA} = X^R - X^A$  for  $X = D, \hat{g}$ . Inelastic particle-particle collision self-energies  $\check{\Sigma}_{\text{ee}}$  within the quasiclassical theory have been discussed in Refs. [119, 120].

#### 3.3.1. Electron-phonon coupling

The relaxation due to the electron-phonon coupling is an important limiting mechanism for some of the nonequilibrium effects discussed in subsequent sections. Generally, it becomes weaker towards lower temperatures as the phonon density of states decreases at low energies. As a consequence, the temperatures  $T_{\text{qp}}$  and  $T_{\text{ph}}$  can decouple and the two subsystems can be in different temperatures, and eventually e-ph interaction is dominated by other relaxation processes. As the interaction is also sensitive to the electronic spectrum, it is modified by superconductivity. [119, 103, 121] Below we discuss what this results to in the spin-split case.

The collision integral for electron-phonon processes in a spin-split superconductor was discussed in Ref. [122] and can be obtained from the self-energies described in Eq. (41) [123]. The overall collision integral entering the kinetic equations [Keldysh part of Eq. (8)] is obtained from a commutator between the self-energy and Green's function,  $\check{I}_{\text{eph}} = [\check{\Sigma}_{\text{eph}}, \hat{g}]^K$ . This is still a Nambu-spin matrix, its different matrix components describe the relaxation of the different nonequilibrium modes. Electron-phonon interaction causes inelastic scattering of quasiparticles, which means that energy flow between quasiparticles and phonons becomes possible. That process is described by the collision integral  $I_L \equiv \text{Tr}[\hat{I}_{\text{eph}}]/8$ . Also the other matrix components of the collision integral

are in general non-vanishing; for example the component  $\text{Tr}[\tau_3 \hat{I}_{\text{eph}}]$  affecting  $f_T$  is detailed in [124]. However, since electron-phonon interaction conserves charge and spin, the energy integrals of  $\text{Tr}[\tau_3 \hat{I}_{\text{eph}}]$  and  $\text{Tr}[\sigma_3 \hat{I}_{\text{eph}}]$  vanish (see Appendix A). The remaining component  $\text{Tr}[\tau_3 \sigma_3 \hat{I}_{\text{eph}}]$  describes the relaxation of the difference in the thermal energies of electrons with opposite spins due to electron-phonon interaction [125]. In the following, we only concentrate on energy relaxation. Substituting the self-energy (41) in the equation for the collision integral and assuming that  $\check{f} = f_L \check{1}$  we can write

$$I_L = \frac{g_{\text{eph}}}{4} \int_{-\infty}^{\infty} d\omega \omega |\omega| \text{Tr}[\hat{g}^{RA}(\varepsilon) \hat{g}^{RA}(\varepsilon + \omega)] \times \left\{ f_L(\varepsilon) f_L(\varepsilon + \omega) - 1 - \coth\left(\frac{\omega}{2k_B T_{\text{ph}}}\right) [f_L(\varepsilon) - f_L(\varepsilon + \omega)] \right\}. \quad (42)$$

Typically this collision integral is used to calculate the total heat current  $\dot{Q}_{\text{eph}} = 2\nu_F \Omega \int d\varepsilon \varepsilon I_L(\varepsilon)$  between the electron and phonon systems in a volume  $\Omega$ . Assuming that the electron system resides in temperature  $T_{\text{qp}}$ , we have  $f_L = \tanh[\varepsilon/(2k_B T_{\text{qp}})]$  and thus the heat current is [126, 127],

$$\dot{Q}_{\text{eph}} = \frac{\Sigma \Omega}{96\zeta(5)k_B^5} \int_{-\infty}^{\infty} d\varepsilon \varepsilon \int_{-\infty}^{\infty} d\omega \omega |\omega| L_{\varepsilon, \varepsilon + \omega} \times \left\{ \coth\left(\frac{\omega}{2k_B T_{\text{ph}}}\right) \times \left[ \tanh\left(\frac{\varepsilon + \omega}{2k_B T_{\text{qp}}}\right) - \tanh\left(\frac{\varepsilon}{2k_B T_{\text{qp}}}\right) \right] + \tanh\left(\frac{\varepsilon}{2k_B T_{\text{qp}}}\right) \tanh\left(\frac{\varepsilon + \omega}{2k_B T_{\text{qp}}}\right) - 1 \right\}. \quad (43)$$

Here  $\Sigma = 3072\zeta(5)\nu_F k_B^5 g_{\text{eph}}$  describes the materials dependent magnitude of the electron-phonon coupling (see tabulated values in [128]) typically used for heat flow, and  $\zeta(x)$  is the Riemann zeta function. The kernel  $L_{E, E'}$  depends on the spin-splitting field, as it is

$$L_{\varepsilon, \varepsilon'} = \frac{1}{2} \sum_{\sigma=\pm} N_{\sigma}(\varepsilon) N_{\sigma}(\varepsilon') - F_{\sigma}(\varepsilon) F_{\sigma}(\varepsilon') = \frac{1}{2} \sum_{\sigma=\pm} N_{\sigma}(\varepsilon) N_{\sigma}(\varepsilon') \left[ 1 - \frac{\Delta^2(T_{\text{qp}})}{(\varepsilon + \sigma h)(\varepsilon' + \sigma h)} \right], \quad (44)$$

where  $N_{\sigma}(\varepsilon) = \text{Re}(g_{03} + \sigma g_{33})/2$  is the density of states for electrons with spin  $\sigma$  and  $F_{\sigma} = \text{Re}(g_{01} + \sigma g_{31})/2$  is the anomalous function for spin  $\sigma$  (see Eq. (15) and below it). The latter formula applies in the absence of spin-flip or spin-orbit scattering.

Strictly speaking, Eq. (43) requires two conditions to be met: (i) A well-defined local quasiparticle temperature that may deviate from the phonon temperature. In other words, the quasiparticles should first equilibrate between

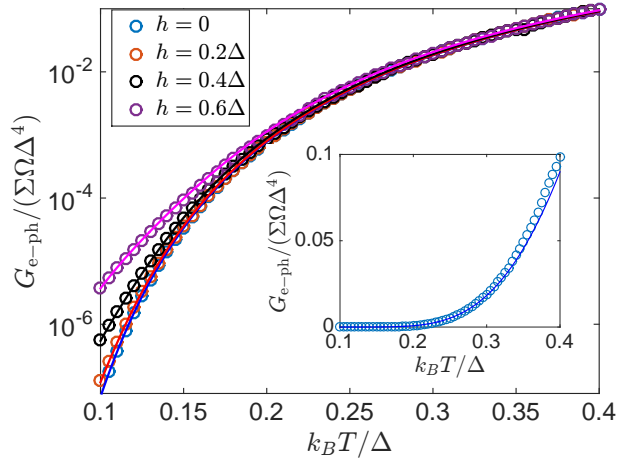


Figure 9: Electron-phonon heat conductance in a spin-split superconductor. Circles show the numerical evaluation based on the linearization of Eq. (43), whereas the lines are from Eq. (46). Note that the vertical axis in the main figure is in a log scale, whereas the inset shows a linear scale for  $h = 0$ . On the linear scale the effects from non-vanishing  $h$  are not visible.

themselves. (ii) In the presence of a spin-splitting field, also spin imbalance affects the quasiparticle-phonon heat flow [122, 123]. Neglecting it therefore requires that the spin relaxation rate exceeds the injection rate causing the out-of-equilibrium situation.<sup>4</sup>

In the general case Eq. (43) needs to be evaluated numerically. However, we may consider two limiting cases. In a normal metal  $\Delta = 0$  implies  $L_{\varepsilon,\varepsilon'} = 1$ . In that case the heat current between the two systems becomes [129]

$$\dot{Q}_{\text{eph}} = \Sigma\Omega(T_{\text{qp}}^5 - T_{\text{ph}}^5). \quad (45)$$

Another tractable limit is that of linear response, where  $T_{\text{qp}} = T_{\text{ph}} + \Delta T$ ,  $\Delta T \ll T_{\text{ph}} \equiv T$ . If moreover  $k_B T \ll \Delta - h$ ,  $\dot{Q}_{\text{eph}} = G_{\text{ph}}\Delta T$  with [33]

$$G_{\text{ph}} \approx \frac{\Sigma\Omega T^4}{96\zeta(5)} \left[ f_1\left(\frac{1}{\tilde{\Delta}}\right) \cosh \tilde{h} e^{-\tilde{\Delta}} + \pi \tilde{\Delta}^5 f_2\left(\frac{1}{\tilde{\Delta}}\right) e^{-2\tilde{\Delta}} \right], \quad (46)$$

where  $\tilde{\Delta} = \Delta/k_B T$ ,  $\tilde{h} = h/k_B T$ , and  $f_1(x) = \sum_{n=0}^3 C_n x^n$ ,  $f_2(x) = \sum_{n=0}^2 B_n x^n$ ,  $C_0 \approx 440$ ,  $C_1 \approx 500$ ,  $C_2 \approx 1400$ ,  $C_3 \approx 4700$ ,  $B_0 = 64$ ,  $B_1 = 144$ ,  $B_2 = 258$ . The two terms in Eq. (46) describe scattering and recombination processes, respectively. Equation (46) is compared to the exact result in Fig. 9. The recombination process, whose heat conductance is almost independent of the

<sup>4</sup>Note that strictly speaking one should then include this spin relaxation into the kernel  $L_{E,E'}$  as spin relaxation affects the spectral functions, see Fig. 4. The relevant scales for the two effects differ, however, as the kernel is significantly modified only when  $\hbar/\tau_{sn}$  is not very much weaker than  $\Delta$ . This is further quantified in Sec. 5.5.

spin splitting (as long as  $\hbar \ll \Delta$ ), dominates at high temperatures, whereas the two become of the same order of magnitude for  $T \approx 0.1\Delta$ . Note that the exponential suppression of the electron-phonon heat conductance  $\sim e^{-\Delta/T}$  at low temperatures does not directly make it irrelevant in a superconductor, because any effect related to quasiparticles contains such exponential terms due to the gap in the superconducting density of states. However, as lowering the temperature reduces the phase space available for acoustic phonons, also the prefactor of the exponential becomes small low temperatures. Thus, at very low temperatures quasiparticles decouple from phonons, and other heat conduction mechanisms become relevant.

### 3.3.2. Particle-particle collisions

The particle-particle collision integrals generally reflect symmetries and conservation laws of the electron system. Below, we only point out conservation laws that a consistent formulation of the collision integrals must imply in a system involving collinear magnetizations. The conservation of charge, spin, and overall energy by spin-rotation symmetric scattering within the particle system can be expressed as:

$$\int d\varepsilon \text{Tr}[\tau_3 \sigma_0 \hat{I}_{ee}] = 0 \quad (47a)$$

$$\int d\varepsilon \text{Tr}[\tau_0 \sigma_3 \hat{I}_{ee}] = 0 \quad (47b)$$

$$\int d\varepsilon \varepsilon \text{Tr}[\tau_0 \sigma_0 \hat{I}_{ee}] = 0. \quad (47c)$$

The spin energy, involving the component  $\varepsilon \tau_3 \sigma_3$  of the collision integral, is generally not conserved in electron-electron collisions, because electrons with opposite spins can exchange energy [125]. The specific forms for  $I_{ee}$  for superfluids have been discussed in [119, 103, 120], however, typically in the absence of spin splitting of the spectrum.

The above conservation laws are relevant in terms of studying what happens in the limit of strong electron-electron scattering. In that case, the usually assumed model is that the quasiparticle distribution functions tend to equilibrium forms, but retaining some effective temperature and a spin-dependent chemical potential. This *quasiequilibrium* limit (without spin accumulation) is often used in analyzing heat transport in superconductors driven out of equilibrium (for example, see [130]).

### 3.4. Description of hybrid interfaces

The spectral current density (19) appearing in the kinetic equation is defined in the bulk of a superconductor (S) or a normal metal (N). In addition, we need a description of interfaces between different materials in order to model transport in hybrid structures. At such interfaces, potentials and materials parameters vary over atomic distances, and therefore they cannot directly be described by quasiclassical equations that are valid only when changes occur over distances

much larger than  $\lambda_F$ . Rather, such interfaces are included in the theoretical description via the derivation of suitable boundary conditions for the Green's functions. This was first done in Ref. [131], and later extended in Refs. [132, 133, 134]. Magnetic interfaces were discussed in Ref. [14] for the S/FI case and extended to metallic interfaces and general cases in Refs. [135, 136, 137, 29, 138].

To get a qualitative understanding of the phenomena related with spin-polarized tunneling into superconductors, we consider below low-transmissive interfaces between superconductors and normal or magnetic leads, using the description in Ref. [137]. Fixing the  $z$  direction in the polarization direction of the interface, the transmission through it can be described by the tunneling matrix  $\hat{\Gamma} = t\tau_3 + u\sigma_3$ . It is defined through the normalized transparencies satisfying  $t^2 + u^2 = 1$  and determining the interface polarization via  $2ut = P$ . The possible non-collinearity between the interface and the bulk magnetizations can be described by introducing rotation matrices in spin space. We assume that this interface connects a normal-metal electrode with bulk Green's function  $\check{g}_N$  with a spin-split superconductor with GF  $\check{g}$ . The boundary condition gives an expression for the matrix current density through the interface in terms of  $\hat{\Gamma}$ ,  $\check{g}_N$  and  $\check{g}$ :

$$\check{g}\nabla_k\check{g} = -\frac{1}{R_{\square}\sigma_N} \left[ \hat{\Gamma}\check{g}_N\hat{\Gamma}^\dagger, \check{g} \right], \quad (48)$$

where  $R_{\square}$  characterizes the spin-averaged barrier resistance per unit area. Its precise microscopic definition is given in Refs. [137, 138]. In experiments it is usually used as a fitting parameter. Equation (48) is valid for an arbitrary spin polarization  $P \in [-1, 1]$  of the interface. From this condition and Eqs. (29–32) we obtain the spectral current densities through spin-polarized barriers as

$$I_{ab} = -\frac{1}{16e^2R_{\square}} \text{Tr}\tau_b\sigma_a \left[ \hat{\Gamma}\check{g}_N\hat{\Gamma}^\dagger, \check{g} \right]^K. \quad (49)$$

The normal electrode Green's function  $\check{g}_N$  is defined by  $\hat{g}_N^{R(A)} = \pm\sigma_0\tau_3$  and  $\hat{g}_N^K = 2\tau_3\hat{f}^{(N)}$ , where  $f^{(N)}$  is the distribution function of the normal metal. The boundary conditions for both spectral GF ( $R$ ) and distribution functions ( $K$ ) are then given by the continuity of the matrix current density,  $n_k j_{kb}^a = I_{ab}$ , where the tunneling current  $I_{ab}$  and bulk current  $j_{kb}^a$  are provided by Eqs. (49) and (19), respectively, and  $n_k$  are the components of the unit vector normal to the interface. For small enough junctions, the approximate conservation of matrix current at short distances implied by Eq. (8) [134] allows neglecting the precise 3D structure of the junction. Hence, in quasi-1D problems, the boundary condition can be integrated over the cross-sectional areas of the wire  $A$  and tunnel interface  $A_T$  and written in the form  $Aj_{1D,b}^a = A_T I_{ab}$ .

Low effective transmissivity of interfaces, which corresponds to a large interface resistance (tunneling limit), also allows for further simplified approximations to be made in the description of nonequilibrium effects. In such a case, changes in the spectrum due to the coupling can be neglected, and the probability for Andreev reflection [83] vanishes. In the lowest order in transmissivity,



we can also assume the electrodes to be in local thermal equilibrium. If, in addition,  $P = 0$ , the charge current between two electrodes is given by the usual tunneling expression Eq. (3) with  $G_T = A_T/R_{\square}$ . In Sec. 4 we describe the more general limit of an arbitrary  $P$ , and the different components of the spectral current.

It is worth emphasizing that the boundary condition, Eq. (48), when combined with the quasiclassical equations, allows for the description of effects which are beyond the quasiclassical limit and that involve strong ferromagnets with large spin polarization [139, 140].

### 3.5. Free energy

The quasiclassical approach can be used to describe the collapse of superconductivity caused by an applied exchange field, including the part of the parameter space where a first-order phase transition occurs. The main physical features of this are discussed in Sec. 2.3. In particular, a necessary condition for the stability of a superconducting state is that the free energy density of the superconducting state compared to the normal state is negative,  $\Omega < 0$ . Below, we express this condition in the quasiclassical framework, neglecting the FFLO state.

The free energy density of a uniform superconductor relative to the normal state can be written in terms of the quasiclassical Green functions, [95, 120, 141, 142, 143]:

$$\Omega[\hat{g}, \hat{\Sigma}] = -\frac{1}{2} \int_0^1 d\lambda \operatorname{Tr}[\hat{\Sigma}(\hat{g}_\lambda[\hat{\Sigma}] - \hat{g})] + \Phi[\hat{g}], \quad (50)$$

where the auxiliary Green function  $\hat{g}_\lambda[\hat{\Sigma}]$  satisfies

$$0 = [\hat{\Lambda} + \lambda\hat{\Sigma}, \hat{g}_\lambda[\hat{\Sigma}]], \quad \hat{g}_\lambda[\hat{\Sigma}]^2 = 1. \quad (51)$$

Here,  $\hat{\Lambda} = (\omega_m + i\mathbf{h} \cdot \boldsymbol{\sigma})\hat{\tau}_3$ , and  $\operatorname{Tr} = \pi TN(0) \sum_{\omega_n} \operatorname{tr}$  contains a Matsubara sum and Nambu and spin traces. Variation of  $\Omega$  vs.  $\hat{g}$  produces the relation  $\delta\Phi[\hat{g}] = -\frac{1}{2} \operatorname{Tr}[\hat{\Sigma}_* \delta\hat{g}]$  between the self-consistent self-energies  $\hat{\Sigma}_*$  and the subtracted quasiclassical  $\Phi$ -functional, with value  $\Phi[\hat{g}_{*,N}] = 0$  in the normal state. Variations and derivatives of  $\hat{g}$  need to retain the condition  $\hat{g}^2 = 1$ , and can generally be expressed in the form  $\delta\hat{g} = \delta\hat{X}\hat{g} - \hat{g}\delta\hat{X}$  for some  $\delta\hat{X}$ . This observation, and making use of Eq. (51), allows the evaluation of the  $\lambda$  integral:

$$\operatorname{Tr}[\hat{\Sigma}(\hat{g}_\lambda[\hat{\Sigma}] - \hat{g})] = \frac{d}{d\lambda} \operatorname{Tr}[(\hat{\Lambda} + \lambda\hat{\Sigma})(\hat{g}_\lambda[\hat{\Sigma}] - \hat{g})]. \quad (52)$$

This enables writing the self-consistent free energy as

$$\Omega[\hat{g}_*, \hat{\Sigma}_*] = \frac{1}{2} \operatorname{Tr}[\hat{\Lambda}(\hat{g}_{\lambda=0} - \hat{g}_{\lambda=1})] + \Phi[\hat{g}_{\lambda=1}]. \quad (53)$$

Note that in a spatially non-uniform situation, gradient terms would complicate the  $\lambda$ -integration. This still allows for including the magnetic orbital effect, given

the approximation in Eq. (8) where Eq. (51) retains its spatially uniform form also in the presence of the vector potential [144]. The  $\Phi$ -functional producing the elastic scattering self-energies discussed in preceding sections reads

$$\begin{aligned} \Phi = & \frac{1}{2} \text{Tr} \left\{ -\frac{1}{2} \Delta [\hat{g}] \hat{g} + \frac{1}{2\tau_{orb}} [1 - (\hat{\tau}_3 \hat{g})^2] \right. \\ & \left. + \frac{1}{16\tau_{so}} [3 - (\boldsymbol{\sigma} \hat{g})^2] + \frac{1}{16\tau_{sf}} [3 - (\boldsymbol{\sigma} \hat{\tau}_3 \hat{g})^2] \right\}, \end{aligned} \quad (54)$$

$$\Delta[\hat{g}] = N(0)V\pi T \sum_{\omega_n} \frac{1}{2} (\hat{\tau}_+ \text{tr}[\hat{\tau}_- \hat{g}] + \hat{\tau}_- \text{tr}[\hat{\tau}_+ \hat{g}]). \quad (55)$$

For  $\tau_{orb}, \tau_{so}, \tau_{sf} \gg \Delta^{-1}$ , direct evaluation yields

$$\Omega = 2\pi T N(0) \text{Re} \sum_{\omega_n > 0} \frac{2w_n \sqrt{w_n^2 + \Delta^2} - 2w_n^2 - \Delta^2}{\sqrt{w_n^2 + \Delta^2}}, \quad (56)$$

where  $w_n = \omega_n + ih$ . At low temperatures  $T/\Delta \ll 1$ ,  $\Omega/N(0) \simeq -\frac{\Delta^2}{2} + h^2 + \frac{\pi^2 T^2}{3}$  [62], producing the Chandrasekhar–Clogston result discussed in Sec. 2.3.

### 3.6. Linear response and generalized Onsager relations

A way of exciting the nonequilibrium modes in superconductors is by injecting electrons from either a voltage or temperature biased metallic lead. In this case, and in the language of Eq. (14), the distribution function in the normal metal is given by  $\hat{f}^{(N)} = f_L^{(N)} + \tau_3 f_T^{(N)}$ , where  $f_{L/T}^{(N)} = [f_{\text{eq}}(\varepsilon - eV) \pm f_{\text{eq}}(\varepsilon + eV)]/2$  is the voltage-biased distribution function in the normal-metal electrode and  $f_{\text{eq}}(\varepsilon) = \tanh(\varepsilon/2T_N)$  is the equilibrium distribution corresponding to the normal-metal temperature  $T_N$ .

In a more general situation, all components of the distribution function, Eq. (14), have to be taken into account. The different components of the spectral current through a tunneling contact between a normal electrode and a superconductor can be derived from the boundary condition in Eq. (49). In the case of collinear magnetizations the relevant components are the spectral charge  $I_{30}$ , energy  $I_{00}$ , spin  $I_{03}$  and spin energy  $I_{33}$  currents. They satisfy

$$\begin{pmatrix} I_{30} \\ I_{00} \\ I_{03} \\ I_{33} \end{pmatrix} = \kappa \begin{pmatrix} N_+ & PN_- & PN_+ & N_- \\ PN_- & N_+ & N_- & PN_+ \\ PN_+ & N_- & N_+ & PN_- \\ N_- & PN_+ & PN_- & N_+ \end{pmatrix} \begin{pmatrix} \tilde{f}_T \\ \tilde{f}_L \\ \tilde{f}_{T3} \\ \tilde{f}_{L3} \end{pmatrix}, \quad (57)$$

where the parameter  $\kappa = 1/(R_{\square} e^2)$  describes the interface transparency and  $\tilde{f}_k = f_k^{(S)} - f_k^{(N)}$  are the differences of the various distribution functions  $\tilde{f}_k = f_k^{(S)} - f_k^{(N)}$ , with  $k = T, L, T3, L3$ , between the superconductor and normal-metal electrodes. The response matrix is here described by the spin polarization  $P$  and the energy-symmetric and energy-antisymmetric parts of the density of states,  $N_{\pm}$  defined in Eqs. (16-17).

Expression (57) is valid for arbitrarily large deviations from the equilibrium state and describes several intriguing effects which come into play in the nonequilibrium situation in junctions combining spin-split superconductors ( $N_- \neq 0$ ) and a spin-polarized injector, modeled by a nonzero spin polarization  $P \neq 0$ . If both  $N_- \neq 0$  and  $P \neq 0$  simultaneously, all the nonequilibrium modes are coupled. In turn, this coupling results in a rich variety of cross-couplings between different potentials and currents.

To illustrate the basic phenomena which can be expected in such a tunneling contact, let us consider the linear response limit. The different components of the distribution function can be described by spin-dependent temperatures<sup>5</sup> and voltages introduced according to Ref. [145]:

$$\begin{pmatrix} \Delta f_T \\ \Delta f_L \\ \Delta f_{T3} \\ \Delta f_{L3} \end{pmatrix} = \frac{\partial f_{\text{eq}}}{\partial \varepsilon} \begin{pmatrix} eV \\ -\Delta T \varepsilon / T \\ eV_s / 2 \\ -\Delta T_s \varepsilon / 2T \end{pmatrix}, \quad (58)$$

where  $V$  and  $\Delta T$  are the voltage and the temperature bias and  $V_s$  and  $\Delta T_s$  the spin-dependent biases.

Integrating Eq. (57) over energy allows us to calculate the total charge  $I = e \int_{-\infty}^{\infty} I_{30} d\varepsilon$ , energy  $\dot{Q} = \int_{-\infty}^{\infty} \varepsilon I_{00} d\varepsilon$ , spin  $I_s = \int_{-\infty}^{\infty} I_{03} d\varepsilon$ , and spin energy  $\dot{Q}_s = \int_{-\infty}^{\infty} \varepsilon I_{33} d\varepsilon$  currents. They are related to the generalized potentials via a  $4 \times 4$  Onsager matrix<sup>6</sup>

$$\begin{pmatrix} I \\ \dot{Q} \\ I_s \\ \dot{Q}_s \end{pmatrix} = \begin{pmatrix} G & P\alpha & PG & \alpha \\ P\alpha & G_{\text{th}}T & \alpha & PG_{\text{th}}T \\ PG & \alpha & G & P\alpha \\ \alpha & PG_{\text{th}}T & P\alpha & G_{\text{th}}T \end{pmatrix} \begin{pmatrix} V \\ -\Delta T/T \\ V_s/2 \\ -\Delta T_s/2T \end{pmatrix}, \quad (59)$$

where the conductance, heat conductance and thermoelectric coefficient are given by

$$G = e^2 \kappa \int_{-\infty}^{\infty} N_+ \frac{\partial f_{\text{eq}}}{\partial \varepsilon} d\varepsilon \quad (60)$$

$$G_{\text{th}} = \frac{\kappa}{T} \int_{-\infty}^{\infty} N_+ \varepsilon^2 \frac{\partial f_{\text{eq}}}{\partial \varepsilon} d\varepsilon \quad (61)$$

$$\alpha = -e\kappa \int_{-\infty}^{\infty} N_- \varepsilon \frac{\partial f_{\text{eq}}}{\partial \varepsilon} d\varepsilon, \quad (62)$$

<sup>5</sup>Note that the notion of spin-dependent temperatures in an out-of-equilibrium setup is questionable [125]. However, for linear response  $\Delta T_s$  can be strictly defined to characterize the nonequilibrium mode via Eq. (58).

<sup>6</sup>In Eq. (59) we assume that the biases are calculated as the shifts of the corresponding quantities in the normal metal with respect to the superconductor and the currents flow from the superconductor into the normal metal.

respectively.<sup>7</sup> In the absence of spin-orbit or spin-flip scattering, these integrals can be evaluated analytically in the limit  $T \ll \Delta - h$ . The results are in Eqs. (147).

Note that the four  $2 \times 2$  quadrants of the response matrix have different time-reversal symmetries: the quadrants on the diagonal are symmetric, whereas the off-diagonal quadrants coupling spin and charge are antisymmetric. This result follows from the fact that  $G$  and  $G_{\text{th}}$  are symmetric whereas  $\alpha$  and  $P$  are antisymmetric in time reversal.

From Eq. (59) we can, for example, study the spin and charge currents created at the SF interface in response to a temperature bias between the normal lead and the superconductor. These are the thermospin and thermoelectric effects. Interestingly, Eq. (59) demonstrates also that the charge current can be induced by the spin-dependent temperature bias  $\Delta T_s$  even without spin-filtering ( $P = 0$ ) but in the presence of a spin-split DOS,  $N_- \neq 0$ . Qualitatively the corresponding non-equilibrium mode  $f_{L3}$  [Fig. 7(e)] can be interpreted as the spin-dependent particle-hole imbalance which produces electric signal due to  $N_- \neq 0$ .

Let us focus on the case where the nonequilibrium state is generated by applying a voltage and a temperature bias to the injecting normal electrode in the absence of spin-dependent potentials,  $\Delta T_s = 0$  and  $V_s = 0$ . If the interface lacks spin polarization,  $P = 0$ , then from Eq. (59) it follows that all currents are decoupled from each other, recovering standard expressions for charge and heat currents in terms of the local electrical and thermal conductances  $I = GV$  and  $\dot{Q} = -G_{\text{th}}\Delta T/T$ . In addition, the remaining block of the Onsager matrix leads to nonzero spin current  $I_s = -\alpha\Delta T/T$  and spin heat current  $\dot{Q}_s = \alpha V$ . From this linear response analysis we can conclude that in a setup consisting of a normal and a spin-split superconducting electrode, a spin current can be generated even in the absence of ferromagnetic electrodes. It is worth mentioning that this thermospin effect leads to a pure spin current  $I_s$  that does not carry electric charge and therefore does not produce Joule heating and Ohmic losses. Clearly this situation is very different from the one occurring in normal metal systems, where spin currents can be generated only by injecting a charge current from a ferromagnet — a process corresponding to the relation  $I_s = PGV$  obtained from Eq. (59).

If  $P \neq 0$  all four types of currents are injected into the superconducting region just by applying the temperature bias  $\Delta T$ . In particular a very large thermoelectric effect can be generated, described by  $I = -P\alpha\Delta T/T$ . This effect is discussed in detail in Sec. 5.

### 3.7. Nonequilibrium effects on the superconducting order parameter

Nonequilibrium also affects the superconducting state by modifying its order parameter. This can be seen by inserting the parametrization (13,14) of the

---

<sup>7</sup>We denote the full thermoelectric coefficient by  $\tilde{\alpha}$  and separate the dependence on the polarization  $P$  in  $\alpha$  to clarify the dependence on  $P$ . Thus, here  $\tilde{\alpha} = P\alpha$ .

nonequilibrium Green's function in Eq. (12):

$$\Delta = \frac{\lambda}{2} \int_{-\Omega_D}^{\Omega_D} d\varepsilon \text{Im} g_{01}^R f_L + \text{Im} g_{31}^R f_{T3} + i(\text{Re} g_{01}^R f_T + \text{Re} g_{31}^R f_{L3}). \quad (63)$$

In equilibrium, only the first term contributes with  $f_L = f_{\text{eq}} = \tanh[\varepsilon/(2T)]$ . The imaginary terms affect the phase of  $\Delta$  and ensure charge current conservation in situations where quasiparticle current is converted to supercurrent (described by the  $R^{ab}$  term in Eq. (18)). In the absence of spin splitting, the nonequilibrium modifications in the size of the gap, described by the first term, are the most relevant. Often such modifications are studied within the Rothwarf–Taylor phenomenological model [146] that neglects the energy dependence of the distribution functions, and rather concentrates on the overall number of quasiparticles. This model was derived under some simplifying assumptions from the full energy dependent kinetic equations in Ref. [147]. It has been used to study the gap suppression due to nonequilibrium injection, see for example Ref. [148]. According to that work, for small changes around equilibrium, such models agree with the predictions of the phenomenological models of Refs. [149, 150]. For large changes, the full kinetic equations with energy dependent distribution functions should be used. An extreme example is given in Ref. [151] describing a voltage-driven transition of a superconducting wire to the normal state.

In the spin-dependent case we need to consider both the effects of spin splitting and the spin-dependent distribution functions describing spin accumulation. Disregarding the terms affecting mostly only the phase of the order parameter, we can also write Eq. (63) as

$$\Delta = 2\lambda \sum_{\sigma=\pm} \int_{-\Omega_D}^{\Omega_D} d\varepsilon \text{Im} F_{\sigma} f_{\sigma}, \quad (64)$$

where  $F_{\sigma} = (g_{01}^R + \sigma g_{31}^R)/2$  and  $f_{\sigma} = (f_L + \sigma f_{T3})/2$ ; the different signs of  $\sigma = \pm$  representing the two spin directions. Ref. [152] went a step further, assuming that the spin accumulation in a superconductor can be described in terms of a simple spin-dependent chemical potential shift  $\mu_s$ , neglecting all other nonequilibrium effects. In that case  $f_{\sigma} = f_{\text{eq}}(\varepsilon - \sigma\mu_s)$ . As a result, by a simple shift of the energy ( $\varepsilon \mapsto \varepsilon + \sigma\mu_s$ ) in Eq. (64),  $\mu_s$  shows up as a shift of the energy of the anomalous function  $F_{\sigma}$  and a small shift of the cutoff  $\Omega_D$ . When  $\Omega_D \gg \mu_s$ , the latter effect can be disregarded, and the net effect of the spin accumulation is the same as that of the spin splitting field, explained in Sec. 2, eventually leading to the suppression of superconductivity. Moreover, in the presence of both spin splitting and spin accumulation, this model shows how in the special case  $h = \mu_s$  spin accumulation can actually lead to the recovery of superconductivity suppressed by spin splitting [153].

This physics can be probed in a FISIF system where a superconducting island or layer is placed between two ferromagnetic electrodes. In this case, the current induced suppression of the superconducting gap should be larger

when the magnetizations of the two ferromagnets are antiparallel than when they are parallel [152]. Only in the previous case the spin accumulation builds up. This effect was measured in Ref. [154]. They indeed found a stronger suppression of superconductivity in the antiparallel configuration. However, they found that the required spin relaxation time for fitting the results to the above theory is much longer than that expected from the normal-state measurements. This discrepancy may result from the somewhat simplified model for the spin accumulation described above.

The suppression of superconducting properties due to spin injection has been measured in the case of high-temperature superconductors [155, 156, 157, 158]. However, these features are typically attributed to the non-conventional character of superconductivity, and are therefore outside the scope of this review.

Besides the superconducting gap, in principle also the induced spin-splitting field can obtain nonequilibrium corrections in the presence of spin injection. The theory for such effects was outlined already in Ref. [75], but to our knowledge such effects have not been thoroughly examined in spin-split superconductors.

### *3.8. Overall strategy to explore the transport and spectral properties of hybrid superconducting systems*

Spectral and transport properties of a diffusive metal or superconductor of mesoscopic size attached to electrodes can be fully described by using the theoretical framework presented in this section. Specifically, one should solve the boundary problem defined by the Keldysh-Usadel equation (8), the normalization condition for  $\check{g}$ , Eq. (9), and the boundary conditions at the interfaces with the electrodes, Eq. (48). Once the Green's functions are determined one can compute the currents and potentials from Eqs. (21-32).

If the system under consideration is in the normal state, the equations for the retarded and advanced GFs are decoupled from each other and from the Keldysh one. The solution of the spectral equations within the quasiclassical approach is trivial and leads to  $\hat{g}^{R(A)} = \pm\tau_3$ . Thus the problem reduces to solving the equation for the distribution functions.

If the system is a superconductor attached to leads, the equations for the retarded and advanced GFs are coupled to the Keldysh component through the self-consistency equation for the superconducting order parameter, Eq. (12). This complication can be overcome if the superconductor and the electrodes are coupled via tunneling junctions. In such a case the spectral properties of the superconductor remain unchanged within the leading order in the interface transmission. This means that retarded and advanced GFs coincide with those of the homogeneous superconductor. In Sec. 4, we concentrate on the case where the normal-state tunnel junction conductance satisfies  $G_T R_{\ell_E} \ll 1$ , where  $R_{\ell_E}$  is the normal-state resistance of a wire with length equal to the energy relaxation length (due to electron-phonon or electron-electron scattering)  $\ell_E$  at the energy around the amplitude of the superconducting gap. On the other hand, in Sec. 5, we mostly consider the cooling of the superconducting island with a starting temperature much below  $T_c$ . In these cases we can disregard the nonequilibrium effects on the energy gap, and can rather use the self-consistent

gap that is calculated from the equilibrium version of self-consistency equation, i.e., Eq. (63), with  $f_L = \tanh[\varepsilon/(2k_B T)]$ .

In most of the discussed examples of this review we follow this approach and use the self-consistent  $\Delta$  calculated in the decoupled spin-split superconductor. From this we obtain the spectral functions of the spin-split superconductor that yield the coefficients of the kinetic equation for the nonequilibrium distribution functions. The latter is obtained from the Keldysh component of Eq. (8). Only in Sec. 4.5, where we study the effect of an ac field on the spectrum of a spin-split superconductor, we compute the self-consistent gap using the nonequilibrium distribution function (see Fig. 20).

Inspection of the different components in Keldysh space of Eq. (8) provides a first insight about the characteristic lengths involved in the different situations. In a superconductor changes of the spectral properties due, for example, to the magnetic proximity effect with a ferromagnetic insulator, occur over the superconducting coherence length  $\xi_s$ . On the other hand, this  $\xi_s$  depends on the temperature, and on the concentration of magnetic and spin-orbit impurities via the self-consistent  $\Delta$ .

Different length scales govern the decay of nonequilibrium components of the distribution function generated, for example, by injecting a current through a contact with an electrode. In this case the characteristic lengths depend on the nature of the excited mode (charge, energy or spin) and the type of relaxation process in the system. The calculation of these characteristic lengths is one of the main goals of Sec. 4. As we show there, the spin splitting plays a crucial role in determining these length scales, since it couples the different nonequilibrium modes, and hence changes the range over which non-local spin and charge signals can be detected.

#### 4. Transport properties of ferromagnetic insulator–superconductor heterostructures

Electrical injection of spins into a superconductor was first studied in Ref. [159]. The injection of an electric current from a F electrode into a superconductor creates not only spin, but also charge imbalance. Moreover, such imbalances relax away from the injection point over distances different from those in the normal state.

In the absence of a spin-splitting field in the superconductor the spin imbalance is decoupled from the other modes. However, in spin-split superconductors charge, spin and energy modes couple with each other. The goal of this section is to describe this coupling, the characteristic relaxation lengths of the different nonequilibrium modes and effects that occur in superconducting structures as a consequence of such coupling.

We start by reviewing experiments on charge and spin injection in superconductors and by summarizing the main theoretical works on spin injection in superconductors with no spin splitting.

Further on, with the help of kinetic equations derived in Sec. 3.1.1 we describe how the spin splitting affects transport properties in S/FI structures,

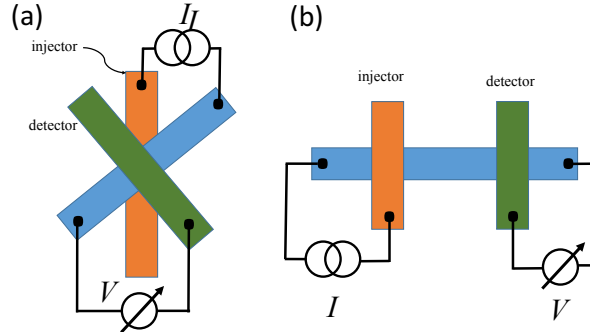


Figure 10: Non-local detection of charge and spin imbalances via transport measurements. Sketch of (a) the original setup [98] for charge imbalance measurement in a superconductor (blue) and (b) a lateral structure used in several more recent experiments for both spin and charge imbalance detection.

and discuss several possible experimental situations both with collinear and non-collinear spin configurations.

#### 4.1. Detection of spin and charge imbalance: non-local transport measurements

Nonequilibrium states in superconducting systems can be experimentally accessed using the non-local transport measurement setup invented in Ref. [98]. The geometry used in that experiment was a vertical structure such as the one sketched in Fig. 10(a). Injection of a current from a normal metal (injector) into the superconductor (blue stripe) generates the charge imbalance mode shown schematically in Fig. 7(b). Qualitatively this mode can be understood as the difference between the chemical potentials of the quasiparticles and the superconducting condensate. This relative shift of chemical potentials induces an electric signal (voltage or current), depending on the measurement setting at the detector electrode [green stripe in Fig. 10(a)]. First experiments demonstrating the charge imbalance induced in superconductors by current injection were performed at temperatures close to the critical temperature  $T_c$  by using vertical samples with large cross sections, such as the one depicted in Fig. 10(a). More recent experiments have allowed for non-local transport measurements at lower temperatures using lateral structures such as the one sketched in Fig. 10(b) [160, 161, 162, 163, 38, 115]. Such structures allow for an accurate measurement of the charge imbalance and nonequilibrium energy mode and their spatial dependence by placing contacts (detectors) at different distances from the injector. For example, in an aluminum wire at 100 mK the charge and energy modes decay over 5 and 10  $\mu\text{m}$ , respectively, as reported in Ref. [164].

Substituting the normal injector by a ferromagnet, the injected current becomes spin polarized and the charge injection is accompanied by a spin injection into the superconductor. The nonequilibrium charge and spin relax over different lengths. When the superconductor shown by the blue wire in Fig. 10b is in the normal state, charge accumulation is negligible at the detector and



only a spin imbalance contributes to the nonlocal signal. The nonequilibrium spin density induced at the interface is polarized in the direction of the injector's magnetization and it diffuses into the normal wire over the spin-relaxation length, which can be several hundreds of nanometers. The spin accumulation can be detected by measuring the non-local voltage between a ferromagnetic detector and the N wire.

First measurement of the nonequilibrium spin accumulation was reported in Ref. [101] on a single-crystal aluminum bar at temperatures below 77 K. This pioneering experiment did not only demonstrate the spin accumulation associated with the injection from a ferromagnetic electrode, but also the coherent spin precession, the Hanle effect, that occurs when an external magnetic field non-collinear with the injector magnetization is applied. Later these effects have been reported at room temperature in Al-based nanostructures in Refs. [165, 166]. Since then, electrical injection of spins have been used in several experiments on metallic spintronics devices, for example for the direct detection of the spin Hall effect in metallic structures [167], electronic spin transport in graphene [168], and modulation of the spin density in metal/ferromagnetic insulator bilayers [169, 170].

In the superconducting state the situation drastically changes, as reported in several experiments on lateral superconducting structures with ferromagnetic electrodes. In contrast to the charge imbalance, which has been well understood since the 1980s, spin injection and accumulation in superconductors is a more recent research line. In 1990 Kivelson [171] suggested that charge and spin should exhibit different relaxation times in superconductors, leading to the possibility of separating charge and spin transport. Also Ref. [172] studied the spin injection from a ferromagnet to a bulk superconductor and found theoretically that, while the charge imbalance survives only within the field penetration length from the surface, the spin imbalance may also exist in the bulk. However, early experiments measuring spin diffusion length in Nb did not show any evidence of such a long-range spin signal [173, 174]. Thus the possibility of having strongly different relaxation scales for spin accumulation and charge imbalance in superconducting state was not confirmed at that time.

More recently, clearer insight into the spin and charge modes has been obtained in experiments using lateral nanostructures with ferromagnetic injectors and detectors [160, 175, 176, 31, 177, 163, 42, 115, 38, 154]. First, the decrease of spin relaxation length in the superconducting state as compared to the normal one has been observed [115] by measuring the non-local spin-dependent resistances. Later, by applying the external spin-splitting field to the superconducting wire it has been possible to prove experimentally the charge-spin separation [32]. A detailed overview of the recent experiments on charge, energy and spin imbalance in superconductors can be found in the recent topical reviews in Refs. [32, 178].

In order to describe theoretically the different modes excited in experiments on lateral S/F structures, it is convenient to use the generalized quasiclassical model introduced in Sec. 3.1. First theoretical works on spin injection into mesoscopic superconductors [118, 179] addressed the question of how spin re-

laxation changes in the superconducting state and how these changes depend on the spin relaxation mechanism. These works pointed out that in the presence of spin-polarized injected currents additional spin-resolved components of the distribution function may appear. The main conclusion of Refs. [118, 179] was that the spin-relaxation length changes significantly in the superconducting state and depends on the energy of the injected quasiparticles. In particular, it has been shown that for electrons with energy close to the superconducting gap the spin relaxation length can decrease in agreement with the experiment [115]. However, two important features observed in subsequent studies of spin transport in superconductors with spin-splitting field could not be understood in terms of that theory. One intriguing observation was the drastic increase of the spin accumulation length in the superconducting state as compared to the normal one [38, 31, 163]. In addition, it has been observed that spin accumulation in such a setup can be created by the current injection from a non-magnetic electrode [163].

As we discuss in this section, to explain these two observations we need to use the kinetic theory which takes into account the modification of the quasiparticle spectrum due to the spin splitting. If it is caused by the Zeeman effect from the external magnetic field, it is also important to take into account the orbital depairing effect which leads to the suppression of superconductivity. Recent works showed that such a modification of the spectrum of the superconductor leads to an intriguing coupling between the nonequilibrium modes in a superconductor [180, 35, 123, 37, 36, 181]. The effect of this coupling between the modes on the transport properties of a multi-terminal superconducting structure can be theoretically explored with the quasiclassical formalism developed in Sec. 3. Here we review these theory works and provide a quantitative explanation of the long-range spin accumulation detected in multi-terminal superconducting devices.

#### *4.2. Nonequilibrium properties of a superconductor with spin splitting*

Spin accumulation and transport in superconductors has been considered in a number of theory papers [182, 118, 179, 183, 180, 35, 123, 37, 36, 181]. Here we follow the approach developed in [35] that enables the description of all non-equilibrium modes, the effect of the spin-splitting field, and the various relaxation mechanisms. As discussed in Sec. 3.1, nonequilibrium conditions lead to the excitation of charge, energy and spin modes in superconducting systems. These modes are related to the different components of the distribution function introduced in Eq. (14). A prototypical experimental geometry to reveal the different nonequilibrium modes in superconductors is the lateral structure shown in Fig. 11. It consists of a mesoscopic superconductor attached to four electrodes. One of them serves as an injector for the current, whereas another one is used as a detector. The other two electrodes serve as separate charge current sinks, allowing for such a non-local measurement.

We assume first that both electrodes, injector and detector, are ferromag-

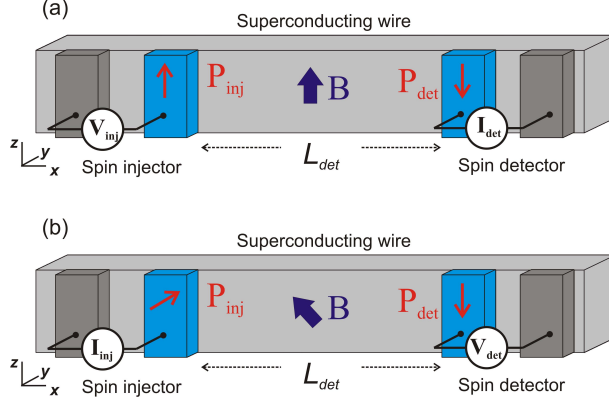


Figure 11: Schematic view of the setup for nonlocal transport measurements. (a) Collinear configuration where the polarizations of the magnetic contacts are collinear with the magnetic field,  $\mathbf{P}_{inj} \parallel \mathbf{P}_{det} \parallel \mathbf{B}$ . The non-local conductance  $g_{nl} = dI_{det}/dV_{inj}$  is measured. (b) General non-collinear case with the magnetic field having finite transverse component with respect to the polarizations  $\mathbf{P}_{inj}, \mathbf{P}_{det}$ . The non-local voltage  $V_{det}$  is measured in the absence of the current in the detector electrode,  $I_{det} = 0$ . The latter detection scheme enhances the spin signal in the superconducting state, see discussion in the text.

netic and that their magnetizations are collinear as in Fig.11a

$$\mathbf{P}_{inj} \parallel \mathbf{B} \parallel \mathbf{P}_{det} .$$

The tunnelling current at the detector can be expressed through the charge imbalance  $\mu$  and spin accumulation  $\mu_z$  (25,26)

$$I_{det} = (\mu + P_{det}\mu_z)/R_{det}, \quad (65)$$

where  $R_{det} = R_{\square}/A$  is the detector interface resistance in the normal state, and  $A$  is the cross-sectional area of the detector. Here we consider collinear magnetizations along the  $z$ -axis and therefore only the spin components  $f_{T3}$  and  $f_{L3}$  enter these expressions. A non-collinear case is discussed in Sec. 4.3.

If the current through the detector is measured at zero bias  $V_{det} = 0$ , then the nonlocal differential conductance is defined as

$$g_{nl} = \frac{dI_{det}}{dV_{inj}} . \quad (66)$$

This quantity provides information about the modes that, being excited at the injector via the injected current, reach the detector by diffusing in the superconducting wire. The nonlocal conductance  $g_{nl}$  depends on the distance  $L_{det}$  between the injector and the detector. This dependence reveals the characteristic length scale over which the modes relax and in practice it is measured by using several detectors at different distances to the injector.

According to Eqs. (25,26) the non-local current is determined, in the most general case, by the contributions of all four non-equilibrium modes shown

schematically in Fig. 7. Here the quantities  $\mu$  and  $\mu_z$  characterize arbitrary nonequilibrium states of the superconducting wire, including those that cannot be described by the effective potentials  $V$ ,  $\Delta T$ ,  $V_s$  and  $\Delta T_s$  introduced in Sec. 3.6. However, if we restrict the analysis to linear response then Eq. (65) reduces to the expression for the current obtained from Eq. (59) with  $P = P_{\text{det}}$ ,  $\kappa = A/(e^2 R_{\text{det}})$ ,  $\mu = R_{\text{det}}(\alpha \Delta T_s/2T - GV)$  and  $\mu_z = R_{\text{det}}(\alpha \Delta T/T - GV_s/2)$ .

When the distance between the injector and detector electrodes is much larger than the charge imbalance relaxation length, the contribution of  $\mu$  to the detected current can be neglected [36, 181]. In the absence of spin splitting  $h = 0$  ( $N_- = 0$ ), the spin-dependent part of  $I_{\text{det}}$  is determined only by the  $f_{T3}$  mode related to the spin-dependent chemical potential shift [182, 118, 179] (see Eq. (58)). In this case in the linear response regime and at low temperatures  $|eV_s|, T \ll \Delta$ , the spin accumulation generated by a spin-dependent chemical potential shift  $\delta\mu = eV_s/2$  is exponentially small. This can be seen from the first term on the r.h.s of Eq. (26), by noticing that if the energy gap  $\Delta$  is non-zero then  $N_+(|\varepsilon| < \Delta) = 0$ . In this case the nonequilibrium spin state is described by  $f_{T3} = (\partial f_{\text{eq}}/\partial \varepsilon)eV_s/2$  and hence the spin accumulation is given by  $\mu_z = -(eV_s/2) \int_{\Delta}^{\infty} d\varepsilon N_+(\partial f_{\text{eq}}/\partial \varepsilon)$  so that  $\mu_z \propto e^{-\Delta/T}$  at  $T \ll \Delta$ .

The non-trivial behaviour of spin accumulation  $\mu_z$  is determined by the second term in the r.h.s of Eq. (26). It appears when the spin splitting becomes non-zero, i.e.,  $h \neq 0$ ,  $N_- \neq 0$ . This term allows for the spin-charge separation which explains experiments in [38, 31, 163]. On the qualitative level the physics related to this term can be described as follows. When  $N_- \neq 0$  the spin accumulation has a contribution from energy nonequilibrium mode  $f_L$  shown schematically in Fig. 7. This mode, once excited, can only relax via inelastic processes, especially mediated by the electron-phonon interaction. At low temperatures in metals the electron-phonon relaxation can be much slower than the spin decay in the normal state. This mechanism explains the long-range spin accumulation observed in experiments. Since the nonequilibrium mode  $f_L$  can be generated in particular by the temperature rise in the quasiparticle system, the long-range non-local spin signals can be explained in terms of the thermo-spin effect. Its essence is the generation of spin accumulation by heating up quasiparticles in the superconductor. In practice this effective heating can be achieved with the help of the voltage-biased tunnel junction which can inject the nonequilibrium quasiparticles with energies larger than the gap into the superconducting wire [180, 35, 123, 37, 36, 181]. Such a mechanism does not require injector electrode to be spin-polarized. Thus the spin accumulation can be generated by an injected current even from a non-ferromagnetic electrode. This can be seen from the second term in the r.h.s. of Eq. (26), which shows that  $\mu_z$  can be non-zero even if the injection occurs from a non-magnetic lead, provided that  $N_- \neq 0$ , i.e., if the superconductor shows a spin-split spectrum [163].

In addition, with the help of the qualitative picture described above one can understand the antisymmetric shape of the non-local spin signal in  $g_{nl}$  with respect to  $V_{\text{inj}}$  observed in the experiments [38, 31, 163]. The origin of such a  $g_{nl}(V_{\text{inj}})$  dependence is again the thermo-spin effect in the superconductor

with  $N_- \neq 0$ . The spin accumulation generated in this way is an even function of the bias voltage at the injector electrode  $\mu_z(V_{\text{inj}}) = \mu_z(-V_{\text{inj}})$  because the effective heating of quasiparticles is not sensitive to the sign of  $V_{\text{inj}}$ . Hence the non-local spin signal (66), that is a derivative of  $\mu_z$ , is an odd function  $g_{nl}(V_{\text{inj}}) = -g_{nl}(-V_{\text{inj}})$ . This is also what has been observed in the experiments [162].

#### 4.2.1. Relaxation of the nonequilibrium modes

To provide a quantitative description of the effects discussed in the previous section, we now calculate the potentials  $\mu$ ,  $\mu_z$  and the non-local conductance by using the kinetic equations for superconductors with spin-split subbands introduced in Sec. 3.1.1.

Our starting point is the general Usadel equation (8). By assuming that the transparencies of the interfaces between the superconductor and the electrodes are small we can neglect the changes of the spectral properties of the superconductor due to the proximity effect. This means that the retarded and advanced GFs correspond to the homogeneous superconducting state (*cf.* Sec. 2), and we only have to focus on the calculation of the components of the distribution function, Eq. (14). In this discussion we disregard inelastic relaxation, assuming the corresponding scattering length to far exceed the spin relaxation length. We thus set  $\tilde{\Sigma}_{in} = 0$ .

In the collinear situation considered here only the four components of the distribution function entering Eqs. (25-26) are finite. In a homogeneous superconductor, for example in the absence of the supercurrent they are pairwise coupled. The expressions for different currents can be obtained by combining Eqs. (13,14,18,19). It is instructive to represent these expressions in a matrix form

$$\begin{pmatrix} \mathbf{j}_e \\ \mathbf{j}_s \\ \mathbf{j}_c \\ \mathbf{j}_{se} \end{pmatrix} = \begin{pmatrix} D_L \nabla & D_{T3} \nabla & 0 & 0 \\ D_{T3} \nabla & D_L \nabla & 0 & 0 \\ 0 & 0 & D_T \nabla & D_{L3} \nabla \\ 0 & 0 & D_{L3} \nabla & D_T \nabla \end{pmatrix} \begin{pmatrix} f_L \\ f_{T3} \\ f_T \\ f_{L3} \end{pmatrix}. \quad (67)$$

Here, following the notation in Eq. (18),  $\mathbf{j}_c \cdot \mathbf{e}_k = D j_{k3}^0$ ,  $\mathbf{j}_{se} \cdot \mathbf{e}_k = D j_{k3}^3$ ,  $\mathbf{j}_e \cdot \mathbf{e}_k = D j_{k0}^0$  and  $\mathbf{j}_s \cdot \mathbf{e}_k = D j_{k0}^3$  where  $\mathbf{e}_k$  is the unit vector in direction  $k = x, y, z$ . The components  $f_L$  and  $f_{T3}$  determine the spectral energy  $\mathbf{j}_e$  and spin  $\mathbf{j}_s$  currents, whereas the components  $f_T$  and  $f_{L3}$  determine the spectral charge  $\mathbf{j}_c$  and spin-heat  $\mathbf{j}_{se}$  currents. The spectral coefficients appearing here are defined in terms of the spectral GFs discussed in Eq. (15), and the diffusion coefficient  $D$

$$\mathcal{D}_T = \frac{D}{2} (1 + |g_{01}|^2 + |g_{03}|^2 + |g_{31}|^2 + |g_{33}|^2) \quad (68)$$

$$\mathcal{D}_{L3} = D \text{Re}(g_{03} g_{33}^* + g_{01} g_{31}^*) \quad (69)$$

$$\mathcal{D}_L = \frac{D}{2} (1 - |g_{01}|^2 + |g_{03}|^2 - |g_{31}|^2 + |g_{33}|^2) \quad (70)$$

$$\mathcal{D}_{T3} = D \text{Re}(g_{03} g_{33}^* - g_{01} g_{31}^*). \quad (71)$$

According to Eq. (8) the modes  $f_T$  and  $f_{L3}$  satisfy the diffusion equations

$$\nabla \cdot \mathbf{j}_c = R_T f_T + R_{L3} f_{L3} \quad (72)$$

$$\nabla \cdot \mathbf{j}_{se} = (R_T + S_{L3}) f_{L3} + R_{L3} f_T, \quad (73)$$

where  $R_T = 2\Delta \text{Reg}_{01}$ ,  $R_{L3} = 2\Delta \text{Reg}_{31}$  describe the coupling of the quasi-particles to the superconducting condensate, and the collision integral for spin relaxation  $S_{L3}$  is given by Eq. (38). They are hence of the form of spectral current conservation equations, except for the source/sink terms provided by the collision integrals.

The kinetic equations (72,73) are supplemented by the boundary conditions at the injector electrode given by the second and the third rows on the matrix of Eq. (57).

On the other hand, according to Eq.(67) the second pair of modes,  $f_L, f_{T3}$ , determines the energy and spin currents  $\mathbf{j}_e$  and  $\mathbf{j}_s$ , respectively. They satisfy the diffusion equations

$$\nabla \cdot \mathbf{j}_e = 0 \quad (74)$$

$$\nabla \cdot \mathbf{j}_s = S_{T3} f_{T3}. \quad (75)$$

Here the spin-relaxation term  $S_{T3}$  is given by Eq. (37). Typical energy dependencies of the kinetic coefficients in Eqs.(72, 73, 74) in the presence of spin splitting and spin-flip relaxation ( $\beta = 1$ ) are shown in Fig. 12.

*Charge and spin-energy modes.* The two systems of diffusion equations (72-73,74-75) describe the coupled transport of spin, charge and heat in superconductors.

We start by solving the system (72,73) describing the coupled charge and spin energy modes. The solution for  $f_T$  and  $f_{L3}$  is a superposition of two exponentially decaying functions

$$\begin{pmatrix} f_T \\ f_{L3} \end{pmatrix} = \sum_{j=1,2} A_j e^{-k_j x} \begin{pmatrix} R_T - \mathcal{D}_L k_j^2 \\ \mathcal{D}_T k_j^2 - R_{L3} \end{pmatrix}, \quad (76)$$

where the coefficients  $A_i$  have to be determined from the boundary conditions. The inverse lengths  $k_{1,2}$  are energy dependent. This dependence is shown in Figs. 13(a-d). Notice that both the charge and the spin-heat imbalance relaxation are nonvanishing for all energies, below and above the gap, due to the magnetic pair breaking effects [97, 105]. In the absence of spin splitting,  $h = 0$ ,  $R_{L3} = \mathcal{D}_{L3} = 0$ , and the charge and spin-energy modes are decoupled [*cf.* Eqs. (72,73)]. Then  $k_1$  and  $k_2$  can be ascribed to the spin energy and charge imbalance relaxation, respectively. The non-zero Zeeman splitting  $h \neq 0$  leads to the coupling of  $f_T$  and  $f_{L3}$ , at low energies. At high energies  $\varepsilon \gg \Delta$  though, when the superconducting correlations become negligible, the decoupled behavior is restored. This can be seen in the asymptotic behavior for  $\varepsilon \rightarrow \infty$  shown in Figs. 13(b,d). In this limit  $k_2 \rightarrow 0$  corresponding to a vanishing charge relaxation, whereas  $k_1 \rightarrow \lambda_{sn}^{-1}$  which is the spin-energy relaxation length in the normal state.

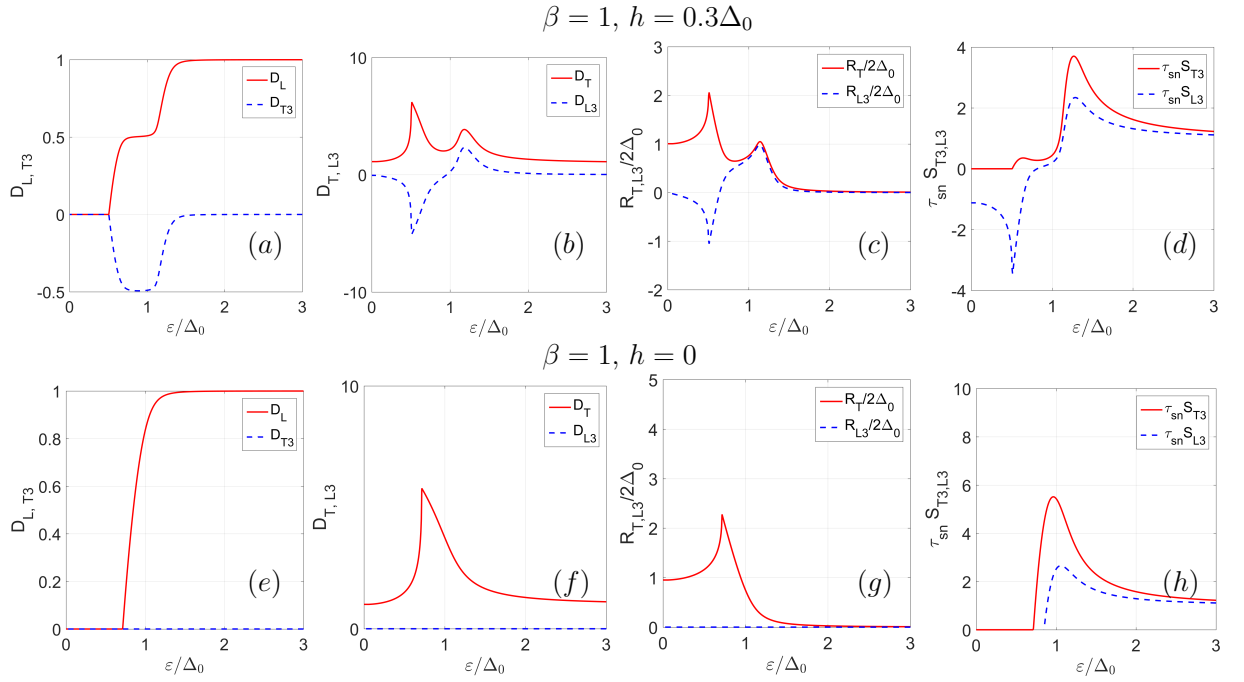


Figure 12: Kinetic coefficients in the presence of Zeeman splitting for  $\beta = 1$ ,  $h = 0.3\Delta_0$  (upper panel) and in the absence of Zeeman splitting  $h = 0$  for the same parameters (lower panel). The normal state spin relaxation rate  $(\tau_{sn}\Delta_0)^{-1} = 0.1$ , temperature  $T = 0.1T_{c0}$ . (a,e) Diffusion coefficients for energy and spin imbalance modes, (b,f) diffusion coefficients for spin energy and charge imbalance modes, (c,g) Andreev reflection-related coefficients  $R_{T,L3}$ , and (d,h) spin relaxation  $S_{L3,T3}$  coefficients.

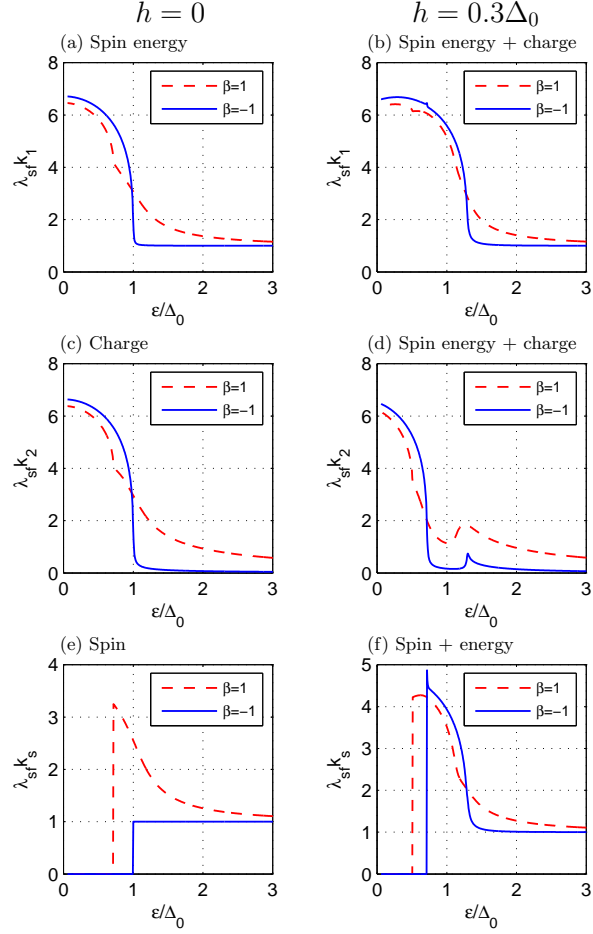


Figure 13: Energy dependence of the inverse length scales  $k_1$ ,  $k_2$  and  $k_s$  for  $h = 0$  (left panels) and  $h = 0.3\Delta_0$  (right panels). In each plot  $\beta = -1; 1$  corresponding to dominating spin-orbit and spin-flip scattering, respectively. The temperature is  $T = 0.1T_{c0}$ , normal-state spin relaxation rate  $(\tau_{sn}\Delta_0)^{-1} = 0.1$ .



*Spin and energy modes.* We now analyze the system of equations (74-75) that describes the coupling between the spin and energy modes, i.e., the components  $f_L$  and  $f_{T3}$  of the distribution function. The solution of the system can be written as the sum of two qualitatively different terms

$$\begin{pmatrix} f_L \\ f_{T3} \end{pmatrix} = B_1 \begin{pmatrix} \mathcal{D}_{T3} \\ -\mathcal{D}_L \end{pmatrix} e^{-k_s x} + B_2 \begin{pmatrix} x - L \\ 0 \end{pmatrix} + \begin{pmatrix} f_{\text{eq}} \\ 0 \end{pmatrix}, \quad (77)$$

with coefficients  $B_j$  determined by the boundary conditions. The first term in (77) describes a decay of the (spectral) spin imbalance with a characteristic length scale  $k_s = \sqrt{S_{T3}\mathcal{D}_L/(\mathcal{D}_L^2 - \mathcal{D}_{T3}^2)}$ . In the absence of a spin-splitting field and depairing mechanisms the expression for  $k_{se}$  yields the energy dependent spin-relaxation length in superconductors obtained in Ref. [179]:  $k_s^{-1} = \lambda_{sn}\sqrt{\varepsilon^2 - \Delta^2}/\sqrt{\varepsilon^2 + \beta\Delta^2}$ . This length is strongly renormalized by superconductivity if the spin-flip scattering rate is nonzero,  $\beta \neq -1$ . A more accurate calculation of  $k_{se}(\varepsilon)$ , including the modification of spectral functions in the superconductor due to the spin relaxation, is shown in Fig. 13(c). We see that  $k_s$  is constant for  $\beta = -1$  and has a pronounced peak near the self-consistent gap edge for  $\beta = 1$ . Note that the spectral gap is reduced by spin-flip scattering to the values smaller than  $\Delta_0$ . Comparing Figs. 13(c,e) one can see that the relaxation lengths of charge imbalance and spin accumulation are very different even in the absence of a spin-splitting field. For example at subgap energies  $k_s < k_2$ . In contrast, for quasiparticles with energies  $\varepsilon \gg \Delta$  the charge relaxation vanishes whereas the spin relaxation remains non-zero. Hence particle injection at voltages  $V_{inj}$  well above the gap leads at large distances from the injector mainly to a charge imbalance.

It is worth noticing that in the presence of a non-zero spin-splitting field the behavior of  $k_s(\varepsilon)$  is very similar for spin-orbit and spin-flip relaxation mechanisms as shown in Fig. 13(d).

The second term in the r.h.s. of Eq. (77). It describes an effective increase of the quasiparticle temperature associated with the  $f_L$  nonequilibrium mode. This mode can only decay via inelastic scattering which is disregarded in the above analysis. In the following we assume the presence of an electrode at a distance  $L$  much larger than the spin relaxation length, and assume that the energy mode relaxes there.

#### 4.2.2. Kinetic equations with supercurrent

The expressions for the current in Eq. (67) and hence the kinetic equations can be modified by driving a supercurrent through the superconducting wire. Its effect can be included by assuming a constant phase gradient  $\nabla\phi$  of the order parameter [184], i.e.,  $\Delta(\mathbf{r}) = |\Delta|e^{i\phi(\mathbf{r})}$ . As a result, two new spectral coefficients appear: the spectral supercurrent  $j_E$  and the spectral spin supercurrent  $j_{Es}$ , defined as  $j_E = D\text{Tr}[\tau_3(\hat{g}^R\nabla\hat{g}^R - \hat{g}^A\nabla\hat{g}^A)]/(8\nabla\phi)$  and  $j_{Es} = D\text{Tr}[\tau_3\sigma_3(\hat{g}^R\nabla\hat{g}^R - \hat{g}^A\nabla\hat{g}^A)]/(8\nabla\phi)$ , respectively. In their presence all distribution function components are coupled so that the spectral currents

appearing in Eqs. (72,73,74,75) read

$$\begin{pmatrix} \mathbf{j}_e \\ \mathbf{j}_s \\ \mathbf{j}_c \\ \mathbf{j}_{se} \end{pmatrix} = \begin{pmatrix} D_L \nabla & D_{T3} \nabla & j_E \nabla \phi & j_{Es} \nabla \phi \\ D_{T3} \nabla & D_L \nabla & j_{Es} \nabla \phi & j_E \nabla \phi \\ j_E \nabla \phi & j_{Es} \nabla \phi & D_T \nabla & D_{L3} \nabla \\ j_{Es} \nabla \phi & j_E \nabla \phi & D_{L3} \nabla & D_T \nabla \end{pmatrix} \begin{pmatrix} f_L \\ f_{T3} \\ f_T \\ f_{L3} \end{pmatrix}. \quad (78)$$

Hence in this case the presence of spin-splitting and supercurrent leads to a coupling between all nonequilibrium modes. This is in contrast to the case without supercurrent when the matrix in Eq. (67) has a block-diagonal form so that the modes are coupled only pairwise.

In the absence of spin splitting, this leads to a coupling between charge and energy modes, and hence for example to the possibility of creating charge imbalance from temperature gradients [185, 186, 187]. For a spin-split superconductor, the supercurrent couples charge and spin modes [184] so that one can be converted into another one. In practice this conversion can be measured by analysing the different symmetry components of the non-local conductance with respect to the injection voltage and the spin polarization of the detector.

Strictly speaking, the assumption of a constant phase gradient together with the excitation of the nonequilibrium modes leads to a non-conserved total (energy integrated) charge current in the setup. Therefore, the non-linear problem of analysing the dynamics of modes for supercurrent needs to be coupled with the self-consistency equation (63), where the presence of the modes  $f_T$  and  $f_{L3}$  affects the phase of the self-consistent order parameter and therefore the phase gradient.

#### 4.2.3. Non-local conductance measurements

In a typical experiment quasiparticles are injected from a normal or a ferromagnetic metal electrode by applying a voltage  $V_{inj}$  between the electrode and the superconductor. In this way the nonequilibrium states described by Eqs. (76,77) can be excited. We determine the coefficients  $A_{1,2}$  and  $B_{1,2}$  using the general boundary conditions (57) for the currents, where the voltage-biased normal electrodes are described by the distribution functions  $f_T^{(N)}(\varepsilon) = [f_{eq}(\varepsilon + V) - f_{eq}(\varepsilon - V)]/2$  and  $f_L^{(N)}(\varepsilon) = [f_{eq}(\varepsilon + V) + f_{eq}(\varepsilon - V)]/2$  while the remaining components are zero,  $f_{L3}^{(N)} = 0$  and  $f_{T3}^{(N)} = 0$ .

The current at the detector, Eq. (65), is obtained by substitution of Eqs. (76,77) into the expressions (25,26) for the chemical potentials. Finally we obtain the non-local conductance from Eq. (66). The result for  $g_{nl}$  as a function of the injecting voltage  $V_{inj}$  is shown in Fig. 14. It reproduces the main features observed in experiments in Refs. [38, 31, 162].

We plot the non-local conductance in three different cases (the three curves in Fig. 14). The blue curve is for a vanishing spin-splitting field and injector polarization. In that case the signal is solely due to charge imbalance. The black curve is with a non-zero spin-splitting field, but vanishing injector polarization, and in the red curve both the spin-splitting field and the injector polarization are non-zero. As discussed below, the former shows the thermally created spin

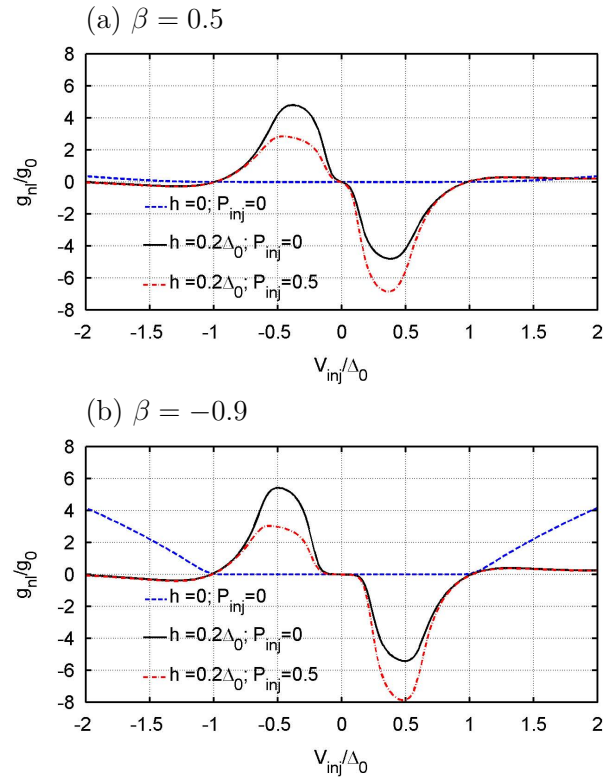


Figure 14: Nonlocal conductance as a function of the injecting voltage,  $g_{nl}(V_{inj})$  for  $\alpha_{orb} = 1.33$ , spin relaxation rate  $(\tau_{sn}T_{c0})^{-1} = 0.2$  and  $T = 0.05 T_{c0}$ , effective inelastic relaxation length  $L = 20\lambda_{sn}$ ,  $L_{det} = 5\lambda_{sn}$  and detector polarization  $P_{det} = -0.5$ . Spin relaxation mechanism is (a) spin-flip dominated  $\beta = 0.5$ ; (b) spin-orbit dominated  $\beta = -0.9$ . The conductance is normalized to  $g_0 = R_{\xi}/(R_{inj}R_{det})$ , where  $R_{\xi} = \xi/(A_s\sigma_N)$  is the normal-state resistance of the wire with length  $\xi$  and cross section  $A_s$ .

accumulation, whereas the latter shows a combination of the thermally and electrically created spin accumulations.

In an experiment where the spin-splitting field is controlled by an external magnetic field, we also need to take into account the orbital depairing effect [Eq. (35)] of the magnetic field in addition to the Zeeman effect. Whereas the latter leads to the coupling of the energy and spin modes, the former affects especially the relaxation of charge imbalance. For the results in Fig. 14, we describe the relative strength of the orbital depairing and the spin-splitting field by setting  $(\tau_{\text{orb}}T_{c0})^{-1} = \alpha_{\text{orb}}(\mu_B B/T_{c0})^2$  and choosing for the dimensionless quantity  $\alpha_{\text{orb}}$  a value close to the experiments in [31].

First, in the absence of a Zeeman field,  $N_- = 0$ , and according to Eqs. (26,66) only the modes  $f_T$  and  $f_{T3}$  contribute to  $g_{nl}$ . In such a case the contribution stemming from the spin accumulation is nonzero only if  $P_{\text{inj}} \neq 0$ , which is the condition to obtain a nonvanishing  $f_{T3}$ . However, this function decays over the spin diffusion length and therefore is negligibly small at the distances  $L_{\text{det}} > \lambda_{sn} = \sqrt{D\tau_{sn}}$  from the injector. Thus, the detected signal in this case is mostly determined by the charge imbalance  $\mu$ . This explains the approximate symmetry with respect to the injecting voltage:  $g_{nl}(V_{\text{inj}}) = g_{nl}(-V_{\text{inj}})$  (blue curves in Fig. 14). The charge imbalance contribution to  $g_{nl}$  grows monotonically when  $|eV_{\text{inj}}| > \Delta_g$ . This behavior is determined by the increase of the charge relaxation scale at high energies,  $k_2^{-1} \rightarrow \infty$  shown in Fig. 13(c).

In the presence of an applied magnetic field the charge relaxation is strongly enhanced due to the orbital depairing. As a result, the charge imbalance background signal is strongly suppressed by an increased  $h$ . On the other hand the spin imbalance contribution stemming from the  $f_L$  mode is large. This term describes heat injection in the presence of a finite spin-splitting field  $h$  and has a long-range behavior. This contribution leads to the large peaks in  $g_{nl}(V_{\text{inj}})$  shown in Fig. 14. The non-linear heating produced by quasiparticles injected at voltages exceeding the energy gap explains the large electric signal observed in the experiments [38, 31, 162]. Notice that the peaks do not have exactly the same form so that  $g_{nl}(V_{\text{inj}}) \neq -g_{nl}(-V_{\text{inj}})$ . The deviation from the perfect antisymmetric form is due to the small but finite injector polarization  $P_{\text{inj}}$ , which modifies the boundary conditions for the spin current.

One important feature shown in Fig. 14 is that the spin polarization peaks exist always in the presence of spin splitting,  $h \neq 0$ , even if the injector electrode is not ferromagnetic,  $P_{\text{inj}} = 0$ . This explains the non-local conductance measurements of Ref. [163] by using a normal metal as injector.

The results summarized in Fig. 14 can have direct applications in the field of spintronics. On the one hand spin accumulation can be created without using ferromagnets as injectors. On the other hand, due to the coupling between the spin and energy mode, the spin signal can be controlled over a very long range. The only requirement for these two features to occur is to use a superconductor with a spin-split DOS due to a Zeeman or an exchange field.

### 4.3. Spin Hanle effect in normal metals and superconductors

In the previous section we study the spin injection and spin accumulation in a superconductor assuming that the magnetization of the injector and the applied field are collinear. We now lift this assumption and consider non-collinear field and magnetizations. This situation has been widely studied in the normal state. The non-collinearity between the external field and the spin of the injected electrons leads to a precession of the latter. This is the spin Hanle effect [101, 165, 166, 169, 188]. This precession can be measured via the non-local conductance in a multi-terminal sample as a function of the applied field.

In order to understand the spin Hanle effect in superconductors it is instructive to first discuss the spin precession in a normal metal within the formalism described above. We then demonstrate that in the superconducting state the spin precession can be either enhanced or suppressed, depending on the spin relaxation mechanism.

#### 4.3.1. Normal-metal non-local spin valve

In the normal state the Usadel equation can be drastically simplified because the retarded and advanced Green's functions do not depend on energy and have the simple form  $\hat{g}^{R(A)} = \pm\tau_3$ . Thus the reduced density of states equals to unity according to Eqs. (16)–(17). It follows from Eq. (13) that the Keldysh component is then proportional to the distribution matrix:  $\hat{g}^K = 2\tau_3\hat{f}$ .

It is then useful to integrate Eq. (8) over energies and take the trace after multiplication with the Pauli matrices. This results in a diffusion equation for the nonequilibrium spin density  $\mathbf{S}$

$$\mathbf{S} = -\frac{\nu_F}{8} \int dE \text{Tr}[\tau_3 \boldsymbol{\sigma} \check{g}^K]$$

given by

$$D\nabla^2 S_a(\mathbf{r}) - i[\boldsymbol{\sigma}\mathbf{h}, \boldsymbol{\sigma}\mathbf{S}(\mathbf{r})]^a = \frac{S_a}{\tau_{sn}}. \quad (79)$$

This is the spin diffusion equation [189, 190, 191] widely used in spintronics. Generalization of this equation in the presence of spin-orbit coupling has been done in several works [192, 193, 194, 195]. Its right hand side describes the effective spin relaxation time defined as  $\tau_{sn}^{-1} = \tau_{so}^{-1} + \tau_{sf}^{-1}$ . The second term on the left hand side describes the torque induced by the external field via the spin splitting field. This torque leads to the spin Hanle effect, studied in the language of quasiclassics in Ref. [196].

Let us consider a lateral spin valve as the one sketched in Fig. 11(b). We assume that a field is applied in the  $x$ -direction whereas the injector and detectors are polarized in the  $z$ -direction. If the width and thickness of the N wire are smaller than the spin relaxation length the problem reduces to a quasi 1D

geometry along the length of the wire. In such a case Eq. (79) leads to two linear coupled equations for the components  $S_{y,z}$ ,

$$\begin{pmatrix} \partial_{xx}^2 - \lambda_{sn}^{-2} & l_h^2 \\ -l_h^2 & \partial_{xx}^2 - \lambda_{sn}^{-2} \end{pmatrix} \begin{pmatrix} S_z \\ S_y \end{pmatrix} = 0,$$

with solutions

$$\begin{aligned} S_z &= Ae^{-\kappa x} + Be^{-\kappa^* x} \\ S_y &= -iAe^{-\kappa x} + iBe^{-\kappa^* x}. \end{aligned}$$

We have defined the spin diffusion length  $\lambda_{sn}^2 = D\tau_{sn}$ , the magnetic length  $l_h^2 = D/h$  and  $\kappa = \lambda_{sn}^{-1} \sqrt{1 + i(\lambda_{sn}/l_h)^2}$ . The coefficients  $A$  and  $B$  have to be determined from the boundary condition, Eq. (48), which in this particular case has the simple form

$$\partial_x S_z|_{x=0} = \frac{\nu_F P V_I}{2R_I \sigma_N}.$$

Here  $V_I$  is the voltage across the injector/N interface and  $R_I$  the resistance per unit area of the barrier. The resulting spin accumulation in the N wire is

$$\begin{aligned} S_z(x) &= -\frac{\nu_F P V_I}{2R_I \sigma_N} \operatorname{Re} \left[ \frac{e^{-\kappa x}}{\kappa} \right] \\ S_y(x) &= -\frac{\nu_F P V_I}{2R_I \sigma_N} \operatorname{Im} \left[ \frac{e^{-\kappa x}}{\kappa} \right], \end{aligned} \quad (80)$$

where  $V_I$  and  $R_I$  are the voltage drop and the resistance of the injector, respectively. A ferromagnetic voltage detector at a distance  $x = L$  from the injector detects the spin potential  $\mu_z = S_z(L)/\nu_F$ . The resulting  $\mu_z(B)$  dependence, described by Eq. (80), coincides with the Hanle-shaped curves measured experimentally [165, 166].

#### 4.3.2. Hanle effect in spin-split superconductors

If the wire in Fig. 11 is in the superconducting state the non-local signal can change drastically as discussed in Ref. [180]. In contrast to the normal-metal case, the retarded and advanced GFs have non-trivial energy dependencies and therefore one cannot integrate straightforwardly the diffusion equation over the energy.

As in previous sections, we assume that the retarded and advanced GFs are position independent and the density of states is the one shown in Fig. 4. In contrast to the normal case the non-local Hanle signal in a superconducting wire depends on the dominating spin relaxation mechanism. We consider again the two mechanisms: magnetic impurities, Eq. (34), and extrinsic spin-orbit coupling, Eq. (33), and introduce again the parameter  $\beta$  describing the relative strength between them  $\beta = (\tau_{so} - \tau_{sf})/(\tau_{so} + \tau_{sf})$ .

In principle the Hanle signal in the superconductor would include contributions from the long-range energy mode discussed in Sec. 4.2 for the case

of collinear field and magnetizations. To separate that contribution from the bare Hanle effect, we concentrate on the linear response regime of low injector and detector voltages, where the effect of the energy mode can be disregarded (*cf.* Fig. 14). In such a case the non-local conductance is exponentially small ( $\sim \exp(-\Delta/T)$ ) and therefore we focus on the non-local resistance  $V_{\text{det}}/I_{\text{inj}}$ , where  $V_{\text{det}}$  is the voltage at the detector in the absence of a current and  $I_{\text{inj}}$  is the current at the injector. To uncover the Hanle effect, we furthermore study the difference  $V_S$  between the voltages for the parallel and anti-parallel orientations of the detector and injector polarizations. The non-local resistance of interest is thus  $R_S = V_S/I_{\text{inj}}$ .

If we assume that the external field is applied in the  $z$ -direction and disregard the orbital effects, the retarded quasiclassical Green's function is described by only four nonzero components in Eq. (15). The energy dependence of these components is shown in Fig. 6.

Whereas the spectral terms remain constant in the S region, the spin-polarized current  $I_{\text{inj}}$  that flows through the interface with the injector causes a spin accumulation characterized by the vector  $\boldsymbol{\mu}_s$ . The current measured at the detector is then given by [180]

$$I_{\text{det}} = -\frac{V_{\text{det}}Y}{R_{\text{det}}} + \frac{\boldsymbol{\mu}_s \cdot \mathbf{P}_{\text{det}}}{R_{\text{det}}}, \quad (81)$$

where  $R_{\text{det}} = R_{\square}/A$  is the normal-state barrier resistance between the superconducting wire and the detector with cross sectional area  $A$  and spin polarization  $\mathbf{P}_{\text{det}}$ , and  $V_{\text{det}}$  is the voltage measured at the detector with respect to the superconductor.  $Y = \int_0^\infty d\varepsilon N_+ \partial_\varepsilon f_{\text{eq}}$  describes the effect of the density of states in Eq. (60). Its low-temperature analytical estimate for weak spin relaxation is given in Eq. (147a) below.

To find the voltage induced in the electrically open detector circuit we set  $I_{\text{det}} = 0$  in Eq. (81). The spin-dependent part of the non-local resistance  $R_S = [V_{\text{det}}(\mathbf{P}_{\text{det}}) - V_{\text{det}}(-\mathbf{P}_{\text{det}})]/I_{\text{inj}}$  can be found using the linear response relation for the injector current  $I_{\text{inj}} = V_{\text{inj}}Y/R_{\text{inj}}$  with the normal-state resistance  $R_{\text{inj}}$  of the injector:

$$R_S = \frac{2R_{\text{inj}}}{V_{\text{inj}}Y^2} \boldsymbol{\mu}_s \cdot \mathbf{P}_{\text{det}}, \quad (82)$$

where  $V_{\text{inj}}$  is the voltage applied at the injector in order to inject the current.

We then need to determine the spin accumulation  $\boldsymbol{\mu}_s(x)$  induced along the S wire which can be written in terms of the Keldysh component of the GF as

$$\boldsymbol{\mu}_s(x) = \int_0^\infty \mathbf{m}(\varepsilon, x) d\varepsilon, \quad (83)$$

with  $\mathbf{m}(\varepsilon, x) = \text{Tr}(\tau_3 \mathbf{S} g^K)/8$ . For simplicity we assume that  $\mathbf{P}_{\text{inj}} \perp \mathbf{h}$  so that the  $f_L$  mode is not induced by the thermoelectric coupling at linear response, see Sec. 5.4.3. Therefore the spin accumulation does not contain the long-range contribution discussed in Sec. 4.2. The remaining part of  $\mathbf{m}$  in Eq. (83) is given

by:

$$\mathbf{m} = N_+ \mathbf{f}_T + \frac{\text{Im}g_{33}}{h} (\mathbf{f}_T \times \mathbf{h}), \quad (84)$$

where the vector  $\mathbf{f}_T = (f_{T1}, f_{T2}, f_{T3})$  contains the spin components of the general distribution function (14). The first term in this expression is the usual quasiparticle contribution which also appears in the normal state. It is determined by the nonequilibrium distribution function at energies larger than the superconducting gap, that is where the total density of states is non-zero. In contrast, the second term in Eq. (84) only appears in the superconducting case and is finite for subgap energies due to the prefactor  $\text{Im}g_{33}$  (*cf.* Fig. 6). This term can be related to the difference  $N_-$  between the DOS in spin subbands using the Kramers-Kronig relation for the retarded GF  $\text{Im}g_{33}(\varepsilon) = -\mathcal{P} \int_{-\infty}^{\infty} \frac{N_-(\varepsilon')}{\varepsilon' - \varepsilon} \frac{d\varepsilon'}{\pi}$ .

Let us assume that the spin-splitting field in the superconductor points in the  $z$ -direction,  $\mathbf{h} = h\mathbf{e}_z$ . Then the transverse components  $f_{T1}, f_{T2}$  satisfy the kinetic equations obtained from Eq. (8),

$$\mathcal{D}_{T1} \nabla^2 f_{T1} + \mathcal{D}_{T2} \nabla^2 f_{T2} = X_1 f_{T1} + X_2 f_{T2} \quad (85a)$$

$$\mathcal{D}_{T1} \nabla^2 f_{T2} - \mathcal{D}_{T2} \nabla^2 f_{T1} = X_1 f_{T2} - X_2 f_{T1}. \quad (85b)$$

In contrast to the normal case, Eq. (79), the diffusion coefficient is now a tensor with components that depend on energy,

$$\mathcal{D}_{T1} = D(1 + |g_{03}|^2 - |g_{01}|^2 + |g_{31}|^2 - |g_{33}|^2) \quad (86)$$

$$\mathcal{D}_{T2} = 2D \text{Im} (g_{33}g_{03}^* - g_{31}g_{01}^*). \quad (87)$$

The terms on the right hand side of Eq. (85) are  $X_1 = (S_{T1} - H_1)$ ,  $X_2 = (S_{T2} + H_2)$ , with

$$H_1 = 4h\text{Im}g_{33}, \quad H_2 = 4hN_+, \quad (88)$$

$$S_{T1} = 2\tau_{sn}^{-1} [(\text{Re}g_{03})^2 + \beta(\text{Im}g_{01})^2], \quad (89)$$

$$S_{T2} = 2\tau_{sn}^{-1} (\text{Im}g_{33}\text{Re}g_{03} - \beta\text{Im}g_{01}\text{Re}g_{31}). \quad (90)$$

The  $H_{1,2}$  terms are the "Hanle" terms that describe the coherent spin rotation and relaxation due to the action of the external field. In the normal case only  $H_2$  and the first term of  $S_{T1}$  are non-zero and we recover Eq. (79).

In order to solve Eqs. (85a-85b) we need the boundary conditions at the interface with the injector. They can be obtained from Eq. (48). By keeping terms to leading order in the interface parameter  $\kappa_I = 1/(R_{I\Box}\sigma_N)$  we obtain [180]

$$\mathcal{D}_{T1} \nabla f_{T1} + \mathcal{D}_{T2} \nabla f_{T2} = -2\kappa_I \text{Im}g_{33} P_I n_- \quad (91a)$$

$$\mathcal{D}_{T1} \nabla f_{T2} - \mathcal{D}_{T2} \nabla f_{T1} = -2\kappa_I N_+ P_I n_- . \quad (91b)$$

These are evaluated at the position of the interface.

Equations (85a,85b) can be re-written for the spectral density of spin polarization, Eq. (84), in a more familiar form, similar to the Bloch-Torrey transport



equation [197] for the magnetic moment:

$$\nabla_k \cdot \mathbf{j}_{sk} = \gamma \mathbf{m} \times (\mathbf{h} + \mathbf{h}_s) - \mathbf{m}/\tau_S, \quad (92)$$

$$\mathbf{j}_{sk} = -\mathcal{D}_{\parallel} \nabla_k \mathbf{m} - \mathcal{D}_{\perp} \nabla_k \mathbf{m} \times \mathbf{h}. \quad (93)$$

Here  $\gamma = -2$  is the electron gyromagnetic ratio and  $\mathbf{j}_{sk}$  is the spin current density in the  $k$ -th spatial direction. The diffusion coefficients are defined as

$$\mathcal{D}_{\parallel} = \frac{\mathcal{D}_{T1} N_+ + \mathcal{D}_{T2} \text{Im} g_{33}}{N_+^2 + \text{Im} g_{33}^2} \quad (94)$$

$$\mathcal{D}_{\perp} = \frac{\mathcal{D}_{T2} N_+ - \mathcal{D}_{T1} \text{Im} g_{33}}{N_+^2 + \text{Im} g_{33}^2}. \quad (95)$$

Equations (92-93) are written in the steady-state limit, which is enough for the description of the spin Hanle effect. In the dynamical case, the magnetization depends explicitly on time  $\mathbf{m} = \mathbf{m}(\varepsilon, t)$ , and the l.h.s. of Eq. (92) contains additional terms. When the spin dynamics is slow enough, with a characteristic frequency much smaller than the superconducting energy gap,  $\omega \ll \Delta$ , the Bloch-Torrey equation in the superconducting state can be written as<sup>8</sup>

$$\frac{\partial \mathbf{m}}{\partial t} + \nabla_k \cdot \mathbf{j}_{sk} = \gamma \mathbf{m} \times (\mathbf{h} + \mathbf{h}_s) - \mathbf{m}/\tau_S. \quad (96)$$

In Eqs. (92,96),  $\tau_S$  and  $\mathbf{h}_s$  are the transverse spin relaxation time and a correction to the effective Zeeman field appearing in the presence of spin-relaxation processes. The latter determines the (Larmor) precession frequency of the spins. Specifically,

$$\tau_S^{-1} = \frac{2h(H_2 S_{T1} + H_1 S_{T2})}{H_1^2 + H_2^2}, \quad (97a)$$

$$\mathbf{h}_s = \mathbf{h} \frac{H_2 S_{T2} - H_1 S_{T1}}{H_1^2 + H_2^2}. \quad (97b)$$

Both the transverse relaxation rate  $\tau_S^{-1}$  and the effective field shift  $h_s = |\mathbf{h}_s|$  are proportional to the normal-state spin relaxation rate  $\tau_{sn}^{-1}$ . In the superconducting state  $\tau_S^{-1}$  and  $h_s$  depend differently on energy for different spin-relaxation mechanisms. The typical dependencies are shown in Fig. 15 for  $\beta = \pm 1$ . One can see that  $\tau_S^{-1}$  has a step-wise behavior as a function of energy when the spin-orbit relaxation dominates [Fig. 15(a)]. In contrast,  $\tau_S^{-1}(\varepsilon)$  shows peaks near the spin-split gap edges for spin-flip relaxation [Fig. 15(b)]. The effective field shift  $h_s$  has different signs for  $\beta = \mp 1$  as shown in Fig. 15(c,d). Interestingly, the transverse spin relaxation  $\tau_S^{-1}$  vanishes at the subgap energies.

Equations (85a-85b) imply that the transverse components of  $\mathbf{f}_T$  have the general form

$$f_{T1} = -\text{Im}(Ae^{-k_T z}) \quad (98)$$

$$f_{T2} = \text{Re}(Ae^{-k_T z}), \quad (99)$$

---

<sup>8</sup>For the general case of arbitrary large frequencies in the absence of gradients, see Eq. (108).

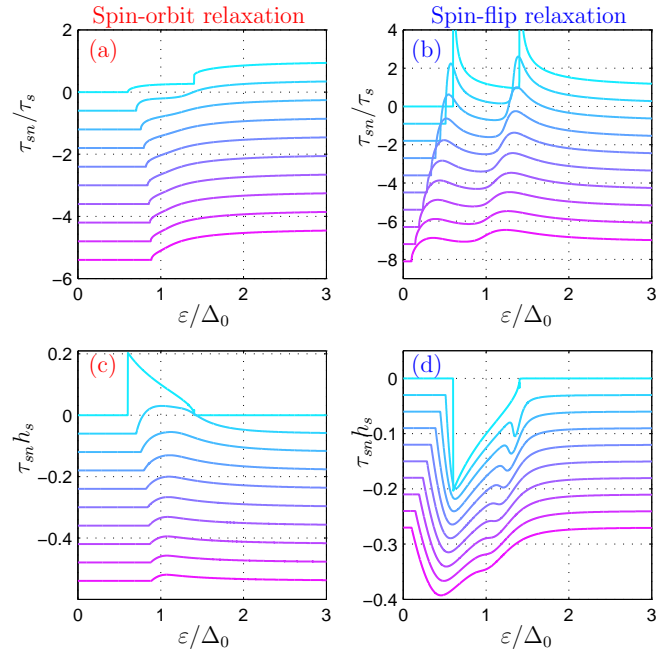


Figure 15: (a,b) Transverse relaxation time of magnetic precession Eq. (97a) and (c,d) shift of the field determining the precession frequency, Eq. (97b). For spin-orbit mediated spin relaxation (a,c)  $\beta = -1$  the curves from top to bottom are for  $(T_{c0}\tau_{sn})^{-1} = 0.001 - 30.001$  with steps of 3. For spin-flip relaxation  $\beta = 1$  (b,d) the curves from top to bottom are for  $(T_{c0}\tau_{sn})^{-1} = 0.001 - 0.601$  with steps of 0.06. The spin-splitting field is  $h = 0.4\Delta_0$  in all panels.

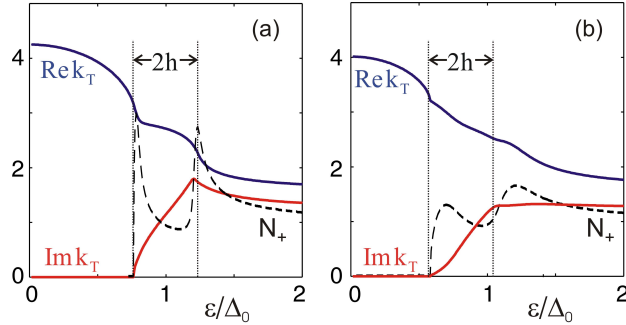


Figure 16: Energy dependencies of the inverse length scales that determine spin relaxation  $\text{Re}k_T$  (blue solid curve) and spin precession  $\text{Im}k_T$  (red solid curve). The length scales are normalized by  $\lambda_{sn}$ . Dashed curves show the total DOS  $N_+$ . (a)  $\beta = -0.9$  (b)  $\beta = 0.5$ . Exchange field  $h = 0.22\Delta_0$  and spin relaxation rate  $(\tau_{sn}T_{c0})^{-1} = 0.2$ . The precession  $\text{Im}k_T$  vanishes at subgap energies and  $k_T(\varepsilon = 0) \sim \xi_s^{-1}$  is given by the superconducting coherence length  $\xi_s = \sqrt{D/\Delta_0}$ .

where  $A$  is an integration constant determined by the boundary conditions, and

$$k_T = \left[ \frac{(S_{T1} - H_1) - i(S_{T2} + H_2)}{D(\mathcal{D}_{T1} - i\mathcal{D}_{T2})} \right]^{1/2} \quad (100)$$

with  $\text{Re}k_T > 0$ . In contrast to the normal metal case considered in Sec. 4.3.1, there is no straightforward relation between  $k_T$  and the parameters  $\tau_S$  and  $h_s$ . This is because the diffusion coefficients in the superconducting state entering Eq. (93) are energy dependent and hence the spectral spin current has a complicated expression that couples the different components of the spin polarization.

The real part  $\text{Re}k_T$  determines the spin relaxation length and the imaginary part  $\text{Im}k_T$  gives the quasiparticle spin precession. In the superconducting state both these scales are energy dependent. In Fig. 16 we show how the precession and relaxation scales depend on energy and on the parameter  $\beta$ .

It follows that at low energies  $\text{Re}k_T$  is larger than in the normal-metal case which corresponds to the limit  $\varepsilon \gg \Delta$ . At  $\varepsilon = 0$  the characteristic relaxation length  $k_T^{-1}(0)$  is determined by the coherence length  $\xi_s = \sqrt{D/\Delta_0}$  rather than by the normal-state spin relaxation length  $\lambda_{sn}$ . In contrast, the imaginary part of  $k_T$  vanishes at the energies below the spectral gap where the DOS shown by the dashed lined in Fig. 16 is absent, i.e.,  $N_+ = 0$ . In the case of dominating spin-orbit scattering ( $\beta < 0$ ), the precession  $\text{Im}k_T$  has a shallow peak at  $\varepsilon \approx \Delta + h$  [see Fig. 16(a)]. If the spin-flip mechanism dominates ( $\beta > 0$ ), this peak of  $\text{Im}k_T$  is suppressed, Fig. 16(b).

Putting all this together allows us to evaluate the non-local resistance  $R_S$  exhibiting the Hanle curves in the superconducting state as shown in Fig. 17. The data at  $T = T_c$  corresponds to the normal-metal Hanle signal. The result depends on the relative directions of the injector and detector polarizations. Panels a and c show the non-local signal  $R_{S_y}$  obtained from Eq. (82) when

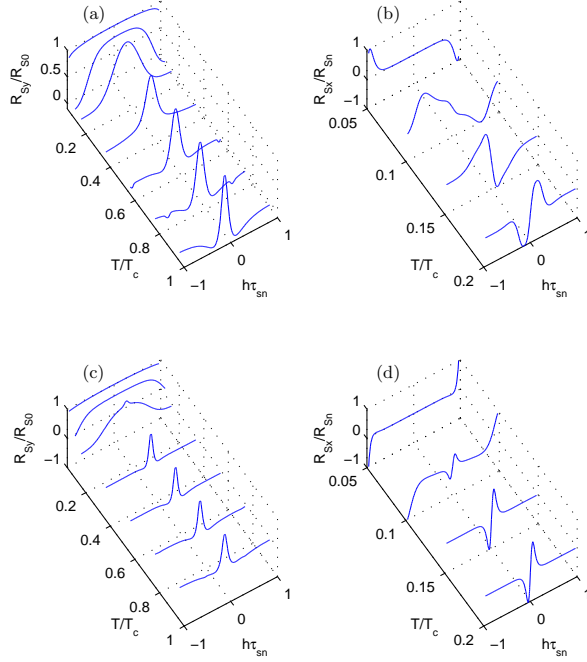


Figure 17: Hanle signals  $R_{sy}$  and  $R_{sx}$  at the distance  $L_D = 2\lambda_{sn}$  from the injector for (a,b)  $\beta = 0.5$  and (c,d)  $\beta = -0.9$ . The temperatures are  $T/T_c = 0.05, 0.1, 0.15, 0.35, 0.55, 0.75, 0.95$  in panels (a,c) and  $T/T_c = 0.05, 0.1, 0.15, 0.2$  in panels (b,d). The resistance  $R_{sy}$  is normalized by its maximum value obtained at  $h = 0$  and  $R_{sx}$  is normalized to the local normal state resistance.

the detector polarization  $\mathbf{P}_{\text{det}} = P_{\text{det}}\mathbf{e}_y$  so that  $\mathbf{P}_{\text{det}} \parallel \mathbf{P}_{\text{inj}} \perp \mathbf{h}$ . One can see that both, the precession and decay of the nonlocal signal, disappear at  $T \rightarrow 0$ , whereas the shape of the curves at intermediate temperatures depends on the type of spin relaxation.

If instead of the above configuration we assume that the three vectors  $(\mathbf{P}_{\text{det}}, \mathbf{P}_{\text{inj}}, \mathbf{h})$  are perpendicular to each other (e.g.,  $\mathbf{P}_{\text{det}} = P_{\text{det}}\mathbf{e}_x$ ,  $\mathbf{P}_{\text{inj}} = P_{\text{inj}}\mathbf{e}_y$ ,  $\mathbf{h} = h\mathbf{e}_z$ ), the subgap current is absent in the detector circuit and the corresponding spin signal  $R_{sx}$  has a strong dependence on  $h$  even at the temperatures well below  $T_c$ . This is shown in Figs. 17(c,d).

We are not aware of the measurement of the spin Hanle signals in the superconducting state. We emphasize that the above results are obtained in the linear response regime of small voltages. They disregard the thermal effects coming into play at higher voltages, especially at those of the order of the energy gap  $\Delta \pm h$ . In the linear response regime the transport quantities in superconductors are exponentially suppressed due to the gap in the density of states, and hence the above theory is rather made for the thermally activated quasiparticles. Because of this, the best way to uncover the superconducting effects on the Hanle response would be to study it rather close but below the critical temperature

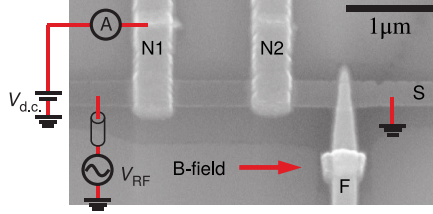


Figure 18: Experimental setup from Ref. [198]. An applied RF field excites quasiparticle spin resonance in a thin Al film (S), which is indirectly probed by observing modification of the  $I(V)$  curve of probe N1. Figure adapted from Ref. [198] (Creative Commons Attribution 4.0 International License).

$T_c$ .

To summarize: The kinetic equations for the nonequilibrium modes constitute a rather generic theoretical tool that we have used in this section to provide a quantitative description of some transport properties, such as spin injection and precession, occurring in superconducting structures in the presence of a spin-splitting field. The predictive capability of the derived kinetic equations has been proven in this section by contrasting the results with existing experiments especially in the case of collinear magnetizations. This makes these equations an ideal tool to study further effects that involve the coupling between different nonequilibrium modes in superconductors, as for example, the possible thermal spin Hanle effect and other non-linear effects taking place in systems with non-collinear magnetizations.

In section 5 we focus on thermoelectric effects that are also direct manifestations of the spin-splitting fields in the superconductor. However, in contrast to the section here where the focus is on the diffusion of the nonequilibrium modes within the superconducting wire, section 5 deals mainly with interface effects, and disregards the position dependence of the nonequilibrium modes within the superconductors. The next section discusses applications of the quasiclassical method to time-dependent nonequilibrium problems and for example generalizes the Bloch-Torrey equation (92) to large frequencies.

sectionNon-equilibrium quasiparticle dynamics

The conduction electrons of a superconductor in an oscillating electromagnetic field can absorb energy via excitation of the existing quasiparticles, and by creation of new quasiparticles from breaking of Cooper pairs. In a stationary state, the excitation is balanced by corresponding relaxation processes. These are sensitive to the spectrum of states available in a spin-split superconductor.

Electrons couple to the electromagnetic field via the Zeeman and the orbital terms. The Zeeman coupling is the source for the conduction electron spin resonance (CESR), which was theoretically considered in early works [199, 200, 201, 202, 203]. The corresponding dynamical susceptibility for the spin-split case was discussed in Refs. [204, 205, 206]. The linewidth of the resonant absorption peak is determined by the spin relaxation time in the normal state,  $\tau_{sn}$ , and is not af-

ected by the slow relaxation of the thermal long-range spin imbalance discussed in Sec. 4.2. The magnetic screening complicates the experimental observation of the resonance. Results however exist in the mixed state of type II superconductors as reported in Refs. [207, 208, 209], and more recently, also in spin-split Al thin films in Ref. [198] [see Fig. 18]. For the Al films, linewidths of 100 ps were observed, consistent with the expected magnitude of  $\tau_{sn}$  in aluminum.

The CESR physics is also related to pumping effects, where an externally driven spin precession drives a nonequilibrium state or currents in the superconductor, or currents across a junction. Effects of this type have been considered in different ferromagnet/superconductor structures in several works, in adiabatic [210, 211] and nonadiabatic cases [212, 213, 214, 215].

As mentioned above, a rf field also couples to the orbital degree of freedom of the electrons. This coupling drives ac currents that also excite quasiparticles. In the absence of spin splitting, the linear and nonlinear response of superconductors has been extensively studied [17]. In the linear response regime, the complex impedance for spin-split superconducting films was considered theoretically and experimentally in Ref. [216] adding Zeeman energy shifts to BCS theory results [217, 218]. In the nonlinear regime, strong driving can modify the observed quasiparticle spectrum [219]. Moreover, at temperatures close to  $T_c$ , exciting quasiparticles can lead to an increase of the superconducting gap  $\Delta$  [220, 221, 222]. In spin-split superconductors, this effect is modified by the spin-split density of states and spin-flip scattering [123].

In this section we discuss the dynamic response of spin-split superconductors in terms of the time-dependent quasiclassical equations, both in the linear and nonlinear regimes. In addition to these effects, oscillating fields can excite magnetic impurities and nuclear moments. Discussion of such extrinsic resonance effects can be found in the articles [223, 224, 225, 226], and are beyond the scope of this review. We also do not discuss magnetization dynamics and how superconductivity affects it; reviews on this active topic can be found in other works [227, 228].

#### 4.4. Linear response of a spin-split superconductor to a rf field

The dynamic nonequilibrium response of spin-split dirty superconducting thin films can be studied on the basis of the Usadel equation, Eq. (8), which in time-dependent representation [103] we write in a compact form

$$D\hat{\nabla}(\check{g} \circ \hat{\nabla}\check{g}) = [\check{X} \circ \check{g}], \quad (101)$$

where

$$\check{X} = -i\epsilon\hat{\tau}_3 + i\phi + i\mathbf{h} \cdot \boldsymbol{\sigma}\hat{\tau}_3 + \check{\Delta} + \check{\Sigma}. \quad (102)$$

Now  $\check{g}(\omega, \omega') = \int_{-\infty}^{\infty} dt dt' e^{i\omega t - i\omega' t'} \check{g}(t, t')$  depends on both time indices and matrix products involve energy convolutions,  $(a \circ b)(\omega, \omega') = \int \frac{d\omega_1}{2\pi} a(\omega, \omega_1) b(\omega_1, \omega')$ . Above,  $\epsilon(\omega, \omega') = 2\pi\delta(\omega - \omega')\omega$ , and  $\hat{\nabla}X = \nabla X - i[\mathbf{A}\tau_3 \circ X]$ . External classical electromagnetic fields couple to the electrons via the exchange field  $\mathbf{h}(\omega - \omega')$  and the vector potential  $\mathbf{A}(\omega - \omega')$ . We choose the gauge such that the local

charge neutrality [229, 102] fixes the scalar potential to  $\phi(t) = \frac{\pi}{4} \text{Tr} \hat{g}^K(t, t)$ , and in the spatially uniform cases discussed below  $\phi = 0$ . As above, we consider thin films, and neglect magnetic screening.

The kinetic equation for the distribution function  $\hat{f}$  follows from Eq. (101) and the above assumptions,

$$\frac{1}{8} D \hat{\nabla} [\hat{\nabla} \hat{f} - \hat{g}^R \circ (\hat{\nabla} f) \circ \hat{g}^A] + \frac{1}{8} \hat{j}^R \circ \hat{\nabla} f - \frac{1}{8} \hat{\nabla} f \circ \hat{j}^A = \hat{\mathcal{I}}, \quad (103)$$

where  $\hat{j}^{R/A} \equiv D \hat{g}^{R/A} \circ \hat{\nabla} \hat{g}^{R/A}$  and the collision integral is defined as

$$\hat{\mathcal{I}} = \frac{1}{8} [\hat{g}^R \circ \hat{Z} - \hat{Z} \circ \hat{g}^A] \quad (104)$$

and

$$\hat{Z} = \hat{X}^R \circ \hat{f} - \hat{f} \circ \hat{X}^A - \hat{X}^K. \quad (105)$$

Note that the definition of collision integrals in Eq. (103) differs from Eq. (18), as several terms in the kinetic equation have here been canceled by making use of the R/A components of the Usadel equation. In a spatially uniform case with  $\mathbf{A} = 0$ , the l.h.s of Eq. (103) vanishes and the kinetic equation reduces to the condition  $\hat{\mathcal{I}} = 0$ .

The CESR emerges when considering a Zeeman field of the form  $\mathbf{h}(\omega) = h_0 \hat{z} + h_1(\omega) \hat{x}$ , where an ac field  $h_1$  perpendicular to a static exchange field  $h_0$  excites the electron spins. The spin dynamics follows a Bloch-like equation including spin relaxation, similar to the spin Hanle effect (see Sec. 4.3 and Eq. (92)). Such equations can be derived from the Usadel equation in linear response to  $h_1$ , and from other approaches [204, 205, 206, 230]. Here we briefly discuss the physics within the Usadel framework.

It is useful to separate the corrections to the Keldysh Green's function in Eq. (101) due to the distribution function from those due to the modification of the spectral functions:  $\delta \hat{g}^K = \delta \hat{g}_{\text{reg}}^K + \delta \hat{g}_{\text{an}}^K$ , defining  $\delta \hat{g}_{\text{reg}}^K = \delta \hat{g}^R \circ f_{\text{eq}} - f_{\text{eq}} \circ \delta \hat{g}^A$ . We split  $\delta \hat{X}^K$  similarly. The equation  $[\hat{X} \circ \hat{g}]^K = 0$  then reduces in linear response to

$$\hat{X}_{\text{eq}}^R \circ \delta \hat{g}_{\text{an}}^K - \delta \hat{g}_{\text{an}}^K \circ \hat{X}_{\text{eq}}^A = \hat{g}_{\text{eq}}^R \circ \delta \hat{X}_{\text{an}}^K - \delta \hat{X}_{\text{an}}^K \circ \hat{g}_{\text{eq}}^A, \quad (106)$$

$$\begin{aligned} \delta \hat{X}_{\text{an}}^K &= -i \sigma_x \tau_3 [h_1 \circ f_{\text{eq}}] + \frac{1}{8 \tau_{so}} \boldsymbol{\sigma} \delta \hat{g}_{\text{an}}^K \cdot \boldsymbol{\sigma} \\ &+ \frac{1}{8 \tau_{sf}} \boldsymbol{\sigma} \hat{\tau}_3 \delta \hat{g}_{\text{an}}^K \cdot \boldsymbol{\sigma} \hat{\tau}_3 + \frac{1}{\tau_{orb}} \hat{\tau}_3 \delta \hat{g}_{\text{an}}^K \hat{\tau}_3. \end{aligned} \quad (107)$$

The solution to Eq. (106) can be obtained with the Ansatz  $\delta \hat{g}_{\text{an}}^K = \hat{g}_{\text{eq}}^R \circ \delta f - \delta f \circ \hat{g}_{\text{eq}}^A$ , where  $\delta f = f_{Tx} \sigma_x + f_{Ty} \sigma_y$ . To determine the solution components, we can take the trace  $\frac{1}{8} \text{Tr}[(\dots) \boldsymbol{\sigma}]$  of the  $(\varepsilon, \varepsilon - \omega)$  frequency component of Eq. (106). This results in

$$\begin{aligned} -i \omega \mathbf{m} &= -2 \mathbf{m} \times h_0 \hat{z} - \frac{N'_+ \mathbf{m} + \beta F'_+ \mathbf{m}'}{\tau_{sn}} + \mathbf{I}' \\ &= -2 \mathbf{m} \times (\mathbf{h}_0 + \mathbf{h}_s) - \frac{\mathbf{m}}{\tau_S} + \mathbf{I}', \end{aligned} \quad (108)$$

where  $\mathbf{m} = \frac{1}{8} \text{Tr}[\tau_3 \boldsymbol{\sigma} \delta \hat{g}_{\text{an}}^K(\varepsilon, \varepsilon - \omega)]$  describes the nonequilibrium magnetization (spin accumulation),  $\mathbf{m}' = \frac{1}{8i} \text{Tr}[\tau_1 \boldsymbol{\sigma} \delta \hat{g}_{\text{an}}^K(\varepsilon, \varepsilon - \omega)]$  describes a correction to spin scattering by superconductivity, and  $N'_+ = [g_{03}(\varepsilon) + g_{03}(\varepsilon - \omega)^*]/2$ ,  $F'_+ = [g_{01}(\varepsilon) - g_{01}(\varepsilon - \omega)^*]/(2i)$  are finite-frequency generalizations of the spin-averaged density of states and anomalous functions, respectively. The term  $\mathbf{I}' = ih_1(\omega)[N'_+ \hat{x} - N'_z \hat{y}][f_{\text{eq}}(\varepsilon) - f_{\text{eq}}(\varepsilon - \omega)]$  describes the exciting field. There is redundancy in the representation, which enables writing  $\mathbf{m}'$  in terms of  $\mathbf{m}$ , resulting in the final Bloch equation. Analogously to the spin Hanle effect discussed in Sec. 4.3.2, the spin relaxation time  $\tau_S$  is renormalized with respect to the one in the normal state,  $\tau_{\text{sn}}$ , and there is also a correction  $\mathbf{h}_s$  to the Zeeman field:

$$\frac{1}{\tau_S} = \frac{N'_+}{\tau_{\text{sn}}} + \beta \frac{F'_+ F'_+ N'_+ - F'_z N'_z}{\tau_{\text{sn}} (N'_+)^2 + (N'_z)^2} \quad (109)$$

$$\mathbf{h}_s = -\hat{z} \beta \frac{F'_+ F'_+ N'_z + F'_z N'_+}{2\tau_{\text{sn}} (N'_+)^2 + (N'_z)^2}, \quad (110)$$

where  $N'_z = [g_{33}(\varepsilon) - g_{33}(\varepsilon - \omega)^*]/(2i)$  and  $F'_z = [g_{31}(\varepsilon) + g_{31}(\varepsilon - \omega)^*]/2$ . For slow driving,  $\omega \rightarrow 0$ , the spin relaxation time  $\tau_S$  and the Zeeman field correction  $\mathbf{h}_s$  coincide with those visible in the Hanle effect (cf. Eq. (97) and Fig. 15), which also involves precession of the transverse spin component.

The result (108) describes resonant excitation of the transversal modes,  $f_{Tj}$ , which correspond to a nonequilibrium contribution to the spin accumulation (22),

$$\delta \boldsymbol{\mu}_s(t) = \delta \boldsymbol{\mu}_s^{\text{reg}}(t) + \int_{-\infty}^{\infty} \frac{d\varepsilon d\omega}{2\pi} e^{-i\omega t} \mathbf{m}(\varepsilon, \varepsilon - \omega), \quad (111)$$

where  $\delta \boldsymbol{\mu}_s^{\text{reg}}$  arises from the modification of the spectral functions,  $\delta g^{R/A}$ . The result contains the conduction electron spin resonance peak,  $\delta \boldsymbol{\mu}_s \propto h_1(\omega)/[4(h + h_s)^2 - (\omega + i/\tau_S)^2]$  at frequency  $\omega \simeq 2|h_0|$ . As discussed in Sec. 4.2, the  $f_{Tj}$  modes can relax due to elastic spin-flip scattering, which determines the peak absorption linewidth  $\frac{1}{\tau_S} \propto \tau_{\text{sn}}^{-1}$ . The result in Ref. [203] can be obtained from Eq. (108) in the quasiequilibrium approximation  $\delta f \simeq (\partial_E f_{\text{eq}}) \boldsymbol{\mu}_s \cdot \boldsymbol{\sigma}$  and in the limit  $h_0 \ll \Delta$ . Equation (108) also coincides with the result in Ref. [204].

If we focus on the orbital effects, the complex impedance of the superconductor, *i.e.*, the linear response to an oscillating electric field described by  $\mathbf{A}(\omega)$ , can also be obtained within the Usadel framework. In the above chosen (London) gauge, the perturbation to time-averaged  $\check{g}$  is of the order  $D|\mathbf{A}(\omega)|^2/\omega$  [220] and can be neglected in linear response at nonzero frequency. The charge



current response is then given by

$$\begin{aligned} j(\omega) &= \frac{\sigma_N}{16} \int_{-\infty}^{\infty} d\varepsilon \operatorname{Tr} \tau_3 (\check{g} \circ [-i\mathbf{A}\tau_3 \circ \check{g}])^K(\varepsilon, \varepsilon - \omega) \\ &= -i\omega \mathbf{A}(\omega) [\sigma_1(\omega) - i\sigma_2(\omega)] \end{aligned} \quad (112)$$

$$\frac{\sigma_1(\omega)}{\sigma_N} = \sum_{\sigma} \int_{-\infty}^{\infty} d\varepsilon 2R_{\sigma}(\varepsilon, \varepsilon - \omega) \frac{f_L(\varepsilon - \omega) - f_L(\varepsilon)}{\omega}, \quad (113)$$

$$\frac{\sigma_2(\omega)}{\sigma_N} = \sum_{\sigma} \int_{-\infty}^{\infty} d\varepsilon 2R'_{\sigma}(\varepsilon, \varepsilon - \omega) \frac{2f_L(\varepsilon - \omega) - 1}{\omega}, \quad (114)$$

where

$$R_{\sigma}(\varepsilon, \varepsilon') = N_{\sigma}(\varepsilon)N_{\sigma}(\varepsilon') + \operatorname{Im} g_{\sigma,1}(\varepsilon) \operatorname{Im} g_{\sigma,1}(\varepsilon'), \quad (115)$$

$$R'_{\sigma}(\varepsilon, \varepsilon') = \operatorname{Im} g_{\sigma,3}(\varepsilon)N_{\sigma}(\varepsilon') - \operatorname{Re} g_{\sigma,1}(\varepsilon) \operatorname{Im} g_{\sigma,1}(\varepsilon'), \quad (116)$$

and  $g_{\uparrow/\downarrow,1} = (g_{01} \pm g_{31})/2$ ,  $N_{\uparrow/\downarrow} = \operatorname{Re}[g_{03} \pm g_{33}]/2$ . The prefactors in Eqs. (112)-(114) are given by the normal-state conductivity,  $\sigma_N = 2e^2\nu_F D$ , and the kernels  $R_{\sigma}$  have the BCS form [217, 218], and are decoupled for each spin species. In other words, the electric field couples to the orbital motion of the electrons and, in our approach, it conserves spin. Therefore, the dissipative response is zero at frequencies  $\omega < 2\Delta$  in the absence of spin flipping. Phenomenological modification of the above by allowing direct spin flips in the coupling matrix element was considered in Ref. [216], obtaining a reduction in the dissipative pair-breaking threshold frequency from  $2\Delta$  to  $2\Delta - 2h$  (c.f. Fig. 19). Note however that the derivation of the Usadel diffusion equation discussed above works in leading order in  $\tau_{el}$  and neglects spin-orbit effects when dealing with the vector potential.

#### 4.5. Nonlinear spin imbalance of a spin-split superconductor in a rf field

We now go beyond the linear response regime and focus on the stationary quasiparticle distribution which enters the observables. This is determined by disregarding the gradients, in which case the collision term in Eq. (103) is equal to the contribution from the time-dependent vector potential. This results in

$$\hat{\mathcal{I}}_{ac}[\hat{f}] + \hat{\mathcal{I}}_{sn}[\hat{f}] + \hat{\mathcal{I}}_{in}[\hat{f}] = 0, \quad (117)$$

This rate equation, similar to that used in Ref. [122], describes the balance between excitation of quasiparticles induced by ac fields ( $\hat{\mathcal{I}}_{ac}$ ), the spin relaxation by the elastic spin-flip scattering ( $\hat{\mathcal{I}}_{sn}$ ), and the inelastic relaxation ( $\hat{\mathcal{I}}_{in}$ ). Each term in Eq. (117) can be described within the quasiclassical approach.

The orbital ac term of the collision integral can be obtained by assuming a time-dependent spatially uniform vector potential  $A(t) = A_0 \cos(\omega t)$ . Here, it is useful to simplify the problem by expanding in  $DA_0^2/\omega \ll 1$ , and reduce it to a form that only involves the dc component of the distribution function. In this

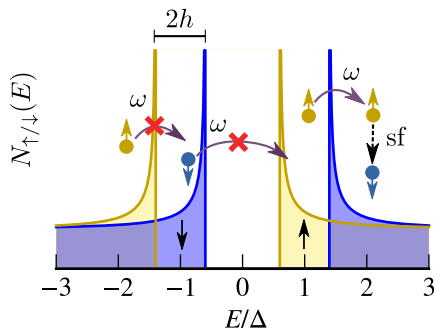


Figure 19: Quasiparticle transitions induced by an orbital electromagnetic field. The energy dependence of the density of states implies an accumulation and depletion of quasiparticles at energy intervals close to gap edges. If direct spin-flip transitions are suppressed (red crosses), relaxation via spin-flip impurity scattering can still transform quasiparticle energy imbalance to spin imbalance.

case [220]

$$\mathcal{I}_{ac,\sigma}(\varepsilon) = DA_0^2 \sum_{\pm} R_{\sigma}(\varepsilon, \varepsilon \pm \omega) [f_{\sigma}(\varepsilon) - f_{\sigma}(\varepsilon \pm \omega)], \quad (118)$$

for the  $\mathcal{I}_{\uparrow/\downarrow} = \text{Tr}[(1 \pm \sigma_z)\hat{\mathcal{I}}/2]$  components. We assume that all spin dependent fields are collinear and hence we can define  $f_{\sigma=\uparrow/\downarrow} = f_L \pm f_{T3}$ , cf. Eq. (14). Notice that the charged modes  $f_T, f_{L3}$  are not excited by a uniform  $A(t)$ .

The absorption kernel  $R$  is the one appearing in the real part of the conductivity, Eq. (115). Qualitatively, this collision integral results in the depletion (accumulation) of quasiparticles in an energy band of width  $\omega$  above (below) the gap edges  $|E| > |\Delta \pm h|$  (see Fig. 19). At higher energies the electron distribution corresponds to an increased temperature.

The collision integrals for the relaxation processes can be written as, cf. Eq. (37),

$$\mathcal{I}_{sn,\sigma} = \frac{S_{T3}}{8} (f_{\sigma} - f_{\bar{\sigma}}), \quad \mathcal{I}_{in,\sigma} = \frac{N_{\sigma}}{\tau_{in}} (f_{\sigma} - f_L^{(0)}), \quad (119)$$

where we describe inelastic scattering in a relaxation time approximation.

The spin-conserving microwave absorption term does not directly generate spin imbalance in the superconductor. However, as illustrated in Fig. 19, spin relaxation converts the accumulation of quasiparticles above the gap to an imbalance in the number of spin-up and spin-down quasiparticles. From the kinetic equation (117) we obtain in the limit  $1/\tau_{sf} \ll 1/\tau_{in}$ ,

$$f_{\sigma} - f_{\sigma}^{(0)} \simeq -\frac{\mathcal{I}_{ac,\sigma}^{(0)} \tau_{in}}{N_{\sigma}} - \sigma \frac{S_{T3} \tau_{in}^2}{8} \frac{N_{\uparrow} \mathcal{I}_{ac,\downarrow}^{(0)} - N_{\downarrow} \mathcal{I}_{ac,\uparrow}^{(0)}}{N_{\uparrow} N_{\downarrow}}. \quad (120)$$

The first term contributes zero total spin imbalance (26), but the second gives a nonzero contribution of the order of  $\tau_{in}/\tau_{sn}$ . A related effect in quasiparticle injection was discussed in Ref. [122].

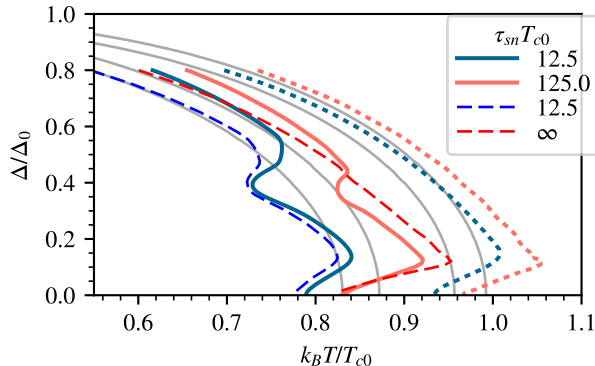


Figure 20: Order parameter  $|\Delta|$  for different magnitudes of spin-flip scattering  $\tau_{sn}$ . We take  $h/\Delta_0 = 0.4$ ,  $\tau_{sn}T_{c0} = 12.5$ ,  $\beta = 0.5$  and  $\alpha_{orb} = 0.01$ ,  $\omega/\Delta_0 = 0.2$ , and  $DA_0^2/\omega = 0.032$ . The inelastic relaxation is modeled either via a phonon model with the collision integral in Eq. (42) (solid lines), or relaxation time approximation (dashed) with  $\tau_{in}T_{c0} = 100$ . Results for  $h = 0$  (dotted) and  $A_0 = 0$  (gray) are also shown.

The generated spin imbalance can be in principle measured by a spin-polarized probe junction, as discussed in Sec. 4.1. Note, however, that in this type of experiments other processes may need to be also considered. On the one hand, photoelectric signals can also occur in the absence of spin splitting as shown in Refs. [231, 232]. These processes, however, generally scale with  $\propto \tau_{e1}$  rather than  $\propto \tau_{in}$ . On the other hand an ac bias over the S/F junction may also result in rectification, as discussed in the next section.

It is interesting to notice that the nonequilibrium quasiparticle accumulation generated by the microwave absorption affects the magnitude of the the superconducting gap  $\Delta$ , leading to deviations from the results in Ref. [220]. Results for the self-consistent  $\Delta(T)$  from numerical calculations [123] are shown in Fig. 20 for  $h = 0$  and  $h > 0$ . In the absence of spin-splitting,  $h = 0$ , a gap enhancement [220] occurs. For  $h > \omega$ , an additional instability develops at  $\Delta(T) = h$ , corresponding to a coexistence of two solutions where the spin-averaged DOS is either gapless ( $|\Delta| < h$ ) or gapped ( $|\Delta| > h$ ). The instability requires the presence of strong spin-flip scattering: for  $\tau_{sn} \gg \tau_{in}$  the exchange field does not cause significant qualitative changes, because in that case the quasiparticle accumulations above the gap edges that generate the enhancement, are approximatively described as two independent copies of the effect at  $h = 0$ .

#### 4.6. S/F tunnel junction dynamics

For adiabatic excitation,  $\omega \ll \Delta$  dynamics of S/F tunnel junctions can be described by the dc relations discussed in Sec. 3 and 5. That this limit can be reached at time scales shorter than the spin-relaxation and inelastic times, was used in a recent experiment [233] to probe the relaxation dynamics in spin-split thin-film superconductors.

At higher frequencies, photoassisted tunneling breaks the adiabatic description. This can be taken into account via a standard tunneling Hamiltonian approach [234, 235, 236]. The result for the tunneling current is

$$I(t) = -2 \operatorname{Re} \sum_{\sigma} \sum_{\mathbf{kq}} \int_{-\infty}^t dt' e^{0^+ t'} |T_{\mathbf{kq}}^{\sigma}|^2 e^{i[\phi(t) - \phi(t')]} \quad (121)$$

$$\times [G_{\mathbf{k}\sigma}^{<}(t', t) G_{\mathbf{q}\sigma}^{>}(t, t') - G_{\mathbf{k}\sigma}^{>}(t', t) G_{\mathbf{q}\sigma}^{<}(t, t')],$$

where  $T$  is the tunneling matrix element,  $G^{>(<)} = \frac{1}{2}G^K \pm \frac{1}{2}(G^R - G^A)$  are (non-quasiclassical) Green functions for the superconducting ( $\mathbf{k}$ ) and non-superconducting ( $\mathbf{q}$ ) sides, and the phase  $\phi(t) = \frac{e}{\hbar} \int^t dt' V(t')$  is related to the time-dependent voltage  $V(t)$  across the junction. The above result applies for spin-conserving tunneling with collinear magnetizations. If the terminals are in an internal equilibrium (no spin or charge imbalance), changing integration variables yields the time-dependent generalization of Eq. (3),

$$I(t) = \operatorname{Re} \int_{-\infty}^{\infty} \frac{dV}{\pi} I_{\text{dc}}(V) \int_{-\infty}^t dt' e^{-i(t-t')V} e^{i[\phi(t) - \phi(t')]} \quad (122)$$

$$= I_{\text{dc}}(V(t)) + \operatorname{Re} \int_{-\infty}^t dt' K(t-t') [e^{i[\phi(t) - \phi(t')]} - e^{iV(t)(t-t')}], \quad (123)$$

where  $I_{\text{dc}}$  is given by Eq. (3), and the memory kernel is [237]

$$K(t) = \int_{-\infty}^{\infty} \frac{dV}{\pi} e^{-itV} [I_{\text{dc}}(V) - \frac{V}{R_T} - I_{\text{dc}}(0)] \quad (124)$$

$$= \frac{\pi T_F \Delta}{R_T} \frac{J_1(t\Delta)}{\sinh(\pi T_F t)} [i \cos ht + P_F \sin ht],$$

and  $J_1$  is a Bessel function.

The resulting current-voltage relation is asymmetric,  $I_{\text{dc}}(-V) \neq -I_{\text{dc}}(V)$  for  $h \neq 0$ . This implies that such junctions rectify ac signals [233]. For an ac signal  $V(t) = V_{\text{dc}} + V_{\text{ac}} \cos(\omega t)$ , from the above we have the average dc current [238]

$$I_{\text{dc}} = \sum_{n=-\infty}^{\infty} J_n^2 \left( \frac{eV_{\text{ac}}}{\hbar\omega} \right) I_{\text{dc}}(V_{\text{dc}} + n\omega) \quad (125)$$

$$\simeq I_{\text{dc}}(V_{\text{dc}}) + \frac{V_{\text{ac}}^2}{4\omega^2} [I_{\text{dc}}(V_{\text{dc}} + \omega) + I_{\text{dc}}(V_{\text{dc}} - \omega)] + \dots \quad (126)$$

At  $V_{\text{dc}} = 0$  and small  $V_{\text{ac}}$  at uniform temperature  $T \gtrsim h, \omega$ , the rectified current is  $I_{\text{dc}} \propto P_F V_{\text{ac}}^2 h / (R_T \Delta^2)$ , [123] proportional to the exchange field in S. Measurements attempting to use F probes for the nonequilibrium ac effects discussed in the previous sections need to take into account such rectification, or try to suppress  $V_{\text{ac}}$  e.g. via a suitable microwave circuit design [239].

While dynamical effects in superconductors have been studied extensively experimentally, we are aware of relatively few studies on spin-split superconductors. Tunnel junction rectification effects were observed for example in Ref. [233]. However, to our knowledge, higher-frequency experiments probing gap enhancement or photoassisted tunneling have not been reported so far.

## 5. Thermoelectric effects in superconducting structures

A temperature difference across an electric contact typically leads to heat currents aiming to relax this difference. In some cases it may also lead to observable charge currents. Reciprocally, an electrical voltage may drive a heat current not only in nonlinear response (due to Joule heating) but also for small voltages. This connection of charge and heat currents is called the thermoelectric effect. The traditional view of thermoelectric effects in superconductors is that if they exist, they must be very weak. In bulk superconductors, this is partially because any thermoelectrically generated quasiparticle current is screened by a supercurrent [240]. Ginzburg suggested [241] to measure this supercurrent by using an additional constraint to the phase of the superconducting order parameter in a multiply connected structure. However, even this thermally created phase gradient tends to be weak, owing to the near-complete electron-hole symmetry in superconductors [242].

Thermoelectric effects typically require strongly energy dependent density of states of the charge carriers. Such energy dependence is present in the BCS density of states of the superconductors. However, typically this density of states is quite symmetric with respect to the Fermi level, and therefore any contribution of the positive energy excitations ("electrons") on thermoelectric effects is cancelled by the negative energy excitations ("holes"). Breaking this electron-hole symmetry would hence allow for the appearance of strong thermoelectric effects. As we discuss in this section, this is what happens in spin-split superconductors, as an exchange field breaks the symmetry in each spin sector, but so that the overall spin-summed energy spectrum remains electron-hole symmetric. Further breaking the spin symmetry in transport through a spin filter can then provide large thermoelectric effects as the two spins are weighed differently [243, 29, 244]. This prediction has been recently confirmed experimentally in [177, 245].

In this section we give an overview of the different types of thermoelectric effects discussed for superconductors, and then concentrate on the ones obtained in superconductors with a spin-splitting field. We discuss both the linear response regime and beyond it, and consider also the limiting features such as the electron-phonon coupling. We show that under suitable conditions, in particular for close-to-optimal spin filters, the efficiency of thermoelectric conversion can become very large and exceed that obtained for best thermoelectric devices operated at or above room temperature. Besides the regular quasiparticle current, in devices coupling two superconductors, one with a spin-splitting field and one without, the thermoelectric effect can also be converted to a phase gradient [30]. This large thermophase effect is discussed in more detail in Ref. [3].

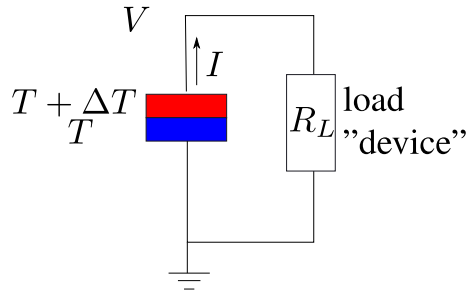


Figure 21: Generic electrical heat engine.

As these effects require low operating temperatures, they obviously cannot be directly used to improve the efficiency of various everyday devices. However, the strong thermoelectric effect may become relevant in other types of applications, such as sensors, where the measured (wide-band) signal consists of heating one part of the system [33]. The thermoelectric conversion can then be used to convert the resulting temperature difference to a charge current.

### 5.1. Thermoelectric effects and heat engines

Biasing a contact with a small voltage  $V$  and a small temperature difference  $\Delta T$  leads to linear-response charge and heat currents  $I$  and  $\dot{Q}$  of the form

$$\begin{pmatrix} I \\ \dot{Q} \end{pmatrix} = \begin{pmatrix} G & \tilde{\alpha} \\ \tilde{\alpha} & G_{\text{th}}T \end{pmatrix} \begin{pmatrix} V \\ -\Delta T/T \end{pmatrix}. \quad (127)$$

The  $2 \times 2$  conductance matrix in Eq. (127) is a part of the generalized  $4 \times 4$  Onsager matrix (59) connecting different interface currents and potentials as discussed in Sec. 3.6. This matrix is symmetric in the presence of time-reversal symmetry, and also in all particular cases considered in this section. Here we consider a conventional situation when the spin-dependent potentials  $V_s$  and  $T_s$  are negligibly small. This is relevant when the spin relaxation rate in the electrodes around the contact exceeds the tunneling rate across the contact. This approximation allows the reduction of the general boundary condition (59) to the simpler one (127) describing thermoelectric response.

When  $\tilde{\alpha}$  is not too small, electrical energy may be converted to heat or cooling (Peltier effect), or reciprocally a temperature difference may be converted to electrical power (Seebeck effect). The efficiency of this conversion can be described by constructing a model for a generic electrical heat engine (see Fig. 21). There, a load with resistance  $R_L$  is driven by the power drawn from the thermoelectric element across which there is a temperature difference  $\Delta T$ . The power dissipated on the load is  $P = IV = R_L I^2$ , whereas the voltage across the thermoelectric element is  $-IR_L$ . Plugging this into Eq. (127) yields

$$I = -\frac{\tilde{\alpha}}{T(1 + GR_L)}\Delta T. \quad (128)$$

The extracted power hence is

$$P = \frac{R_L \tilde{\alpha}^2 (\Delta T)^2}{T^2 (1 + GR_L)^2}. \quad (129)$$

On the other hand, the thermoelectric element extracts heat from the temperature difference, i.e., trying to balance it, with the power

$$\dot{Q} = \left( G_{\text{th}} - \frac{\tilde{\alpha}^2 R_L}{T(1 + GR_L)} \right) \Delta T. \quad (130)$$

The efficiency of thermoelectric conversion is hence

$$\eta = \frac{P}{\dot{Q}} = \frac{\Delta T}{\underbrace{T_{\text{hot}}}_{\eta_{\text{Carnot}}}} \frac{GR_L}{(1 + GR_L)^2} \frac{1}{1/N - \frac{GR_L}{1 + GR_L}}, \quad (131)$$

where  $N = \tilde{\alpha}^2 / (G_{\text{th}} GT) \leq 1$ . Alternatively, we can write  $N$  in terms of the usual thermoelectric figure of merit,

$$ZT \equiv \frac{N}{1 - N} = \frac{\tilde{\alpha}^2}{G_{\text{th}} GT - \tilde{\alpha}^2} = \frac{S^2 GT}{\tilde{G}_{\text{th}}}, \quad (132)$$

where  $S = \tilde{\alpha} / (GT)$  is the thermopower (Seebeck coefficient) and  $\tilde{G}_{\text{th}} = G_{\text{th}} - \tilde{\alpha}^2 / (GT)$  is the thermal conductance at a vanishing current.

Now we should choose  $R_L$  to optimize the device. For example, the maximum efficiency is obtained with  $GR_L = 1 / \sqrt{1 - N} = \sqrt{1 + ZT}$  yielding

$$\max \eta = \eta_{\text{Carnot}} \frac{\sqrt{1 + ZT} - 1}{\sqrt{1 + ZT} + 1}. \quad (133)$$

This result is consistent with that obtained in Ref. [246] in the linear response limit  $T_{\text{cold}} / T_{\text{hot}} \approx 1$ . On the other hand, optimizing the device to yield a maximum power output requires  $GR_L = 1$ , corresponding to the limit [247, 248]

$$\eta = \frac{\Delta T}{\underbrace{2T}_{\eta_{CA}}} \frac{ZT}{2 + ZT}. \quad (134)$$

Here  $\eta_{CA} \equiv 1 - \sqrt{T_{\text{cold}} / T_{\text{hot}}} \approx \Delta T / (2T)$  is the maximum efficiency obtained when  $ZT \rightarrow \infty$ . Both of these efficiencies are maximized when the thermoelectric figure of merit becomes large.

Above room temperature, the highest figures of merit are obtained in certain strongly doped semiconductor structures [249, 250]. The record values are of the order of  $ZT \gtrsim 1 \dots 2$ . The particular value and the optimal temperature where it is obtained results from a competition of two generic temperature dependencies: that of phonon heat conductance, and that of the (typically activated) process yielding the thermopower. Both of these decrease towards low

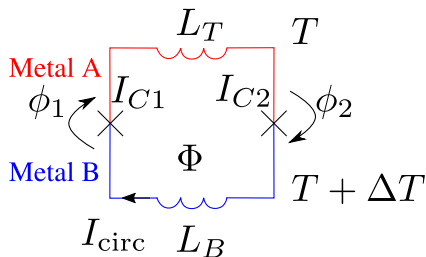


Figure 22: Setup for measuring the thermoelectrically induced circulating current in a bimetallic loop formed by two different superconducting metals A and B. In this case the contact between the metals becomes a Josephson junction.

temperatures, but the previous decreases as a power law, whereas the latter decreases exponentially. In an electron system the heat conductance is typically close to the Wiedemann-Franz limit  $G_{\text{th}}^{\text{el}} \approx \mathcal{L}GT$ , where  $\mathcal{L} = \pi^2 k_B^2 / (3e^2)$ . The total heat conductance is obtained from the sum of the electronic and phononic contributions,  $G_{\text{th}} = G_{\text{th}}^{\text{el}} + G_{\text{th}}^{\text{ph}}$ . Since  $ZT \propto GT/G_{\text{th}} = 1/[\mathcal{L} + G_{\text{th}}^{\text{ph}}/(GT)]$ , the only way to improve this is to minimize the phononic contribution. Generally the latter decreases towards low temperatures faster than linearly. However, the thermopower is typically an exponential function of temperature,  $S \propto \exp(-\Delta/k_B T)$  as the best thermoelectrics contain a gapped dispersion with the gap  $\Delta$ . Therefore, the optimal  $ZT$  takes place at a temperature which is some fraction of  $\Delta$ . As shown in Sec. 5.4 (see in particular Fig. 28), the same is true for a normal metal island coupled to spin-split superconductors. In that case, the magnitude of  $\Delta$  is just orders of magnitude lower than in semiconductor structures.

### 5.2. Thermoelectric effects in superconductors

Research on thermoelectric effects in superconductors dates back to the 1920's, when Meissner [240] concluded them to be absent because any thermoelectric current is cancelled by a counterflowing supercurrent. Ginzburg [241] showed that this is no longer the case in multiply connected bimetallic superconducting structures. This is because the presence of supercurrent is linked to the gradient of the phase of the order parameter, and in multiply connected structures uniqueness of the order parameter imposes a constraint on the relation between the flux through the ring and the circulating supercurrent. This situation can be visualized as in Fig. 22. For definiteness, let us consider a bimetallic superconducting loop, where the thermoelectric effects mostly take place at the two contacts. The current through contact  $i = 1, 2$  consists of a sum of the supercurrent and the thermoelectric current, i.e.,

$$I_o = I_{ci} \sin(\varphi_i) + I_{\text{th},i}. \quad (135)$$

In a closed circuit this current must equal for both junctions, and thereby it yields a relation between the phases  $\varphi_{1,2}$ . A second relation fixing the phases



is obtained in the presence of a flux  $\Phi$  through the loop with inductance  $L = L_T + L_B$ . Without loss of generality the total loop inductance can be described with a single quantity. Namely, the phases must be fixed so that they minimize the energy

$$\frac{\hbar^2}{8e^2L} \left( n2\pi + 2\pi \frac{\Phi}{\Phi_0} - \varphi_1 - \varphi_2 \right)^2 - \frac{\hbar}{2e} \sum_{i=1,2} I_{ci} \cos(\varphi_i), \quad (136)$$

where  $n \in \mathbb{Z}$ ,  $\Phi$  is the magnetic flux through the junction and  $\Phi_0 = h/(2e)$  is the flux quantum. In the following we denote  $\Phi/\Phi_0 = f + 2\pi(m - n)$  with  $f \in [0, 2\pi[$  and  $m \in \mathbb{Z}$ . For  $f \ll 1$  and  $I_{th,i} \ll I_{c,i}$ , the induced phases are small, and we may linearize the current-phase relations. As a result, we obtain a circulating current

$$I_{\text{circ}} = \frac{f + 2m\pi + \frac{I_{th,1}}{I_{c1}} + \frac{I_{th,2}}{I_{c2}}}{2eL_{\text{tot}}/\hbar}, \quad (137)$$

where  $L_{\text{tot}} = L + \hbar(I_{c1}^{-1} + I_{c2}^{-1})/2e$  is the total inductance of the superconducting loop.

Let us assume heating the lower superconductor of the bimetallic loop so that the temperature increases from  $T$  to  $T + \Delta T$ . Such a heating induces thermoelectric currents

$$I_{th,1} = \tilde{\alpha}_1 \Delta T/T, \quad I_{th,2} = -\tilde{\alpha}_2 \Delta T/T. \quad (138)$$

This produces a circulating thermoelectric current

$$I_{\text{circ}}^{\text{th}} = \hbar \frac{\frac{\tilde{\alpha}_1}{I_{c1}} - \frac{\tilde{\alpha}_2}{I_{c2}}}{2eL_{\text{tot}}} \frac{\Delta T}{T}. \quad (139)$$

It can be measured for example by placing a SQUID on top of the bimetallic loop, and measuring the induced flux  $\Phi_{\text{ind}} = MI_{\text{circ}}$ , where  $M$  is the mutual inductance between the two systems.

The size of the coefficient  $\tilde{\alpha}$  was calculated in Ref. [242] to be

$$\tilde{\alpha} = \tilde{\alpha}_N G(\Delta/T), \quad G(x) = \frac{3}{2\pi^2} \int_x^\infty \frac{y^2 dy}{\cosh^2(y/2)}, \quad (140)$$

where the latter form is due to the reduction of the quasiparticle density in the superconducting state, and  $\tilde{\alpha}_N$  is the size of the thermoelectric coefficient in the normal state. The precise value of  $\tilde{\alpha}_N$  depends on the exact electronic spectrum of the metals in question and its calculation needs extending the theory beyond the quasiclassical approximation employed in this review, as within that approximation  $\tilde{\alpha}_N = 0$ . For a quadratic dispersion  $\tilde{\alpha}_N = \frac{\pi^2 G_T k_B^2 T}{6eE_F}$ , where  $E_F$  is the Fermi energy. At temperatures  $T \ll \Delta/k_B$ ,  $\tilde{\alpha}$  is thus a product of two small coefficients,  $\tilde{\alpha}_N \propto k_B T/E_F$ , and  $G(\Delta/T)$ . Such a small  $\tilde{\alpha}$  is not easy to

measure quantitatively. Because of many spurious effects in such measurements, it is not simple to make the experiments agree quantitatively with this theory.

Nevertheless, at least close to the critical temperature the thermoelectric flux should be observable, and the first experiments to measure it were done in the 1970s and early 1980s. One set of experiments [251, 252] followed the idea of Ref. [253] and measured the thermoelectric voltage across a superconductor–normal-metal–superconductor contact as the thermoelectric current exceeded its Josephson critical current. The results of these experiments are in line with the expected magnitude of the thermoelectric signal. On the other hand, Ref. [254] measured the thermoelectrically generated flux in a bimetallic loop formed from superconducting Pb and Ti, close to the critical temperature of the latter. These experiments are also discussed in Ref. [255]. Surprisingly, the experiments demonstrated fluxes five orders of magnitude larger than predicted by theory. This discrepancy annoyed Ginzburg so much that he devoted an entire chapter on the topic in his Nobel colloquium [256].

Recently, Ref. [257] claim to have solved this discrepancy with new experiments performed on much smaller superconducting loops than what was possible in the early 1980s. According to them, the discrepancy originated from the temperature dependence of the inductances  $L_{\text{tot}}$  and  $M$  as well as the flux  $f$  (via the effective area of the loop), and hence they change as one end of the bimetallic loop is being heated. This produces additional contributions to the thermoelectric flux,

$$\begin{aligned} \Phi_{\text{ind}} = \Phi_{\text{ind}}^{\text{th}} & \qquad (141) \\ + \frac{1}{L_{\text{tot}}} & \left[ \left( \frac{dM}{dT} - M \frac{dL_{\text{tot}}}{dT} \right) (f + 2m\pi) + M \frac{df}{dT} \right] \Delta T. \end{aligned}$$

The additional contributions are in practice much larger than the pure thermoelectric effect. According to Ref. [257], whereas the effects from  $f$  can be accounted for by measuring the period of oscillations as the external flux is altered, the effects due to the trapped flux, accounted for by  $m$ , is much harder to deduce, and was likely the reason for the discrepancy, as in the early measurements a geomagnetic field amounted to  $m \sim 10^6$ . Using much smaller loops, Ref. [257] were able to control the number of trapped flux quanta, and hence get rid of the spurious effects. The remaining thermoelectric flux that they observed is more or less in accord with the value obtained from the above theory. However, the temperature dependence of the measured flux depends, besides  $G(x)$  above, also on the temperature dependent inductance, and on the temperature dependence of the main heat contact between the heated electrons and the phonon bath, so the measurement could not directly deduce  $G(x)$ .

The conclusion from these theory and experimental works is that in conventional superconductors thermoelectric effects can be nonzero, but they are extremely weak, and therefore difficult to access. However, other types of superconducting heterostructures besides the bimetallic loop do contain relatively strong thermoelectric effects. In particular, a supercurrent flowing along a temperature gradient leads to an appearance of charge imbalance [187, 258, 185],

which can be measured [186] for example via a non-local geometry similar to those discussed in Sec. 4. A similar type of an effect was found in Andreev interferometers [259, 260, 261] composed of a hybrid multiterminal geometry of a normal metal in contact with a superconducting loop. These effects were considered theoretically in Refs. [262, 263, 264, 265]. Similar effects are also predicted in ballistic systems as discussed in Refs. [266, 267]. Nevertheless, these effects either require complicated multiterminal geometries, and otherwise the thermoelectric effects are typically very weak.

In what follows we show how this situation can be completely reversed in the presence of the spin-splitting field, provided we add a second ingredient into the theory: spin filtering. In this case such superconductor/ferromagnet hybrids can become almost ideal thermoelectric devices. In particular, Ref. [29, 244] showed how three-terminal proximity-coupled superconductor-ferromagnet devices can show non-local thermoelectric effects: in this case the density of states (DOS) in a normal metal coupled both to a superconductor and a ferromagnet becomes spin dependent, and the spin-resolved DOS is also electron-hole asymmetric, resulting in the strong thermoelectric effect. On the other hand, Ref. [268, 269] showed how a metallic bilayer consisting of two superconductors or a superconductor and a normal metal, separated by a spin-active interface (i.e., an interface whose transmission properties are characterized by a spin-dependent scattering matrix), can exhibit large thermoelectric response. Around the same time, Ref. [243] showed how a superconductor with a spin-splitting field, tunnel coupled to a normal metal via a spin-polarized interface, exhibits a thermoelectric effect where the figure of merit can become very large. To our knowledge, only this mechanism has been so far accessed experimentally [177, 245]. We explain this mechanism in more detail below.

Another way to affect the thermoelectric response via magnetism was discussed in Ref. [232] and later in Ref. [270], who argued how magnetic impurities inside a superconductor enhance the thermoelectric coefficient by a large factor  $k_F \ell$  compared to  $\tilde{\alpha}$  in Eq. (140). Here  $\ell$  is the elastic mean free path and  $k_F$  is the Fermi wavenumber. This effect results from the electron-hole asymmetric Andreev states forming in the vicinity of the magnetic impurities.

The above discussion concerns metallic structures. In semiconductor quantum dots the thermoelectric effects can be large when the spectrum of the quantum dot is electron-hole asymmetric [271], even without the presence of superconductivity or magnetism. Theoretical studies showed that the combination of the latter affects the symmetries and may increase the thermoelectric response in quantum dots coupled to superconducting and magnetic electrodes [272, 273].

### 5.3. Thermoelectric effects at a spin-polarized interface to a spin-split superconductor

Tunneling into superconductors has been long used to probe the superconducting density of states [58], for thermometry [128], and for measuring the nonequilibrium distribution functions [274]. We show below that a *spin-polarized* tunnel contact to a superconductor with a spin-splitting field also ex-

hibits a giant thermoelectric effect. Let us denote the spin-dependent normal-state conductance of the tunnel contact by  $G_{\uparrow/\downarrow}$  for spin  $\uparrow / \downarrow$ . In this case the standard tunneling theory yields the spin-resolved charge and heat currents across the tunnel contact from reservoir  $R$  to the spin-split superconductor

$$I_{\sigma} = \frac{G_{\sigma}}{e} \int_{-\infty}^{\infty} dE N^R(\varepsilon - \mu_R) N_{\sigma}(\varepsilon - \mu_L) [f_R(\varepsilon) - f_S(\varepsilon)] \quad (142)$$

$$\dot{Q}_{\sigma}^i = \frac{G_{\sigma}}{e^2} \int_{-\infty}^{\infty} d\varepsilon (\varepsilon - \mu_i) N^R(\varepsilon - \mu_R) N_{\sigma}(\varepsilon - \mu_L) [f_R(\varepsilon) - f_S(\varepsilon)]. \quad (143)$$

The formula for the current is thus the spin-resolved version of Eq. (3). Here  $f_{L/R} = n_F(E - \mu_{L/R}; T_{L/R})$ ,  $n_F(E; T) = \{\exp[E/(k_B T)] + 1\}^{-1}$  are the (Fermi) functions of the reservoirs biased at potentials  $\mu_{L/R}$  and temperatures  $T_{L/R}$ . We assume the reduced density of states  $N^R(\varepsilon)$  (i.e., total density of states at energy  $\varepsilon$  divided by the one at the Fermi energy) of reservoir  $R$  spin independent for simplicity; the possible splitting of the Fermi sea in electrode  $R$  is included in  $G_{\sigma}$ . The reduced density of states in the superconductor for spin  $\sigma$  is  $N_{\sigma}(\varepsilon)$ . The heat current  $\dot{Q}_{\sigma}^i$  is calculated separately for  $i = R, S$ , using the potential  $\mu_{R/S}$ , because the two heat currents differ by the Joule power  $I(\mu_R - \mu_S)/e$ . Let us denote the spin-dependent reduced density of states via  $N_+ = N_{\uparrow} + N_{\downarrow}$  and  $N_- = N_{\uparrow} - N_{\downarrow}$  and define the total tunneling conductance  $G_T = G_{\uparrow} + G_{\downarrow}$  and spin polarization  $P = (G_{\uparrow} - G_{\downarrow})/G_T$ . In that case the spin-averaged tunnel currents  $I = I_{\uparrow} + I_{\downarrow}$  and  $\dot{Q}^i = \dot{Q}_{\uparrow}^i + \dot{Q}_{\downarrow}^i$  are

$$I = \frac{G_T}{2e} \int_{-\infty}^{\infty} d\varepsilon N_R(N_+ + PN_-)(f_R - f_S) \quad (144)$$

$$\dot{Q}_i = \frac{G_T}{2e} \int_{-\infty}^{\infty} d\varepsilon (\varepsilon - \mu_i) N_R(N_+ + PN_-)(f_R - f_S). \quad (145)$$

In the following, we first analyze these currents in detail, and then discuss a method of building a near-optimal heat engine based on such junctions. In particular, we use the densities of states described in Sec. 3. We first disregard the spin relaxation effects on the density of states, because this assumption allows for some analytically treatable limits and because it is a fair approximation for example for Al. This assumption is lifted in Fig. 31.

#### *Heat current beyond linear response*

Let us consider first the case when the reservoir  $R$  is a normal metal and therefore  $N_R(\varepsilon) = 1$ . The heat current  $\dot{Q}$  describing the cooling of the normal metal is positive at voltages  $eV = (\mu_R - \mu_S) \approx \Delta$  even without spin splitting, i.e., the work done by the voltage source can be used to cool the normal metal [275, 276, 277]. However, that heat current is even in the voltage, and therefore it does not result from the usual Peltier effect (Eq. (127) for  $\dot{Q}$ ) where the cooling power is linear in voltage, and therefore can be reversed by reversing the sign of the voltage. As we show below, in the presence of spin polarization

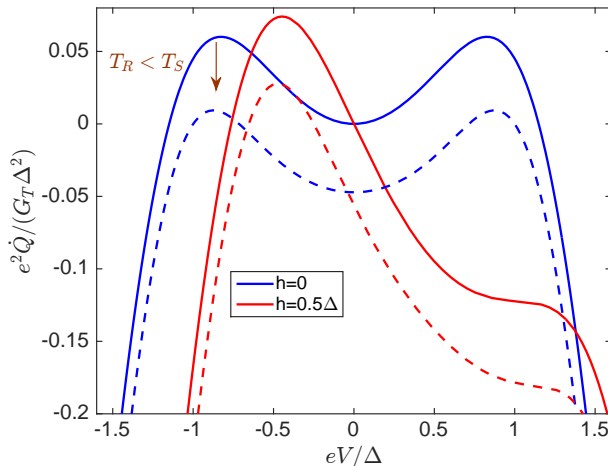


Figure 23: Cooling power vs. voltage without (blue line) and with (red) an exchange field in the superconductor, assuming a unit polarization  $P = 1$ . The solid lines are plotted for  $T_R = T_S = 0.3\Delta/k_B$ , and the dashed lines for  $k_B T_R = 0.22\Delta$  and  $k_B T_S = 0.3\Delta$ . Changing the sign of  $P$  or  $h$  inverts the voltage dependence with respect to  $V = 0$ .

$P$  and with a non-zero spin-splitting field  $h$  in the superconductor, the cooling power obtains also components that are odd in voltage, in analogy with the usual Peltier coolers. This leads to an improved coefficient of performance of electron refrigeration [39, 278].

The cooling power from reservoir  $R$  as a function of voltage is shown in Fig. 23 with and without an exchange field, assuming the ideal case of unit spin polarization  $P = 1$ . The figure also shows how decreasing the normal-metal temperature lowers the cooling power. In the absence of extra heating or energy relaxation processes, the normal-metal temperature at the given voltage would then be fixed to the value nullifying the cooling power.

In an electron refrigerator, the cooled element is an island coupled to two electrodes. Let us consider a normal-metal island playing the role of the reservoir  $R$ , and coupled to two spin-split superconductors via ferromagnetic insulators with polarizations  $P_L$  and  $P_R$ , respectively. The optimal situation is realized when  $P_L = -P_R = \pm 1$  or when the exchange fields in the two superconductors are reversed. The total cooling power from the island is  $\dot{Q}_N = \dot{Q}_R(V/2, P_L) + \dot{Q}_R(-V/2, P_R)$ . It works against other relaxation mechanisms, so that the stationary temperature  $T$  of reservoir  $R$  is determined from heat balance [128],

$$\dot{Q}_N(T, T_S) = \Sigma_N \Omega_N (T_{\text{bath}}^5 - T^5). \quad (146)$$

Here we assume that the dominant heat relaxation mechanism on the reservoir  $R$  with volume  $\Omega_N$  is due to electron-phonon interaction with strength  $\Sigma_N$ , described by Eq. (45). In addition, we assume that the spin accumulation on the island, produced by the nonequilibrium driving, is negligibly small due to

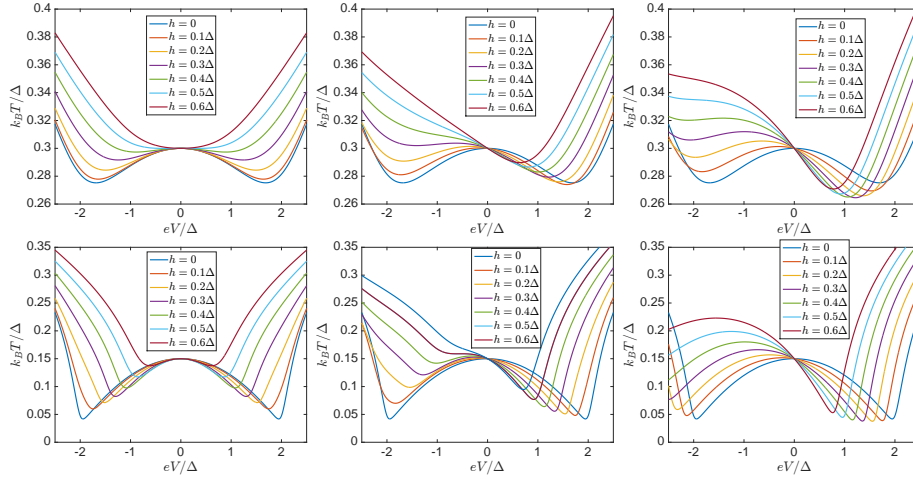


Figure 24: Electron temperature obtained with the S-FI-N-FI-S electron refrigerator as a function of voltage applied across the structure, for different strengths of the exchange field  $h$  inside the superconductor. Top:  $k_B T = 0.3\Delta$  and bottom:  $k_B T = 0.15\Delta$ ; left:  $P = 0$ , middle:  $P = 0.5$  and right:  $P = 1$ . The electron-phonon coupling strength was chosen to be  $\Sigma\Omega = 100G_T k_B^5 / (e^2 \Delta^3)$ .

spin relaxation. The assumptions relevant for this limit are discussed in Sec. 5.5 below.

The resulting island temperatures are shown in Fig. 24 for different parameters of the S-FI-N-FI-S junction. We have chosen the parameters so that for  $h = P = 0$  they correspond to a typical  $T(V)$  curve found experimentally (see for example [276]). In the absence of spin filtering,  $P = 0$ , temperature obtains a minimum at  $eV \approx 2(\Delta - h)$ , and  $T(V)$  is a symmetric function of voltage. Generally, spin splitting in this case makes the cooling worse, so that the minimum reached temperature is higher than in its absence.

The behavior of  $T(V)$  changes in the presence of spin filtering,  $P \neq 0$ . In particular, the curve becomes non-symmetric, and there is cooling even in the linear response regime, i.e., low voltages. This Peltier effect is discussed more below. In addition, the minimum reached electron temperature is generally lowered by an increasing  $P$ , and for a large  $P \approx 1$ , the lowest temperature may be obtained at a non-zero exchange field. However, this effect seems rather weak for the considered parameters.

One possibly relevant aspect of such a magnetic cooler is the fact that the optimum temperature is obtained at a lower absolute value of the voltage [39]. This translates into a somewhat lowered Joule power injected to the device. As this heat is dumped into the superconductor, at the lowest temperatures the heating of the superconductor becomes the dominant limiting obstacle for cooling instead of the electron-phonon coupling [279, 280]. The consequences of this are analyzed in [278].

Besides the normal metal, the magnetic element can be used to refrigerate

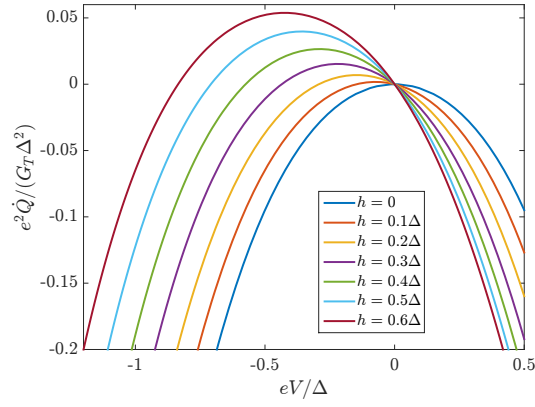


Figure 25: Cooling power from the superconductor in a N-FI-S contact with a superconductor containing a spin-splitting field  $h$ . Here  $P = 1$  and  $k_B T = 0.3\Delta$ , close to the maximum cooling power. Negative cooling power corresponds to heating.

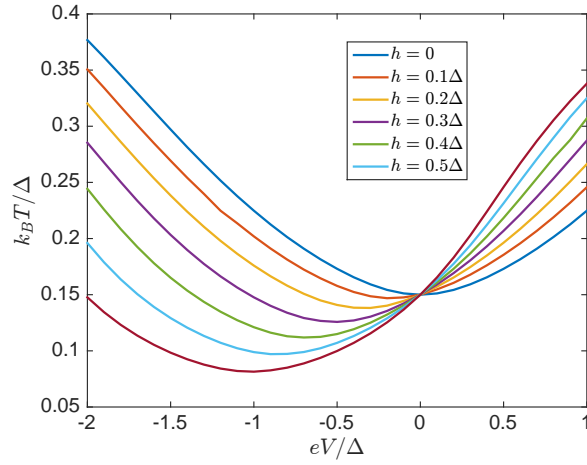


Figure 26: Temperature of the spin-split superconducting island in contact with two normal or ferromagnetic electrodes via spin filters of polarizations  $P = 1$  and  $P = -1$ , respectively. The magnitude of the spin-splitting field  $h$  is indicated in the legends. The calculation was done with the electron-phonon coupling strength  $\Sigma\Omega = 100G_T k_B^3 / (e^2 \Delta^3)$ .

the superconductor [278, 281]. We illustrate this by plotting the cooling power of the superconductor in the case of an N-FI-S junction in Fig. 25. Without spin splitting and a spin-polarized interface, the cooling power is always negative, i.e., corresponding to heating. However, since the Peltier cooling with a non-zero  $P$  is linear in voltage, it has to result to a non-vanishing cooling power also from the superconductor. The maximum cooling power is less than in the case of cooling the normal metal (Fig. 23). However, as indicated in Fig. 26, the resulting temperature drop is nevertheless appreciable because the energy gap also weakens the electron-phonon coupling (see Eq. (46)).

#### 5.4. Linear response and a heat engine

In the presence of non-vanishing spin polarization  $P$  and spin-splitting field  $h$ , the heat current has a linear component in voltage  $V$ . This Peltier effect is visible in the  $h \neq 0$  curves in Figs. 23 and 25. In what follows, let us concentrate on low voltages and small temperature differences  $eV, k_B\Delta T \ll \Delta$ , so that the response of the junction can be described by the linear-response scheme as in Eq. (127). At low temperatures  $k_B T \ll \Delta - h$  the thermoelectric coefficients can be evaluated analytically and they are [243]

$$G \approx G_T \sqrt{2\pi\tilde{\Delta}} \cosh(\tilde{h}) e^{-\tilde{\Delta}}, \quad (147a)$$

$$G_{\text{th}} \approx \frac{k_B G_T \Delta}{e^2} \sqrt{\frac{\pi}{2\tilde{\Delta}}} e^{-\tilde{\Delta}} \left[ e^{\tilde{h}} (\tilde{\Delta} - \tilde{h})^2 + e^{-\tilde{h}} (\tilde{\Delta} + \tilde{h})^2 \right], \quad (147b)$$

$$\tilde{\alpha} \approx \frac{G_T P}{e} \sqrt{2\pi\tilde{\Delta}} e^{-\tilde{\Delta}} \left[ \Delta \sinh(\tilde{h}) - h \cosh(\tilde{h}) \right], \quad (147c)$$

with  $\tilde{\Delta} = \Delta/(k_B T)$  and  $\tilde{h} = h/(k_B T)$ . In an open-circuit configuration ( $I = 0$ ) one rather measures the thermopower

$$S = \frac{\tilde{\alpha}}{G_T} \approx \frac{P\Delta}{eT} [\tanh(\tilde{h}) - h/\Delta]. \quad (148)$$

It is maximized for  $h = k_B T \text{arcosh}[\Delta/(k_B T)]$ , where

$$S_{\text{max}} \approx \frac{k_B}{e} P \left[ \frac{\Delta}{k_B T} - \text{arcosh} \left( \sqrt{\frac{\Delta}{k_B T}} \right) \right]. \quad (149)$$

At low temperatures the thermopower can thus become very large, and within the above scheme it would even diverge for  $k_B T \rightarrow 0$ . However, in practice this divergence would be cut off via either circuit effects (at  $T \rightarrow 0$  the conductance would also tend to zero) or for example the spin relaxation neglected above. Nevertheless, with proper circuit design one should be able to measure a thermopower much exceeding  $k_B/e$  in this setup.

The prediction for the strong thermoelectric effect was confirmed by a recent experiment by [177] via the measurement of the thermoelectric current  $I = -\tilde{\alpha}\Delta T/T$ . This thermoelectric effect also provides a partial explanation [35] for the measurements of the long-range non-local spin signal [31, 38]. In what



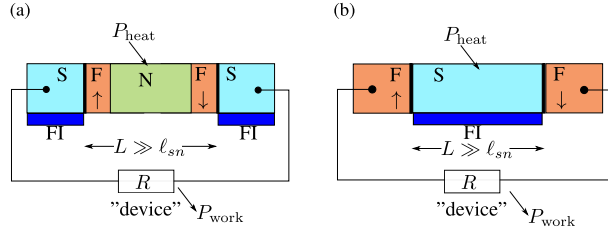


Figure 27: Two realizations of a superconductor/ferromagnet heat engine, where a heating power  $P_{\text{heat}}$  leading to a temperature increase in the absorber can be converted to electrical power  $P_{\text{work}}$  and dissipated in the "device" connected to the heat engine. In both cases the setup requires two junctions with antiparallel magnetization directions. The ferromagnetic insulator FI has a magnetization direction along with the two spin-polarized contacts. To disregard spin accumulation, the island has to be large compared to the spin relaxation length. a) Heat engine with a normal-metal heat absorber. b) Heat engine with a spin-split superconducting island. The ferromagnets can also be replaced by a normal metal if the interfaces to the superconductor contain a ferromagnetic insulator.

follows, we consider the possibility of realizing a true heat engine with a large figure of merit. We discuss this in the case where either a normal metal or the spin-split superconductor realizes an island and therefore works as the heat absorber, see Fig. 27.

Let us first assume that it is only the electrons of the ferromagnetic island that are heated, instead of both the electrons and phonons.<sup>9</sup> In this case the figure of merit of the heat engine is limited by the spurious heat conduction due to the electron-phonon coupling, with heat conductance  $G_{e\text{-ph}} = 5\Sigma\Omega T^4$  [see Eq. (45)], and from the heat conductance to the extra superconducting electrodes  $S$ , with an exponentially suppressed heat conductance, provided the heating current is small. In this case the heat engine has an efficiency described by a figure of merit that for  $k_B T \ll h$  and  $P \neq 1$  tends to

$$ZT = \frac{P^2 \pi (\Delta - h)^2 \Delta^4}{g e^{(\Delta - h)/(k_B T)} T^5 \sqrt{k_B T \Delta} + (1 - P^2) \pi (\Delta - h)^2 \Delta^4 + \pi \Delta^4 (h + \Delta)^2 e^{-2h/(k_B T)}}, \quad (150)$$

where  $g = 5k_B^5 \sqrt{2\pi} e^2 \Sigma \Omega \Delta^3 / (2G_T)$  is a dimensionless quantity characterizing the strength of electron-phonon coupling. Here we take into account the fact that the thermoelectric effect takes place across both contacts, and hence all quantities except the spurious heat conduction channel are doubled. If we do not describe half-metals, i.e.,  $1 - P^2 \gg (h + \Delta)^2 / (h - \Delta)^2 \exp[-2h/(k_B T)]$ , we can simplify this more by dropping the last term in the denominator. We plot this as a function of temperature in Fig. 28 for some representative parameters. For example, for  $\Omega = 0.005 \mu\text{m}^3$ ,  $\Sigma = 10^9 \text{ W } \mu\text{m}^{-3} \text{K}^{-5}$  and  $1/G_T = 3 \text{ k}\Omega$ ,  $g = 100$ . The figure of merit exhibits a peak at around  $k_B T \approx 0.1\Delta$ , and its peak value depends strongly on the relative strength of the spurious heat

<sup>9</sup>The latter would require isolating the phonons of the island from those of the substrate, which can be realized for example by suspending the island.

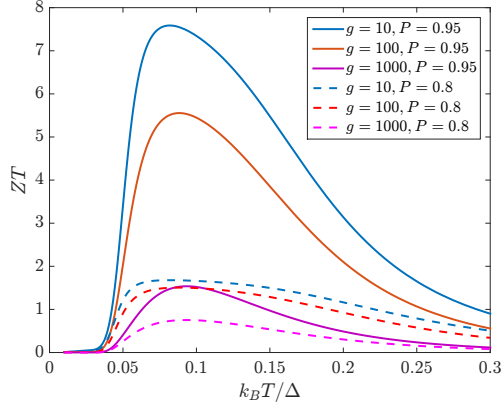


Figure 28: Figure of merit in a S-FI-N-FI-S heat engine as a function of temperature for different magnitudes of the electron-phonon heat conductance, characterized by the coefficient  $g$ , and polarizations  $P$  of the junction. The curves have been calculated with  $h = 0.5\Delta$ , without calculating  $\Delta$  self-consistently. The figure of merit is limited from above by  $P^2/(1 - P^2)$ , which for  $P = 0.95$  is 9.3, and for  $P = 0.8$  it is 1.8.

conduction channels. As seen in the figure, reaching high values for the figure of merit is quite challenging in this way, as besides a high polarization close to one, it requires quite low normal-state resistance of the junctions, a combination not very easy to reach with ferromagnetic insulators.

Note that often such spurious heat conduction mechanism that limit the highest available  $ZT$  are disregarded from the theoretical analysis of the figure of merit, for example in the case of quantum dots [272].

Another possible setting for the heat engine is the one where the island is the spin-split superconductor, and it is connected to normal-metal or ferromagnetic electrodes via spin filters as in Fig. 27(b). In the linear response regime this is otherwise similar to the previous case, except that the electron-phonon coupling inside the island has an exponentially suppressed heat conductance, Eq. (46). In this case, as long as the pure tunneling limit remains valid, and the island volume is not overly large, the low-temperature behavior of  $ZT$  is dictated mostly by the deviation of the polarization from unity as shown in Fig. 29. However, because of the exponentially decaying heat conductance, also in this case other spurious processes besides electron-phonon coupling start to limit  $ZT$ , making it vanish at  $T \rightarrow 0$ . In the case of Fig. 29, the simplest model for them is due to the small but nonvanishing density of states assumed for the superconductor [243], and described by the Dynes parameter  $\Gamma$  [282].<sup>10</sup>

When the heat input into the heat engine is due to electromagnetic radiation coupled to the device, the conversion of this input power to direct charge

<sup>10</sup>All spectral functions, such as the density of states, are calculated here by assuming a nonzero imaginary part of size  $\Gamma$  in the energy. Typically the chosen value for  $\Gamma$  is so small that it does not affect practical quantities. Figure 29 is an exception.

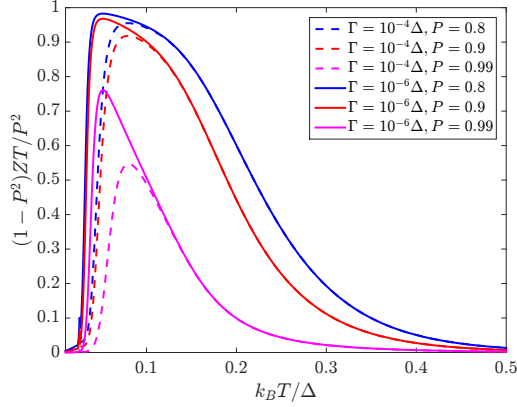


Figure 29: Figure of merit in a N-FI-S-FI-N heat engine as a function of temperature for polarizations  $P$  of the junction. The figure has been calculated with  $h = 0.5\Delta$  and  $g = 1000$ , without calculating  $\Delta$  self-consistently. The figure of merit at low temperatures reaches very close to  $P^2/(1 - P^2)$  unless  $P$  is very close to unity, but the exact temperature scale where this happens depends on the value of polarization. At the lowest temperatures  $ZT$  is limited by another spurious heat conduction process, due to nonzero density of states inside the gap, described here by the Dynes  $\Gamma$  parameter

energy allows realizing a new type of a superconducting thermoelectric detector of radiation [33, 283]. In addition, the thermoelectric effects could be used in non-invasive low-temperature thermometry [34] so that the measured thermovoltage would indicate the temperature profile. At room temperature a scanning thermometer based on thermoelectric effects was realized by [284]. Utilizing spin-polarized tunneling from spin-split superconductors would allow extending this technique to low temperatures.

#### 5.4.1. Effect of spin mixing

Rather than the Dynes parameter, a more relevant limitation of the figure of merit in spin-split superconductors is due to the spin mixing caused by spin-orbit and spin-flip scattering that are disregarded in the above results. This becomes an issue especially in heavy-metal based superconductors where the spin-orbit scattering is strong. As an example, Fig. 30 shows how the figure of merit decays as the spin-orbit relaxation becomes stronger. The high efficiencies are obtained only when the spin relaxation rates are small compared to the gap energy  $\Delta$ . Note that for some materials the stronger spin-orbit relaxation due to the increase in the atomic number  $Z$  (say, compared to Al) is partially compensated by the increased critical temperature and therefore the energy gap.

As shown in in Fig. 31, the suppression of  $ZT$  is monotonous as a function of an increasing spin-orbit scattering. However, in the presence of a non-vanishing Dynes parameter, the spin-flip scattering may also lead to an increased  $ZT$  at low temperatures. For completeness, we also show the effect of spin mixing on the thermopower, i.e., the Seebeck coefficient. The results of the effect of spin-flip scattering are in line with those studied in [285].

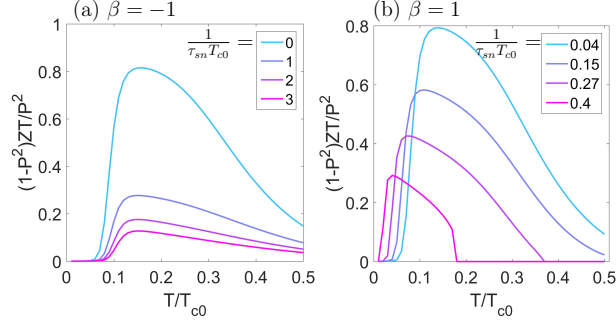


Figure 30: Figure of merit in a N-FI-S-FI-N heat engine as a function of temperature in the presence of (a) spin-orbit mechanism of relaxation with  $\beta = -1$  and (b) spin-flip mechanism of relaxation with  $\beta = 1$ . Thy Dynes parameter is  $\Gamma = 10^{-4}T_{c0}$ , exchange field  $h = 0.5\Delta_0$  and  $P = 0.9$ . Curves in (a,b) correspond to different spin relaxation rates  $1/(\tau_{sn}T_{c0})$ . The electron-phonon coupling is disregarded.

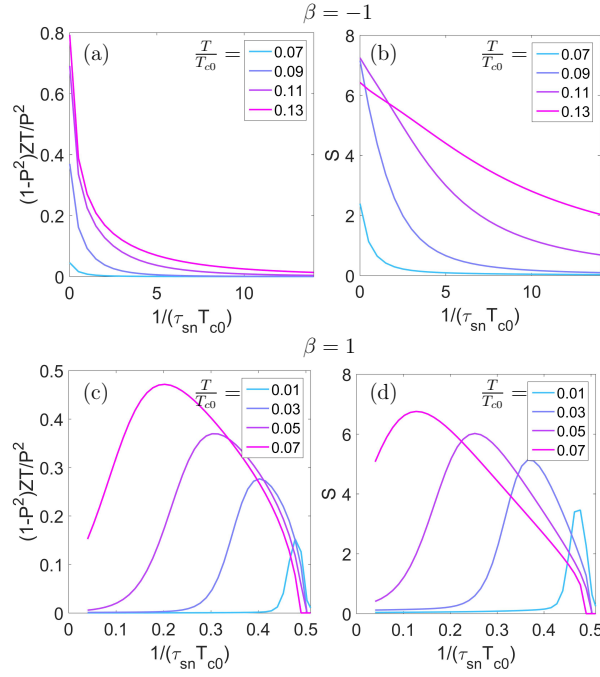


Figure 31: (a,c) Figure of merit in a N-FI-S-FI-N heat engine and (b,d) Seebeck coefficient of the S-FI-N junction as a functions of spin relaxation rate  $\tau_{sn}^{-1}$ . The FI barrier polarization is  $P = 0.9$ , exchange field  $h = 0.5\Delta_0$  and Dynes parameter  $\Gamma = 10^{-4}T_{c0}$ . Panels in the upper row (a,b) correspond to spin-orbit relaxation  $\beta = -1$  and in the lower row (c,d) are for the spin-flip relaxation  $\beta = 1$ . Curves from top to bottom correspond to an increasing temperature. The electron-phonon coupling is disregarded.

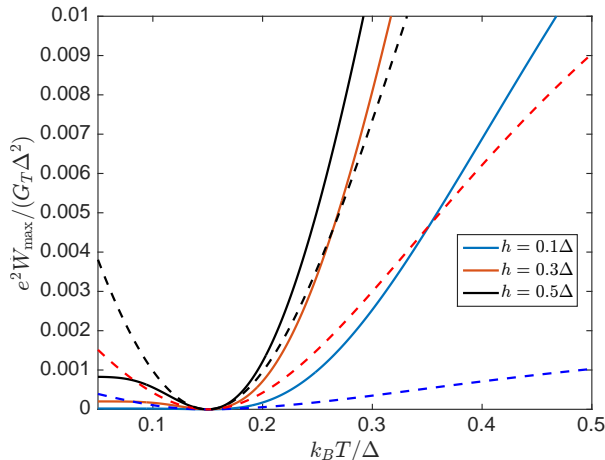


Figure 32: Maximum extractable power from a spin-filter contact to a spin-split superconductor. Solid lines depict the situation with  $T = T_S$ ,  $k_B T_N = 0.15\Delta$ , and dashed lines the one with  $T = T_N$ ,  $k_B T_S = 0.15\Delta$ . The plot has been calculated with  $P = 0.95$ ,  $\Gamma = 10^{-4}\Delta$  and without self-consistency of  $\Delta$  (hence everything should be normalized with respect to  $\Delta(T_S, h)$ ).

#### 5.4.2. Nonlinear response heat engine

The above calculations on the heat engine efficiency have been done in the strict linear response limit  $\Delta T \ll T$ . In this limit both the output power and the Carnot efficiency, proportional to  $\Delta T/T$ , are vanishingly small. However, the device can have a rather large output power and efficiency also at nonlinear response. To illustrate this, we plot the maximum extractable output power  $\dot{W}_{\max} = \max_V(-IV)$  from a N-FI-S junction in Fig. 32 at large differences  $T_S - T_N$  between the spin-split superconductor and a normal-metal reservoir. The output power is somewhat larger for  $T_S > T_N$  than the opposite situation with the same temperature difference. The plotted quantity corresponds to the maximum power that is possible to extract from the junction after optimizing the load resistance — note, however, that this optimized resistance value depends on the exact temperature difference and other parameters. The corresponding efficiency  $\eta = \dot{W}_{\max}/\dot{Q}$  is plotted in Fig. 33. There we take into account only the heat current flowing through the junction itself. The efficiency is reduced if other heat relaxation mechanisms become relevant.

#### 5.4.3. Effect of non-collinear magnetizations

Above we assume that the polarization  $\mathbf{P} = P\hat{u}_P$  of the tunneling contacts is collinear with the exchange field  $\mathbf{h} = h\hat{u}_h$  in the spin-split superconductor. This is the limit that guarantees the largest thermoelectric current, but it is also interesting to consider how non-collinearity would show up in the thermoelectric response, in particular in the coefficient  $\tilde{\alpha}$  of Eq. (147c). This coefficient is by definition a scalar quantity. Therefore, it can only depend on a scalar

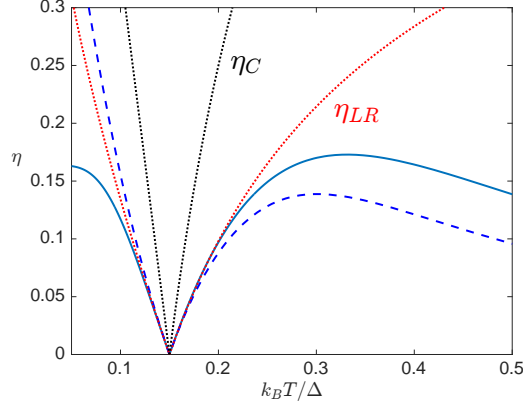


Figure 33: Efficiency of the thermoelectric power conversion of a spin-filter junction to a spin-split superconductor, neglecting spurious contributions to the heat current. Solid lines:  $T = T_S$ ,  $k_B T_N = 0.15\Delta$ , and dashed lines:  $T = T_N$ ,  $k_B T_S = 0.15\Delta$ . The plot has been calculated with  $h = 0.6\Delta$  and otherwise as in Fig. 32. Dotted lines show the Carnot efficiency  $\eta_C = 1 - T_{\text{cold}}/T_{\text{hot}}$  and the linear response result  $\eta_{LR} = ZT/(2 + ZT)(1 - \sqrt{T_{\text{cold}}/T_{\text{hot}}})$ .

combination of the vectors  $\mathbf{P}$  and  $\mathbf{h}$ , or rather,  $\hat{u}_P$  and  $\hat{u}_h$ . This combination is the inner product,  $\hat{u}_P \cdot \hat{u}_h$ . Therefore, the generalization of Eq. (147c) to the non-collinear case is

$$\tilde{\alpha}_{nc} = \hat{u}_P \cdot \hat{u}_h \tilde{\alpha}_c, \quad (151)$$

where  $\tilde{\alpha}_c$  is the thermoelectric coefficient in the collinear case, for example given by Eq. (147c).

### 5.5. Thermally induced spin currents

Besides the large thermoelectric effect discussed above, the contact between spin-split superconductors with other conducting materials can exhibit a large (longitudinal) spin Seebeck effect, where a temperature difference drives spin currents to/from the spin-split superconductor [243]. The spin current  $I_S = I_\uparrow - I_\downarrow$  can be obtained from Eq. (142). In linear response, Eq. (59), it is described by the same coefficient  $\tilde{\alpha}/P = \alpha$  as the thermoelectric coefficient, Eq. (147c), but without the spin polarization  $P$  of the interface. When either of the two materials realizes an island, the spin current can be converted into a spin accumulation  $\mu_z$  that is determined from the balance between thermally induced spin currents and spin relaxation within the island. For weak spin relaxation, the resulting spin Seebeck coefficient  $\mu_z/\Delta T$  can be large [*i.e.*, not proportional to the number of thermally excited quasiparticles  $\sim e^{-(\Delta-h)/(k_B T)}$  as the terms in Eqs. (147a)-(147c)], similar to the thermopower in Eq. (149). The spin currents induced in the case of two spin-split superconductors, and the additional effects of Josephson coupling, magnetization texture and spin-orbit effects are discussed in [286, 287].

The above discussion of the thermoelectric cooling and heat engines disregards the spin accumulation caused by the nonequilibrium biases. This as-

sumption is valid if the overall spin relaxation within the island, described by a spin-flip conductance  $G_{\text{sf}} = e^2 \nu_F \Omega / \tau_{sn}$  is much larger than the conductances of the tunnel junctions. Here  $\nu_F$  is the normal-state density of states in the Fermi level,  $\Omega$  is the volume of the island, and  $\tau_{sn}^{-1}$  is the spin relaxation rate within the island. In the case of a spin-split superconducting island, both the conductance and the spin relaxation rate contain the same exponential term  $\sim e^{-(\Delta-h)/(k_B T)}$ , and for an estimate of the overall magnitude of the effect, it is hence enough to compare  $G_{\text{sf}}$  in the normal state to the normal-state tunnel conductance  $G_T$ . In other words, disregarding the spin accumulation is justified provided  $e^2 \nu_F \Omega / (\tau_{sn} G_T) \gg 1$ . On the other hand, most of the discussion disregards the effect of spin relaxation on the density of states of the spin-split superconductor. As shown in Fig. 31, spin relaxation starts to affect the results when  $\hbar / \tau_{sn} \gtrsim k_B T_c$ . These two constraints can be simultaneously satisfied depending on the precise value of  $\tau_{sn}$ , provided that  $G_T \ll (k_B T_c / \delta_I) e^2 / h$ , where  $\delta_I = 1 / \nu_F \Omega$  is the average energy level spacing on the island. This constraint is always satisfied in tunnel barriers between metallic systems.

To our knowledge, the spin Seebeck effect has not been directly measured in spin-split superconductors driven by a temperature difference. However, outside linear response, this is the effect that causes the long-range spin signal in spin injection experiments as discussed in Sec. 4.2. Besides affecting the nonequilibrium dynamics, the presence of spin accumulation in a superconductor with an exchange field couples to the self-consistency equation for the superconducting order parameter  $\Delta$  as in Sec. 3.7. Ref. [288] utilized this fact and predicted that the thermally induced spin accumulation in a spin-split superconductor can result to changes in the critical temperature: besides only suppressing it at low temperatures, it can enhance the critical temperature at some intermediate temperatures, or even lead to a situation where superconductivity shows up only between two critical temperatures.

This spin Seebeck effect should be contrasted to the analogous phenomenon discussed in non-superconducting materials [289]. There, a major contribution to the spin Seebeck signal comes from the thermally induced spin pumping from ferromagnetic insulators [290].

## 6. Summary

In this work we review the electronic transport properties of superconducting hybrid structures with a spin-split density of states. We mainly focus on ferromagnetic insulator-superconductor systems (FI-S) in which such a splitting field can be achieved without the need of an applied magnetic field. Best FI-S material combinations studied so far are the europium chalcogenides (EuO, EuS and EuSe) together with Aluminum films. Interesting of those materials is that thin films of EuO or EuS can also be used as highly efficient spin filters and therefore they are the best candidates for the realization of the heat engines proposed in Sec. 5.

One of the goals of this review is to provide a complete theoretical framework to study non-equilibrium effects in superconducting structures with spin-split

density of states. In this respect, Sec. 3 gives a detailed introduction to the quasiclassical formalism for diffusive hybrid systems, and a description of the nonequilibrium modes. The advantages of using this formalism are multiple. On the one hand it provides a simple way to identify the quasiparticle nonequilibrium modes. As shown in Sec. 3.1, the combination between superconductivity and magnetism produces, besides the widely studied charge and energy modes, two additional ones: spin and spin energy. The quasiclassical equations show explicitly how all these modes couple to each other in different situations.

On the other hand, quasiclassical kinetic equations are a powerful tool for the study of hybrid multi-terminal systems, with different materials. Effects occurring at hybrid interfaces between different materials can be described by the help of effective boundary conditions. In Sec. 3.4 we discuss this issue and present boundary conditions suitable to describe a S-FI interface. The inclusion of the interfacial spin-orbit effect and the associated coupling between charge and spin would be another interesting further development of the formalism. The extension of the formalism to include additional types of interactions and couplings is in principle rather straightforward. For example, one can include magneto-electric effects associated with the charge-spin coupling in systems with linear-in-momentum spin-orbit coupling, by introducing an effective  $SU(2)$  gauge potential in the quasiclassical equations [291, 292, 112], or, in the case of an extrinsic spin-orbit coupling, by taking into account higher-order terms in the impurity potential [113]. Inclusion of such effects in a non-equilibrium situation and with time-dependent fields, is an interesting further development of the field [293].

We use the power of the quasiclassical approach in Sec. 4, where we study in detail different transport properties of FI-S structures and spin-split superconductors and contrast the results with experimental findings. Both charge and spin dependent properties are determined by the behaviour of the nonequilibrium modes of the superconductor. Specifically we have computed the non-local conductance in a two terminal geometry and the spin Hanle effect in superconductors.

One further perspective of the present work is the extension of the Keldysh quasiclassical formalism used in this review to include magneto-electric effects associated with the spin-orbit coupling (SOC) [291, 292, 112, 113, 111, 293], and the coupling magnetization dynamics to the electronic degrees of freedom via the reciprocal effects of spin transfer torque and spin pumping [227].

In Sec. 4.3.2 we discuss the dynamics of spin-split superconductors in rf fields, and review how nonequilibrium effects induced by them manifest in the quasiclassical theory. Historically, magnetic resonance effects in superconductors are well studied, but fewer experiments have probed spin-split thin films.

Another very interesting aspect in studying superconductors with a spin-split density of states are their thermoelectric properties. In Sec. 5 we focus on thermoelectricity in superconducting structures, both in linear and non-linear regimes and discuss the realization of a heat engine based on FI/S structures. Because of their extremely large thermoelectric figure of merit, using S/FI structures has been proposed for accurate radiation sensing and non-invasive scan-



ning thermometry. These recently proposed applications add up to the the rich physics offered by spin-split superconductors, which have been long used as tools to characterize equilibrium properties of magnets, especially their spin polarization. Most likely there are also many other applications to be uncovered, opened by the possibility for realizing a controlled combination of magnetism and superconductivity. The theoretical framework presented in this review should help in this task.

The major challenge in fabricating real devices is to find FI-S combinations with a large superconducting critical temperature and simultaneously a large spin splitting and efficient spin-filtering. Superconductors with high  $T_c$  usually have larger spin-orbit coupling which leads to a broadening of the spin-split peaks in the density of states, as discussed in Sec. 2. Further material research is needed in this respect in order to find optimal material combinations.

Finally, the phenomena discussed in this review have a direct impact on several fields of condensed matter and quantum technologies, as for example the design of hybrid quantum materials and their use in functional devices. Transport properties of such systems can be controlled by the temperature or by external fields, and to interpret measurements it is essential to understand their nonequilibrium properties, which in turn depend on the quality of interface growth and material combination. This review provides most of the theoretical tools for such analysis.

## Acknowledgments

We thank Faluke Aikebaier, Marco Aprili, Detlef Beckmann, Wolfgang Belzig, Irina Bobkova, Alexander Bobkov, Giorgio De Simoni, Matthias Eschrig, Yuri Galperin, Francesco Giazotto, Vitaly Golovach, Alexander Mel'nikov, Jagadeesh Moodera, Risto Ojajärvi, Asier Ozaeta, Charis Quay, Jason Robinson, Mikel Rouco, and Elia Strambini for useful discussions. This work was supported by the Academy of Finland Center of Excellence (Project No. 284594), Research Fellow (Project No. 297439) and Key Funding (Project No. 305256) programs and project number 317118, the European Research Council (Grant No. 240362-Heatronics), the Spanish Ministerio de Ciencia, Innovacion y Universidades (MICINN) (Project No. FIS2017-82804-P), the European Research Council under the European Union's Seventh Framework Program (FP7/2007-2013)/ERC Grant agreement No. 615187-COMANCHE, Horizon 2020 and innovation programme under grant agreement No. 800923-SUPERTED.

## List of Symbols

$S$	superconductor
$FI$	ferromagnetic insulator
$G_T$	tunneling conductance

$\nu_F$	normal-state density of states (per spin) at the Fermi level
$D$	diffusion constant
$\sigma_N = 2e^2\nu_F D$	normal-state conductivity in a diffusive wire
$\check{g}$	$8 \times 8$ Green's function matrix in Keldysh-Spin-Nambu
$\hat{g}$	$4 \times 4$ Green's function matrix in Spin-Nambu
$N_\sigma(\varepsilon), \sigma = \uparrow, \downarrow$	normalized density of states per spin
$N_+$	$N_\uparrow + N_\downarrow = \text{Re } g_{03}$
$N_-$	$N_\uparrow - N_\downarrow = \text{Re } g_{33}$
$n_F(\varepsilon)$	Fermi distribution function
$f_{eq} = 1 - 2n_F$	quasiclassical equilibrium distribution function
$f_T(\varepsilon)$	non-equilibrium transversal distribution function
$f_L(\varepsilon)$	longitudinal distribution
$f_{Tj}(\varepsilon), j = 1, 2, 3$	spin transversal function
$\sigma_j, j = 1, 2, 3$	Pauli matrices in spin space
$\tau_j, j = 1, 2, 3$	Pauli matrices in Nambu space
$g_{ij}$	$\sigma_i \tau_j$ component of the retarded Green function
$\tau$	elastic relaxation time
$\tau_{sf}$	spin-flip scattering time
$\tau_{so}$	relaxation time at impurities with spin-orbit coupling
$\tau_{sn} = [\tau_{sf}^{-1} + \tau_{so}^{-1}]^{-1}$	normal state spin relaxation time
$R_\square$	barrier resistance per unit area
$\dot{j}_{c,e,s,se}$	charge, energy, spin, spin-energy density currents
$I$	charge current
$\dot{Q}$	energy current
$I_s$	spin current
$\dot{Q}_s$	spin-energy current
$P$	polarization or spin-filter efficiency of FI interface
$\Delta$	superconducting order parameter
$\Delta_0$	value of $\Delta$ at $T = h = 0$ and without spin relaxation

$T_{c0} = \Delta_0/1.76$	BCS critical temperature for $h = 0$ and without spin relaxation
$D$	Diffusion coefficient
$G$	electrical conductance
$G_{th}$	thermal conductance
$\xi_s$	superconducting coherence length

## References

## References

- [1] A. I. Buzdin, Proximity effects in superconductor-ferromagnet heterostructures, *Rev. Mod. Phys.* 77 (2005) 935–976. doi:10.1103/RevModPhys.77.935.
- [2] F. S. Bergeret, A. F. Volkov, K. B. Efetov, Odd triplet superconductivity and related phenomena in superconductor-ferromagnet structures, *Rev. Mod. Phys.* 77 (4) (2005) 1321–1373. doi:10.1103/RevModPhys.77.1321.
- [3] F. S. Bergeret, M. Silaev, P. Virtanen, T. T. Heikkilä, Colloquium: Nonequilibrium effects in superconductors with a spin-splitting field, *Rev. Mod. Phys.* 90 (4) (2018) 041001. doi:10.1103/RevModPhys.90.041001.
- [4] J. Bardeen, L. N. Cooper, J. R. Schrieffer, Theory of superconductivity, *Phys. Rev.* 108 (1957) 1175–1204. doi:10.1103/PhysRev.108.1175. URL <https://link.aps.org/doi/10.1103/PhysRev.108.1175>
- [5] A. I. Buzdin, L. N. Bulaevskii, S. V. Panyukov, Critical-current oscillations as a function of the exchange field and thickness of the ferromagnetic metal (F) in an SFS Josephson junction, *JETP Lett.* 35 (4) (1982) 178. URL [http://jetpletters.ac.ru/ps/1314/article\\_19853.shtml](http://jetpletters.ac.ru/ps/1314/article_19853.shtml)
- [6] V. V. Ryazanov, V. A. Oboznov, A. Yu. Rusanov, A. V. Veretennikov, A. A. Golubov, J. Aarts, Coupling of two superconductors through a ferromagnet: evidence for a  $\pi$  junction, *Phys. Rev. Lett.* 86 (11) (2001) 2427. doi:10.1103/PhysRevLett.86.2427.
- [7] M. Eschrig, Spin-polarized supercurrents for spintronics: a review of current progress, *Rep. Progr. Phys.* 78 (10) (2015) 104501. doi:10.1088/0034-4885/78/10/104501.
- [8] F. S. Bergeret, A. F. Volkov, K. B. Efetov, Induced ferromagnetism due to superconductivity in superconductor-ferromagnet structures, *Phys. Rev. B* 69 (17) (2004) 174504. doi:10.1103/PhysRevB.69.174504.

- [9] F. Bergeret, A. Volkov, K. Efetov, Spin screening of magnetic moments in superconductors, *EPL* 66 (1) (2004) 111. doi:10.1209/epl/i2004-10003-3.
- [10] F. Bergeret, A. L. Yeyati, A. Martin-Rodero, Inverse proximity effect in superconductor-ferromagnet structures: From the ballistic to the diffusive limit, *Phys. Rev. B* 72 (6) (2005) 064524. doi:10.1103/PhysRevB.72.064524.
- [11] M. Y. Kharitonov, A. Volkov, K. Efetov, Oscillations of induced magnetization in superconductor-ferromagnet heterostructures, *Phys. Rev. B* 73 (5) (2006) 054511. doi:10.1103/PhysRevB.73.054511.
- [12] R. Meservey, P. M. Tedrow, Spin-polarized electron tunneling, *Phys. Rep.* 238 (4) (1994) 173–243. doi:10.1016/0370-1573(94)90105-8.
- [13] T. Kontos, M. Aprili, J. Lesueur, F. Genet, B. Stephanidis, R. Boursier, Josephson junction through a thin ferromagnetic layer: negative coupling, *Phys. Rev. Lett.* 89 (13) (2002) 137007. doi:10.1103/PhysRevLett.89.137007.
- [14] T. Tokuyasu, J. A. Sauls, D. Rainer, Proximity effect of a ferromagnetic insulator in contact with a superconductor, *Phys. Rev. B* 38 (1988) 8823–8833. doi:10.1103/PhysRevB.38.8823.
- [15] P. M. Tedrow, J. E. Tkaczyk, A. Kumar, Spin-polarized electron tunneling study of an artificially layered superconductor with internal magnetic field: EuO-Al, *Phys. Rev. Lett.* 56 (1986) 1746–1749. doi:10.1103/PhysRevLett.56.1746.
- [16] X. Hao, J. S. Moodera, R. Meservey, Spin-filter effect of ferromagnetic europium sulfide tunnel barriers, *Phys. Rev. B* 42 (1990) 8235–8243. doi:10.1103/PhysRevB.42.8235.
- [17] M. Tinkham, *Introduction to superconductivity*, Courier Corporation, 1996.
- [18] B. S. Chandrasekhar, A note on the maximum critical field of high-field superconductors, *Appl. Phys. Lett.* 1 (1) (1962) 7–8. doi:10.1063/1.1777362.
- [19] A. M. Clogston, Upper limit for the critical field in hard superconductors, *Phys. Rev. Lett.* 9 (1962) 266–267. doi:10.1103/PhysRevLett.9.266.
- [20] P. Fulde, R. A. Ferrell, Superconductivity in a strong spin-exchange field, *Phys. Rev.* 135 (3A) (1964) A550–A563. doi:10.1103/PhysRev.135.A550.
- [21] A. I. Larkin, Y. N. Ovchinnikov, Inhomogeneous state of superconductors, *Sov. Phys. JETP* 20 (1965) 762–769.

- [22] R. Meservey, P. M. Tedrow, P. Fulde, Magnetic field splitting of the quasi-particle states in superconducting aluminum films, *Phys. Rev. Lett.* 25 (1970) 1270–1272. doi:10.1103/PhysRevLett.25.1270.
- [23] R. Meservey, P. M. Tedrow, R. C. Bruno, Tunneling measurements on spin-paired superconductors with spin-orbit scattering, *Phys. Rev. B* 11 (11) (1975) 4224. doi:10.1103/PhysRevB.11.4224.
- [24] P. M. Tedrow, R. Meservey, Spin-dependent tunneling into ferromagnetic nickel, *Phys. Rev. Lett.* 26 (1971) 192–195. doi:10.1103/PhysRevLett.26.192.
- [25] P. M. Tedrow, R. Meservey, Spin polarization of electrons tunneling from films of Fe, Co, Ni, and Gd, *Phys. Rev. B* 7 (1) (1973) 318. doi:10.1103/PhysRevB.7.318.
- [26] D. Paraskevopoulos, R. Meservey, P. M. Tedrow, Spin polarization of electrons tunneling from *3d* ferromagnetic metals and alloys, *Phys. Rev. B* 16 (1977) 4907–4919. doi:10.1103/PhysRevB.16.4907.
- [27] R. Meservey, D. Paraskevopoulos, P. M. Tedrow, Tunneling measurements of conduction-electron-spin polarization in heavy rare-earth metals, *Phys. Rev. B* 22 (1980) 1331–1337. doi:10.1103/PhysRevB.22.1331.
- [28] G. De Simoni, E. Strambini, J. S. Moodera, F. S. Bergeret, F. Giazotto, Toward the absolute spin-valve effect in superconducting tunnel junctions, *Nano Lett.* 18 (10) (2018) 6369–6374.
- [29] P. Machon, M. Eschrig, W. Belzig, Nonlocal thermoelectric effects and nonlocal Onsager relations in a three-terminal proximity-coupled superconductor-ferromagnet device, *Phys. Rev. Lett.* 110 (4) (2013) 047002. doi:10.1103/PhysRevLett.110.047002.
- [30] F. Giazotto, T. T. Heikkilä, F. S. Bergeret, Very large thermophase in ferromagnetic Josephson junctions, *Phys. Rev. Lett.* 114 (2015) 067001. doi:10.1103/PhysRevLett.114.067001.
- [31] F. Hübler, M. J. Wolf, D. Beckmann, H. v. Löhneysen, Long-range spin-polarized quasiparticle transport in mesoscopic Al superconductors with a Zeeman splitting, *Phys. Rev. Lett.* 109 (20) (2012) 207001. doi:10.1103/PhysRevLett.109.207001.
- [32] D. Beckmann, Spin manipulation in nanoscale superconductors, *J. Phys.: Condens. Matter* 28 (16) (2016) 163001. doi:10.1088/0953-8984/28/16/163001.
- [33] T. T. Heikkilä, R. Ojajarvi, I. J. Maasilta, E. Strambini, F. Giazotto, F. S. Bergeret, Thermoelectric radiation detector based on superconductor-ferromagnet systems, *Phys. Rev. Applied* 10 (2018) 034053. doi:10.1103/PhysRevApplied.10.034053.

- [34] F. Giazotto, P. Solinas, A. Braggio, F. S. Bergeret, Ferromagnetic-insulator-based superconducting junctions as sensitive electron thermometers, *Phys. Rev. Applied* 4 (2015) 044016. doi:10.1103/PhysRevApplied.4.044016.
- [35] M. Silaev, P. Virtanen, F. S. Bergeret, T. T. Heikkilä, Long-range spin accumulation from heat injection in mesoscopic superconductors with Zeeman splitting, *Phys. Rev. Lett.* 114 (16) (2015) 167002. doi:10.1103/PhysRevLett.114.167002.
- [36] I. V. Bobkova, A. M. Bobkov, Long-range spin imbalance in mesoscopic superconductors under Zeeman splitting, *JETP Lett.* 101 (2) (2015) 118. doi:10.1134/S0021364015020022.
- [37] I. V. Bobkova, A. M. Bobkov, Injection of nonequilibrium quasiparticles into Zeeman-split superconductors: a way to create long-range spin imbalance, *Phys. Rev. B* 93 (2) (2016) 024513. doi:10.1103/PhysRevB.93.024513.
- [38] C. H. L. Quay, D. Chevallier, C. Bena, M. Aprili, Spin imbalance and spin-charge separation in a mesoscopic superconductor, *Nat. Phys.* 9 (2) (2013) 84–88. doi:10.1038/nphys2518.
- [39] S. Kolenda, P. Machon, D. Beckmann, W. Belzig, Nonlinear thermoelectric effects in high-field superconductor-ferromagnet tunnel junctions, *Beilstein J. Nanotech.* 7 (1) (2016) 1579. doi:10.3762/bjnano.7.152.
- [40] Y. M. Xiong, S. Stadler, P. W. Adams, G. Catelani, Spin-resolved tunneling studies of the exchange field in EuS/Al bilayers, *Phys. Rev. Lett.* 106 (2011) 247001. doi:10.1103/PhysRevLett.106.247001.
- [41] E. Strambini, V. N. Golovach, G. De Simoni, J. S. Moodera, F. S. Bergeret, F. Giazotto, Revealing the magnetic proximity effect in eus/al bilayers through superconducting tunneling spectroscopy, *Phys. Rev. Materials* 1 (5) (2017) 054402. doi:10.1103/PhysRevMaterials.1.054402.
- [42] M. J. Wolf, C. Sürgers, G. Fischer, D. Beckmann, Spin-polarized quasiparticle transport in exchange-split superconducting aluminum on europium sulfide, *Phys. Rev. B* 90 (2014) 144509. doi:10.1103/PhysRevB.90.144509.
- [43] J. S. Moodera, T. S. Santos, T. Nagahama, The phenomena of spin-filter tunnelling, *J. Phys.: Condens. Matter* 19 (16) (2007) 165202. doi:10.1088/0953-8984/19/16/165202.
- [44] K. Senapati, M. G. Blamire, Z. H. Barber, Spin-filter Josephson junctions, *Nat. Mater* 10 (11) (2011) 849–852. doi:10.1038/nmat3116.

- [45] P. K. Muduli, Spin-polarized quasiparticle control in a double spin-filter tunnel junction, *Phys. Rev. B* 96 (2) (2017) 024514. doi:10.1103/PhysRevB.96.024514.
- [46] J. S. Moodera, X. Hao, G. A. Gibson, R. Meservey, Electron-spin polarization in tunnel junctions in zero applied field with ferromagnetic EuS barriers, *Phys. Rev. Lett.* 61 (1988) 637–640. doi:10.1103/PhysRevLett.61.637.
- [47] A. Pal, M. G. Blamire, Large interfacial exchange fields in a thick superconducting film coupled to a spin-filter tunnel barrier, *Phys. Rev. B* 92 (2015) 180510. doi:10.1103/PhysRevB.92.180510.
- [48] M. G. Khusainov, Indirect RKKY exchange and magnetic states of ferromagnet-superconductor superlattices, *Zh. Eksp. Teor. Fiz.* 109 (2) (1996) 524.  
URL <http://jetp.ac.ru/cgi-bin/e/index/r/109/2/p524?a=list>
- [49] Yu. A. Izyumov, Yu. N. Proshin, M. G. Khusainov, Competition between superconductivity and magnetism in ferromagnet/superconductor heterostructures, *Phys. Usp.* 45 (2002) 109–148. doi:10.1070/PU2002v045n02ABEH001025.
- [50] A. I. Buzdin, L. N. Bulaevskii, Ferromagnetic film on the surface of a superconductor: Possible onset of inhomogeneous magnetic ordering, *Sov. Phys. JETP* 67 (3) (1988) 576–578.  
URL <http://jetp.ac.ru/cgi-bin/e/index/e/67/3/p576?a=list>
- [51] F. S. Bergeret, K. B. Efetov, A. I. Larkin, Nonhomogeneous magnetic order in superconductor-ferromagnet multilayers, *Phys. Rev. B* 62 (17) (2000) 11872–11878. doi:10.1103/PhysRevB.62.11872.
- [52] P. G. de Gennes, Coupling between ferromagnets through a superconducting layer, *Phys. Lett.* 23 (1) (1966) 10–11. doi:10.1016/0031-9163(66)90229-0.
- [53] P. Tischer, Ferromagnetic domains in EuS investigated by low-temperature Lorentz microscopy, *IEEE Trans. Magn.* 9 (1) (1973) 9–12. doi:10.1109/TMAG.1973.1067558.
- [54] F. Aikebaier, P. Virtanen, T. Heikkilä, Superconductivity near a magnetic domain wall, *arXiv:1812.08410* (2018).  
URL <https://arxiv.org/abs/1812.08410>
- [55] A. A. Abrikosov, L. P. Gor’kov, Contribution to the theory of superconducting alloys with paramagnetic impurities, *Zh. Eksp. Teor. Fiz.* 39 (6) (1960) 1781.
- [56] W. Meissner, R. Ochsenfeld, Ein neuer Effekt bei Eintritt der Supraleitfähigkeit, *Naturwissenschaften* 21 (1933) 787.

- [57] R. Meservey, P. M. Tedrow, Properties of very thin aluminum films, *J. Appl. Phys.* 42 (1) (1971) 51–53. doi:10.1063/1.1659648.
- [58] I. Giaever, K. Megerle, Study of superconductors by electron tunneling, *Phys. Rev.* 122 (1961) 1101–1111. doi:10.1103/PhysRev.122.1101.
- [59] K. Maki, Effect of Pauli paramagnetism on magnetic properties of high-field superconductors, *Phys. Rev.* 148 (1) (1966) 362. doi:10.1103/PhysRev.148.362.
- [60] N. R. Werthamer, E. F. Helfand, P. C. Hohenberg, Temperature and purity dependence of the superconducting critical field,  $H_{c2}$ . III. electron spin and spin-orbit effects, *Phys. Rev.* 147 (1) (1966) 295. doi:10.1103/PhysRev.147.295.
- [61] P. Fulde, High field superconductivity in thin films, *Adv. Phys.* 22 (6) (1973) 667–719. doi:10.1080/00018737300101369.
- [62] K. Maki, T. Tsuneto, Pauli paramagnetism and superconducting state, *Prog. Theor. Phys.* 31 (1) (1964) 945–956. doi:10.1143/PTP.31.945.
- [63] R. C. Bruno, B. B. Schwartz, Magnetic field splitting of the density of states of thin superconductors, *Phys. Rev. B* 8 (1973) 3161–3178. doi:10.1103/PhysRevB.8.3161.
- [64] L. G. Aslamazov, Influence of impurities on the existence of an inhomogeneous state in a ferromagnetic superconductor, *Zh. Eksp. Teor. Fiz.* 55 (4) (1969) 1477.  
URL <http://jetp.ac.ru/cgi-bin/e/index/r/55/4/p1477?a=list>
- [65] K. Gloos, R. Modler, H. Schimanski, C. Bredl, C. Geibel, F. Steglich, A. Buzdin, N. Sato, T. Komatsubara, Possible formation of a nonuniform superconducting state in the heavy-fermion compound UPd<sub>2</sub>Al<sub>3</sub>, *Phys. Rev. Lett.* 70 (4) (1993) 501. doi:10.1103/PhysRevLett.70.501.
- [66] T. Koponen, T. Paananen, J.-P. Martikainen, P. Törmä, Finite-temperature phase diagram of a polarized Fermi gas in an optical lattice, *Phys. Rev. Lett.* 99 (12) (2007) 120403. doi:10.1103/PhysRevLett.99.120403.
- [67] A. Korolyuk, F. Massel, P. Törmä, Probing the Fulde-Ferrell-Larkin-Ovchinnikov phase by double occupancy modulation spectroscopy, *Phys. Rev. Lett.* 104 (23) (2010) 236402. doi:10.1103/PhysRevLett.104.236402.
- [68] J. J. Kinnunen, J. E. Baarsma, J.-P. Martikainen, P. Törmä, The Fulde-Ferrell-Larkin-Ovchinnikov state for ultracold fermions in lattice and harmonic potentials: a review, *Rep. Prog. Phys.* 81 (4) (2018) 046401. doi:10.1088/1361-6633/aaa4ad.



- [69] D. E. Sheehy, L. Radzihovsky, BEC-BCS crossover in “magnetized” Feshbach-resonantly paired superfluids, *Phys. Rev. Lett.* 96 (2006) 060401. doi:10.1103/PhysRevLett.96.060401.
- [70] D. E. Sheehy, L. Radzihovsky, BEC-BCS crossover, phase transitions and phase separation in polarized resonantly-paired superfluids, *Ann. Phys.* 322 (8) (2007) 1790–1924. doi:10.1016/j.aop.2006.09.009.
- [71] A. A. Abrikosov, L. P. Gor’kov, On the problem of the Knight shift in superconductors, *Zh. Eksp. Teor. Fiz.* 39 (2) (1960) 480.  
URL <http://www.jetp.ac.ru/cgi-bin/e/index/e/12/2/p337?a=list>
- [72] K. Yosida, Paramagnetic susceptibility in superconductors, *Phys. Rev.* 110 (3) (1958) 769. doi:10.1103/PhysRev.110.769.
- [73] R. Meservey, P. M. Tedrow, Surface relaxation times of conduction-electron spins in superconductors and normal metals, *Phys. Rev. Lett.* 41 (1978) 805–808. doi:10.1103/PhysRevLett.41.805.
- [74] L. D. Landau, The theory of a Fermi liquid, *Zh. Eksp. Teor. Fiz.* 30 (6) (1956) 1058.  
URL <http://www.jetp.ac.ru/cgi-bin/e/index/r/30/6/p1058?a=list>
- [75] J. Alexander, T. Orlando, D. Rainer, P. Tedrow, Theory of Fermi-liquid effects in high-field tunneling, *Phys. Rev. B* 31 (9) (1985) 5811–5825. doi:10.1103/PhysRevB.31.5811.
- [76] G. Catelani, X. S. Wu, P. W. Adams, Fermi-liquid effects in the gapless state of marginally thin superconducting films, *Phys. Rev. B* 78 (2008) 104515. doi:10.1103/PhysRevB.78.104515.
- [77] P. M. Tedrow, J. T. Kucera, D. Rainer, T. P. Orlando, Spin-polarized tunneling measurement of the antisymmetric Fermi-liquid parameter  $G^0$  and renormalization of the Pauli limiting field in A1, *Phys. Rev. Lett.* 52 (1984) 1637–1640. doi:10.1103/PhysRevLett.52.1637.
- [78] G. A. Gibson, R. Meservey, Evidence for spin fluctuations in vanadium from a tunneling study of Fermi-liquid effects, *Phys. Rev. B* 40 (1989) 8705–8713. doi:10.1103/PhysRevB.40.8705.
- [79] F. S. Bergeret, A. F. Volkov, K. B. Efetov, Long-range proximity effects in superconductor-ferromagnet structures, *Phys. Rev. Lett.* 86 (18) (2001) 4096. doi:10.1103/PhysRevLett.86.4096.
- [80] M. Eschrig, Spin-polarized supercurrents for spintronics, *Phys. Today* 64 (1) (2011) 43. doi:10.1063/1.3541944.
- [81] J. Linder, J. W. A. Robinson, Superconducting spintronics, *Nat. Phys.* 11 (4) (2015) 307–315. doi:10.1038/nphys3242.

- [82] P. G. de Gennes, Boundary effects in superconductors, *Rev. Mod. Phys.* 36 (1) (1964) 225. doi:10.1103/RevModPhys.36.225.
- [83] A. F. Andreev, Thermal conductivity of the intermediate state of superconductors, *Zh. Eksp. Teor. Fiz.* 46 (5) (1964) 1823.  
URL <http://jetp.ac.ru/cgi-bin/e/index/r/46/5/p1823?a=list>
- [84] T. Kontos, M. Aprili, J. Lesueur, X. Grison, Inhomogeneous superconductivity induced in a ferromagnet by proximity effect, *Phys. Rev. Lett.* 86 (2) (2001) 304. doi:10.1103/PhysRevLett.86.304.
- [85] G. Verbanck, C. Potter, R. Schad, P. Belien, V. Moshchalkov, Y. Bruynseraede, The superconducting proximity effect in Nb/Fe multilayers, *Physica C* 235 (1994) 3295–3296. doi:10.1016/0921-4534(94)91174-6.
- [86] Y. Blum, A. Tsukernik, M. Karpovski, A. Palevski, Oscillations of the superconducting critical current in Nb-Cu-Ni-Cu-Nb junctions, *Phys. Rev. Lett.* 89 (2002) 187004. doi:10.1103/PhysRevLett.89.187004.
- [87] J. W. A. Robinson, S. Piano, G. Burnell, C. Bell, M. G. Blamire, Critical current oscillations in strong ferromagnetic  $\pi$  junctions, *Phys. Rev. Lett.* 97 (2006) 177003. doi:10.1103/PhysRevLett.97.177003.
- [88] R. Keizer, S. Goennenwein, T. Klapwijk, G. Miao, G. Xiao, A. Gupta, A spin triplet supercurrent through the half-metallic ferromagnet CrO<sub>2</sub>, *Nature* 439 (7078) (2006) 825–827.
- [89] M. Anwar, M. Veldhorst, A. Brinkman, J. Aarts, Long range supercurrents in ferromagnetic CrO<sub>2</sub> using a multilayer contact structure, *Appl. Phys. Lett.* 100 (5) (2012) 052602. doi:10.1063/1.3681138.
- [90] T. S. Khaire, M. A. Khasawneh, W. Pratt Jr, N. O. Birge, Observation of spin-triplet superconductivity in Co-based Josephson junctions, *Phys. Rev. Lett.* 104 (13) (2010) 137002. doi:10.1103/PhysRevLett.104.137002.
- [91] J. Robinson, J. Witt, M. Blamire, Controlled injection of spin-triplet supercurrents into a strong ferromagnet, *Science* 329 (5987) (2010) 59–61. doi:10.1126/science.1189246.
- [92] P. W. Anderson, H. Suhl, Spin alignment in the superconducting state, *Phys. Rev.* 116 (4) (1959) 898. doi:10.1103/PhysRev.116.898.
- [93] L. N. Bulaevskii, A. I. Buzdin, M. L. Kulić, S. V. Panjukov, Coexistence of superconductivity and magnetism theoretical predictions and experimental results, *Adv. Phys.* 34 (2) (1985) 175–261. doi:10.1080/00018738500101741.

- [94] K. D. Usadel, Generalized diffusion equation for superconducting alloys, *Phys. Rev. Lett.* 25 (8) (1970) 507–509. doi:10.1103/PhysRevLett.25.507.
- [95] G. Eilenberger, Transformation of Gorkov’s equation for type II superconductors into transport-like equations, *Z. Phys.* 214 (2) (1968) 195–213. doi:10.1007/BF01379803.
- [96] W. Belzig, F. K. Wilhelm, C. Bruder, G. Schön, A. D. Zaikin, Quasiclassical Green’s function approach to mesoscopic superconductivity, *Superlatt. Microstruct.* 25 (5) (1999) 1251–1288. doi:10.1006/spmi.1999.0710.
- [97] A. Schmid, G. Schön, Linearized kinetic equations and relaxation processes of a superconductor near  $T_c$ , *J. Low Temp. Phys.* 20 (1) (1975) 207–227. doi:10.1007/BF00115264.
- [98] J. Clarke, Experimental observation of pair-quasiparticle potential difference in nonequilibrium superconductors, *Phys. Rev. Lett.* 28 (1972) 1363–1366. doi:10.1103/PhysRevLett.28.1363.
- [99] M. Tinkham, Tunneling generation, relaxation, and tunneling detection of hole-electron imbalance in superconductors, *Phys. Rev. B* 6 (1972) 1747–1756. doi:10.1103/PhysRevB.6.1747.
- [100] M. Tinkham, J. Clarke, Theory of pair-quasiparticle potential difference in nonequilibrium superconductors, *Phys. Rev. Lett.* 28 (1972) 1366–1369. doi:10.1103/PhysRevLett.28.1366.
- [101] M. Johnson, R. H. Silsbee, Interfacial charge-spin coupling: Injection and detection of spin magnetization in metals, *Phys. Rev. Lett.* 55 (1985) 1790–1793. doi:10.1103/PhysRevLett.55.1790.
- [102] S. N. Artemenko, A. F. Volkov, Electric fields and collective oscillations in superconductors, *Sov. Phys. Usp.* 22 (5) (1979) 295. doi:10.1070/PU1979v022n05ABEH005495.
- [103] N. B. Kopnin, Theory of nonequilibrium superconductivity, no. 110 in *International series of monographs on physics*, Oxford University Press, 2001.
- [104] P. G. de Gennes, *Superconductivity of Metals and Alloys*, Advanced book classics, Perseus, Cambridge, MA, 1999.  
URL <https://cds.cern.ch/record/566105>
- [105] J. B. Nielsen, C. J. Pethick, J. Rammer, H. Smith, Pair breaking and charge relaxation in superconductors, *J. Low Temp. Phys.* 46 (5-6) (1982) 565–597. doi:10.1007/BF00683918.
- [106] W. Belzig, C. Bruder, G. Schön, Local density of states in a dirty normal metal connected to a superconductor, *Phys. Rev. B* 54 (1996) 9443–9448. doi:10.1103/PhysRevB.54.9443.

- [107] M. I. Dyakonov, V. I. Perel, Spin relaxation of conduction electrons in noncentrosymmetric semiconductors, *Sov. Phys. Solid State* 13 (12) (1972) 3023–3026.
- [108] I. Žutić, J. Fabian, S. D. Sarma, Spintronics: Fundamentals and applications, *Rev. Mod. Phys.* 76 (2) (2004) 323. doi:10.1103/RevModPhys.76.323.
- [109] J. Sinova, S. O. Valenzuela, J. Wunderlich, C. H. Back, T. Jungwirth, Spin Hall effects, *Rev. Mod. Phys.* 87 (4) (2015) 1213. doi:10.1103/RevModPhys.87.1213.
- [110] V. M. Edelstein, Spin polarization of conduction electrons induced by electric current in two-dimensional asymmetric electron systems, *Solid State Commun.* 73 (3) (1990) 233–235. doi:10.1016/0038-1098(90)90963-C.
- [111] F. Konschelle, I. V. Tokatly, F. S. Bergeret, Theory of the spin-galvanic effect and the anomalous phase shift  $\varphi_0$  in superconductors and Josephson junctions with intrinsic spin-orbit coupling, *Phys. Rev. B* 92 (12) (2015) 125443. doi:10.1103/PhysRevB.92.125443.
- [112] F. S. Bergeret, I. V. Tokatly, Manifestation of extrinsic spin Hall effect in superconducting structures: Nondissipative magnetoelectric effects, *Phys. Rev. B* 94 (18) (2016) 180502. doi:10.1103/PhysRevB.94.180502.
- [113] C. Huang, I. V. Tokatly, F. S. Bergeret, Extrinsic spin-charge coupling in diffusive superconducting systems, *Phys. Rev. B* 98 (14) (2018) 144515. doi:10.1103/PhysRevB.98.144515.
- [114] F. J. Jedema, H. B. Heersche, A. T. Filip, J. J. A. Baselmans, B. J. van Wees, Electrical detection of spin precession in a metallic mesoscopic spin valve, *Nature* 416 (2002) 713. doi:10.1038/416713a.
- [115] N. Poli, J. P. Morten, M. Urech, A. Brataas, D. B. Haviland, V. Korenivski, Spin injection and relaxation in a mesoscopic superconductor, *Phys. Rev. Lett.* 100 (13) (2008) 136601. doi:10.1103/PhysRevLett.100.136601.
- [116] A. A. Abrikosov, L. P. Gor'kov, Spin-orbit interaction and the Knight shift in superconductors, *Zh. Eksp. Teor. Fiz.* 42 (4) (1962) 1088.  
URL <http://jetp.ac.ru/cgi-bin/e/index/e/15/4/p752?a=list>
- [117] T. Wakamura, N. Hasegawa, K. Ohnishi, Y. Niimi, Y. Otani, Spin injection into a superconductor with strong spin-orbit coupling, *Phys. Rev. Lett.* 112 (3) (2014) 036602. doi:10.1103/PhysRevLett.112.036602.
- [118] J. P. Morten, A. Brataas, W. Belzig, Spin transport in diffusive superconductors, *Phys. Rev. B* 70 (21) (2004) 212508. doi:10.1103/PhysRevB.70.212508.

- [119] G. M. Eliashberg, Inelastic electron collisions and nonequilibrium stationary states in superconductors, *Sov. Phys. JETP* 34 (1972) 668.  
URL <http://jetp.ac.ru/cgi-bin/e/index/e/34/3/p668?a=list>
- [120] J. W. Serene, D. Rainer, The quasiclassical approach to superfluid  $^3\text{He}$ , *Phys. Rep.* 101 (1983) 221. doi:10.1016/0370-1573(83)90051-0.
- [121] S. B. Kaplan, C. C. Chi, D. N. Langenberg, J. J. Chang, S. Jafarey, D. J. Scalapino, Quasiparticle and phonon lifetimes in superconductors, *Phys. Rev. B* 14 (1976) 4854–4873. doi:10.1103/PhysRevB.14.4854.
- [122] C. Grimaldi, P. Fulde, Nonequilibrium superconductivity in spin-polarized superconducting tunneling junctions, *Phys. Rev. B* 56 (1997) 2751–2763. doi:10.1103/PhysRevB.56.2751.
- [123] P. Virtanen, T. T. Heikkilä, F. S. Bergeret, Stimulated quasiparticles in spin-split superconductors, *Phys. Rev. B* 93 (1) (2016) 014512. doi:10.1103/PhysRevB.93.014512.
- [124] T. T. Heikkilä, F. Giazotto, Phase sensitive electron-phonon coupling in a superconducting proximity structure, *Phys. Rev. B* 79 (2009) 094514. doi:10.1103/PhysRevB.79.094514.
- [125] T. T. Heikkilä, M. Hatami, G. E. W. Bauer, Spin heat accumulation and its relaxation in spin valves, *Phys. Rev. B* 81 (2010) 100408. doi:10.1103/PhysRevB.81.100408.
- [126] A. V. Timofeev, C. P. García, N. B. Kopnin, A. M. Savin, M. Meschke, F. Giazotto, J. P. Pekola, Recombination-limited energy relaxation in a Bardeen-Cooper-Schrieffer superconductor, *Phys. Rev. Lett.* 102 (2009) 017003. doi:10.1103/PhysRevLett.102.017003.
- [127] V. F. Maisi, S. V. Lotkhov, A. Kemppinen, A. Heimes, J. T. Muhonen, J. P. Pekola, Excitation of single quasiparticles in a small superconducting Al island connected to normal-metal leads by tunnel junctions, *Phys. Rev. Lett.* 111 (2013) 147001. doi:10.1103/PhysRevLett.111.147001.
- [128] F. Giazotto, T. T. Heikkilä, A. Luukanen, A. M. Savin, J. P. Pekola, Opportunities for mesoscopies in thermometry and refrigeration: Physics and applications, *Rev. Mod. Phys.* 78 (2006) 217–274. doi:10.1103/RevModPhys.78.217.
- [129] F. C. Wellstood, C. Urbina, J. Clarke, Hot-electron effects in metals, *Phys. Rev. B* 49 (1994) 5942–5955. doi:10.1103/PhysRevB.49.5942.
- [130] J. T. Muhonen, M. Meschke, J. P. Pekola, Micrometre-scale refrigerators, *Rep. Progr. Phys.* 75 (4) (2012) 046501. doi:10.1088/0034-4885/75/4/046501.

- [131] A. V. Zaitsev, Quasiclassical equations of the theory of superconductivity for contiguous metals and the properties of constricted microcontacts, *Sov. Phys. JETP* 59 (5) (1984) 1015.  
URL <http://jetp.ac.ru/cgi-bin/e/index/e/59/5/p1015?a=list>
- [132] M. Yu. Kupriyanov, V. F. Lukichev, Influence of boundary transparency on the critical current of "dirty" SS'S structures, *Sov. Phys. JETP* 67 (6) (1988) 1163–1168.  
URL <http://www.jetp.ac.ru/cgi-bin/e/index/e/67/6/p1163?a=list>
- [133] C. J. Lambert, R. Raimondi, V. Sweeney, A. F. Volkov, Boundary conditions for quasiclassical equations in the theory of superconductivity, *Phys. Rev. B* 55 (1997) 6015–6021. doi:10.1103/PhysRevB.55.6015.
- [134] Yu. V. Nazarov, Novel circuit theory of Andreev reflection, *Superlatt. Microstruct.* 25 (5-6) (1999) 1221–1231. doi:10.1006/spmi.1999.0738.
- [135] E. Zhao, T. Löfwander, J. A. Sauls, Nonequilibrium superconductivity near spin-active interfaces, *Phys. Rev. B* 70 (2004) 134510. doi:10.1103/PhysRevB.70.134510.
- [136] A. Cottet, D. Huertas-Hernando, W. Belzig, Yu. V. Nazarov, Spin-dependent boundary conditions for isotropic superconducting Green functions, *Phys. Rev. B* 80 (2009) 184511. doi:10.1103/PhysRevB.80.184511.
- [137] F. S. Bergeret, A. Verso, A. F. Volkov, Electronic transport through ferromagnetic and superconducting junctions with spin-filter tunneling barriers, *Phys. Rev. B* 86 (21) (2012) 214516. doi:10.1103/PhysRevB.86.214516.
- [138] M. Eschrig, A. Cottet, W. Belzig, J. Linder, General boundary conditions for quasiclassical theory of superconductivity in the diffusive limit: application to strongly spin-polarized systems, *New. J. Phys.* 17 (8) (2015) 083037. doi:10.1088/1367-2630/17/8/083037.
- [139] F. S. Bergeret, A. Verso, A. F. Volkov, Spin-polarized Josephson and quasiparticle currents in superconducting spin-filter tunnel junctions, *Phys. Rev. B* 86 (6) (2012) 060506. doi:10.1103/PhysRevB.86.060506.
- [140] M. Silaev, I. Tokatly, F. Bergeret, Anomalous current in diffusive ferromagnetic Josephson junctions, *Phys. Rev. B* 95 (18) (2017) 184508. doi:10.1103/PhysRevB.95.184508.
- [141] E. V. Thuneberg, J. Kurkijärvi, D. Rainer, Elementary-flux-pinning potential in type-II superconductors, *Phys. Rev. B* 29 (1984) 3913–3923. doi:10.1103/PhysRevB.29.3913.

- [142] A. B. Vorontsov, J. A. Sauls, Thermodynamic properties of thin films of superfluid  $^3\text{He} - a$ , Phys. Rev. B 68 (2003) 064508. doi:10.1103/PhysRevB.68.064508.
- [143] D. Rainer, J. W. Serene, Free energy of superfluid  $^3\text{He}$ , Phys. Rev. B 13 (1976) 4745–4765. doi:10.1103/PhysRevB.13.4745.
- [144] K. Maki, The behavior of superconducting thin films in the presence of magnetic fields and currents, Prog. Theor. Phys. 31 (5) (1964) 731. doi:10.1143/PTP.31.731.
- [145] G. E. W. Bauer, E. Saitoh, B. J. van Wees, Spin caloritronics, Nature 11 (5) (2012) 391–399. doi:10.1038/nmat3301.
- [146] A. Rothwarf, B. N. Taylor, Measurement of recombination lifetimes in superconductors, Phys. Rev. Lett. 19 (1967) 27–30. doi:10.1103/PhysRevLett.19.27.
- [147] J.-J. Chang, D. J. Scalapino, Kinetic-equation approach to nonequilibrium superconductivity, Phys. Rev. B 15 (1977) 2651–2670. doi:10.1103/PhysRevB.15.2651.
- [148] J. T. C. Yeh, D. N. Langenberg, Gap suppression by self-injection of quasiparticles in tin–tin-oxide–tin tunnel junctions, Phys. Rev. B 17 (1978) 4303–4310. doi:10.1103/PhysRevB.17.4303.
- [149] C. S. Owen, D. J. Scalapino, Superconducting state under the influence of external dynamic pair breaking, Phys. Rev. Lett. 28 (1972) 1559–1561. doi:10.1103/PhysRevLett.28.1559.
- [150] W. H. Parker, Modified heating theory of nonequilibrium superconductors, Phys. Rev. B 12 (1975) 3667–3672. doi:10.1103/PhysRevB.12.3667.
- [151] R. S. Keizer, M. G. Flokstra, J. Aarts, T. M. Klapwijk, Critical voltage of a mesoscopic superconductor, Phys. Rev. Lett. 96 (2006) 147002. doi:10.1103/PhysRevLett.96.147002.
- [152] S. Takahashi, H. Imamura, S. Maekawa, Spin imbalance and magnetoresistance in ferromagnet/superconductor/ferromagnet double tunnel junctions, Phys. Rev. Lett. 82 (1999) 3911–3914. doi:10.1103/PhysRevLett.82.3911.
- [153] I. V. Bobkova, A. M. Bobkov, Recovering the superconducting state via spin accumulation above the pair-breaking magnetic field of superconductor/ferromagnet multilayers, Phys. Rev. B 84 (2011) 140508. doi:10.1103/PhysRevB.84.140508.
- [154] H. Yang, S.-H. Yang, S. Takahashi, S. Maekawa, S. S. P. Parkin, Extremely long quasiparticle spin lifetimes in superconducting aluminium using MgO tunnel spin injectors, Nat. Mater. 9 (7) (2010) 586–593. doi:10.1038/nmat2781.

- [155] V. A. Vas'ko, V. A. Larkin, P. A. Kraus, K. R. Nikolaev, D. E. Grupp, C. A. Nordman, A. M. Goldman, Critical current suppression in a superconductor by injection of spin-polarized carriers from a ferromagnet, *Phys. Rev. Lett.* 78 (1997) 1134–1137. doi:10.1103/PhysRevLett.78.1134.
- [156] D. Koller, M. S. Osofsky, D. B. Chrisey, J. S. Horwitz, R. J. S. Jr., R. M. Stroud, C. R. Eddy, J. Kim, R. C. Y. Auyeung, J. M. Byers, B. F. Woodfield, G. M. Daly, T. W. Clinton, M. Johnson, Suppression of superconductivity by injection of spin-polarized current, *J. Appl. Phys.* 83 (11) (1998) 6774–6776. doi:10.1063/1.367763.
- [157] N.-C. Yeh, R. P. Vasquez, C. C. Fu, A. V. Samoilov, Y. Li, K. Vakil, Nonequilibrium superconductivity under spin-polarized quasiparticle currents in perovskite ferromagnet-insulator-superconductor heterostructures, *Phys. Rev. B* 60 (1999) 10522–10526. doi:10.1103/PhysRevB.60.10522.
- [158] Y. Gim, A. W. Kleinsasser, J. B. Barner, Current injection into high temperature superconductors: Does spin matter?, *J. Appl. Phys.* 90 (8) (2001) 4063–4077. doi:10.1063/1.1404427.
- [159] A. Aronov, Spin injection and polarization of excitations and nuclei in superconductors, *Sov. Phys. - JETP (Engl. Transl.); (United States)* 44:1.
- [160] D. Beckmann, H. B. Weber, H. v. Löhneysen, Evidence for crossed Andreev reflection in superconductor-ferromagnet hybrid structures, *Phys. Rev. Lett.* 93 (19) (2004) 197003. doi:10.1103/PhysRevLett.93.197003.
- [161] F. Hübler, J. C. Lemyre, D. Beckmann, H. v. Löhneysen, Charge imbalance in superconductors in the low-temperature limit, *Phys. Rev. B* 81 (18) (2010) 184524. doi:10.1103/PhysRevB.81.184524.
- [162] M. J. Wolf, F. Hübler, S. Kolenda, D. Beckmann, Charge and spin transport in mesoscopic superconductors, *Beilstein J. Nanotech.* 5 (1) (2014) 180–185. doi:10.3762/bjnano.5.18.
- [163] M. J. Wolf, F. Hübler, S. Kolenda, H. v. Löhneysen, D. Beckmann, Spin injection from a normal metal into a mesoscopic superconductor, *Phys. Rev. B* 87 (2013) 024517. doi:10.1103/PhysRevB.87.024517.
- [164] K. Yu. Arutyunov, H.-P. Auranova, A. S. Vasenko, Spatially resolved measurement of nonequilibrium quasiparticle relaxation in superconducting Al, *Phys. Rev. B* 83 (2011) 104509. doi:10.1103/PhysRevB.83.104509.
- [165] F. J. Jedema, A. T. Filip, B. J. van Wees, Electrical spin injection and accumulation at room temperature in an all-metal mesoscopic spin valve, *Nature* 410 (2001) 345. doi:10.1038/35066533.



- [166] F. J. Jedema, M. S. Nijboer, A. T. Filip, B. J. Van Wees, Spin injection and spin accumulation in all-metal mesoscopic spin valves, *Phys. Rev. B* 67 (8) (2003) 085319. doi:10.1103/PhysRevB.67.085319.
- [167] S. O. Valenzuela, M. Tinkham, Direct electronic measurement of the spin Hall effect, *Nature* 442 (7099) (2006) 176–179. doi:10.1038/nature04937.
- [168] N. Tombros, C. Jozsa, M. Popinciuc, H. T. Jonkman, B. J. Van Wees, Electronic spin transport and spin precession in single graphene layers at room temperature, *Nature* 448 (7153) (2007) 571–574. doi:10.1038/nature06037.
- [169] E. Villamor, M. Isasa, S. Vélez, A. Bedoya-Pinto, P. Vavassori, L. E. Hueso, F. S. Bergeret, F. Casanova, Modulation of pure spin currents with a ferromagnetic insulator, *Phys. Rev. B* 91 (2) (2015) 020403. doi:10.1103/PhysRevB.91.020403.
- [170] F. K. Dejene, N. Vlietstra, D. Luc, X. Waintal, J. Ben Youssef, B. J. van Wees, Control of spin current by a magnetic YIG substrate in NiFe/Al nonlocal spin valves, *Phys. Rev. B* 91 (2015) 100404. doi:10.1103/PhysRevB.91.100404.
- [171] S. A. Kivelson, D. S. Rokhsar, Bogoliubov quasiparticles, spinons, and spin-charge decoupling in superconductors, *Phys. Rev. B* 41 (16) (1990) 11693–11696. doi:10.1103/PhysRevB.41.11693.
- [172] H. L. Zhao, S. Hershfield, Tunneling, relaxation of spin-polarized quasiparticles, and spin-charge separation in superconductors, *Phys. Rev. B* 52 (1995) 3632–3638. doi:10.1103/PhysRevB.52.3632.
- [173] M. Johnson, Spin coupled resistance observed in ferromagnet-superconductor-ferromagnet trilayers, *Appl. Phys. Lett.* 65 (11) (1994) 1460–1462. doi:10.1063/1.112015.
- [174] J. Y. Gu, J. A. Caballero, R. D. Slater, R. Loloee, W. P. Pratt Jr, Direct measurement of quasiparticle evanescent waves in a dirty superconductor, *Phys. Rev. B* 66 (14) (2002) 140507. doi:10.1103/PhysRevB.66.140507.
- [175] Y.-S. Shin, H.-J. Lee, H.-W. Lee, Spin relaxation in mesoscopic superconducting Al wires, *Phys. Rev. B* 71 (2005) 144513. doi:10.1103/PhysRevB.71.144513.
- [176] P. Cadden-Zimansky, Z. Jiang, V. Chandrasekhar, Charge imbalance, crossed Andreev reflection and elastic co-tunnelling in ferromagnet/superconductor/normal-metal structures, *New. J. Phys.* 9 (5) (2007) 116. doi:10.1088/1367-2630/9/5/116.

- [177] S. Kolenda, M. J. Wolf, D. Beckmann, Observation of thermoelectric currents in high-field superconductor-ferromagnet tunnel junctions, *Phys. Rev. Lett.* 116 (2016) 097001. doi:10.1103/PhysRevLett.116.097001.
- [178] C. H. L. Quay, M. Aprili, Out-of-equilibrium spin transport in mesoscopic superconductors, *Philos. Trans. Royal Soc. A* 376 (2017) 20150342. doi:10.1098/rsta.2015.0342.
- [179] J. P. Morten, A. Brataas, W. Belzig, Spin transport and magnetoresistance in ferromagnet/superconductor/ferromagnet spin valves, *Phys. Rev. B* 72 (1) (2005) 014510. doi:10.1103/PhysRevB.72.014510.
- [180] M. Silaev, P. Virtanen, T. T. Heikkilä, F. S. Bergeret, Spin Hanle effect in mesoscopic superconductors, *Phys. Rev. B* 91 (2) (2015) 024506. doi:10.1103/PhysRevB.91.024506.
- [181] T. Krishtop, M. Houzet, J. S. Meyer, Nonequilibrium spin transport in Zeeman-split superconductors, *Phys. Rev. B* 91 (2015) 121407. doi:10.1103/PhysRevB.91.121407.
- [182] S. Takahashi, S. Maekawa, Spin injection and detection in magnetic nanostructures, *Phys. Rev. B* 67 (5) (2003) 052409. doi:10.1103/PhysRevB.67.052409.
- [183] D. Chevallier, M. Trif, C. Dutreix, M. Guigou, C. H. L. Quay, M. Aprili, C. Bena, Superconductor spintronics: modeling spin and charge accumulation in out-of-equilibrium NIS junctions subjected to Zeeman magnetic fields, *New J. Phys.* 20 (1) (2018) 013014. doi:10.1088/1367-2630/aa9cc7.
- [184] F. Aikebaier, M. A. Silaev, T. T. Heikkilä, Supercurrent-induced charge-spin conversion in spin-split superconductors, *Phys. Rev. B* 98 (2018) 024516. doi:10.1103/PhysRevB.98.024516.
- [185] A. Schmid, G. Schön, Generation of branch imbalance by the interaction between supercurrent and thermal gradient, *Phys. Rev. Lett.* 43 (1979) 793–795. doi:10.1103/PhysRevLett.43.793.
- [186] J. Clarke, B. R. Fjordbøge, P. E. Lindelof, Supercurrent-induced charge imbalance measured in a superconductor in the presence of a thermal gradient, *Phys. Rev. Lett.* 43 (1979) 642–645. doi:10.1103/PhysRevLett.43.642.
- [187] C. J. Pethick, H. Smith, Generation of charge imbalance in a superconductor by a temperature gradient, *Phys. Rev. Lett.* 43 (1979) 640–642. doi:10.1103/PhysRevLett.43.640.
- [188] T. Yang, T. Kimura, Y. Otani, Giant spin-accumulation signal and pure spin-current-induced reversible magnetization switching, *Nat. Phys.* 4 (11) (2008) 851–854. doi:10.1038/nphys1095.

- [189] S. Zhang, Spin Hall effect in the presence of spin diffusion, *Phys. Rev. Lett.* 85 (2) (2000) 393. doi:10.1103/PhysRevLett.85.393.
- [190] P. C. van Son, H. van Kempen, P. Wyder, Boundary resistance of the ferromagnetic-nonferromagnetic metal interface, *Phys. Rev. Lett.* 58 (1987) 2271–2273. doi:10.1103/PhysRevLett.58.2271.
- [191] M. I. Dyakonov, A. Khaetskii, Spin Hall effect, in: *Spin Physics in Semiconductors*, Springer, 2008, pp. 211–243.
- [192] E. G. Mishchenko, A. V. Shytov, B. I. Halperin, Spin current and polarization in impure two-dimensional electron systems with spin-orbit coupling, *Phys. Rev. Lett.* 93 (22) (2004) 226602. doi:10.1103/PhysRevLett.93.226602.
- [193] A. Mal'shukov, K.-A. Chao, Spin hall conductivity of a disordered two-dimensional electron gas with dresselhaus spin-orbit interaction, *Phys. Rev. B* 71 (12) (2005) 121308. doi:10.1103/PhysRevB.71.121308.
- [194] T. D. Stanescu, V. Galitski, Spin relaxation in a generic two-dimensional spin-orbit coupled system, *Phys. Rev. B* 75 (12) (2007) 125307. doi:10.1103/PhysRevB.75.125307.
- [195] M. Duckheim, D. L. Maslov, D. Loss, Dynamic spin-Hall effect and driven spin helix for linear spin-orbit interactions, *Phys. Rev. B* 80 (23) (2009) 235327. doi:10.1103/PhysRevB.80.235327.
- [196] D. H. Hernando, Yu. V. Nazarov, A. Brataas, G. E. W. Bauer, Conductance modulation by spin precession in noncollinear ferromagnet normal-metal ferromagnet systems, *Phys. Rev. B* 62 (9) (2000) 5700. doi:10.1103/PhysRevB.62.5700.
- [197] H. C. Torrey, Bloch equations with diffusion terms, *Phys. Rev.* 104 (1956) 563–565. doi:10.1103/PhysRev.104.563.
- [198] C. H. L. Quay, Y. Chiffaudel, C. Strunk, M. Aprili, Quasiparticle spin resonance and coherence in superconducting aluminium, *Nat. Commun.* 6 (2015) 8660. doi:10.1038/ncomms9660.
- [199] K. Aoi, J. C. Swihart, Theory of electron spin resonance in type-I superconductors, *Phys. Rev. B* 2 (1970) 2555–2560. doi:10.1103/PhysRevB.2.2555.
- [200] J. I. Kaplan, Conduction electron spin resonance in a superconductor, *Phys. Lett.* 19 (4) (1965) 266 – 267. doi:10.1016/0031-9163(65)90977-7.
- [201] P. G. de Gennes, Note sur la résonance paramagnétique des supraconducteurs de 2ème espèce, *Solid State Commun.* 4 (2) (1966) 95 – 97. doi:10.1016/0038-1098(66)90280-8.

- [202] C. Tsallis, Conduction electron spin resonance due to exchange and spin-orbit scatterings by silute impurities in superconductors, *Phys. Status Solidi B* 79 (2) (1977) 451–460. doi:10.1002/pssb.2220790207.
- [203] Y. Yafet, Conduction electron spin relaxation in the superconducting state, *Phys. Lett. A* 98 (1983) 287. doi:10.1016/0375-9601(83)90874-5.
- [204] K. Maki, Theory of electron-spin resonance in gapless superconductors, *Phys. Rev. B* 8 (1973) 191–199. doi:10.1103/PhysRevB.8.191.
- [205] A. A. Kosov, B. I. Kochelaev, Electron paramagnetic resonance on localized magnetic moments in gapless superconductors, *Sov. Phys. JETP* 47 (1978) 75.  
URL <http://jetp.ac.ru/cgi-bin/e/index/e/47/1/p75?a=list>
- [206] L. R. Tagirov, K. F. Trutnev, Spin kinetics and EPR in superconductors, *J. Phys. F: Met. Phys.* 17 (3) (1987) 695. doi:10.1088/0305-4608/17/3/014.
- [207] D. C. Vier, S. Schultz, Observation of conduction electron spin resonance in both the normal and superconducting states of niobium, *Phys. Lett. A* 98 (1983) 283. doi:10.1016/0375-9601(83)90873-3.
- [208] Y. Yafet, D. C. Vier, S. Schultz, Conduction electron spin resonance and relaxation in the superconducting state, *J. Appl. Phys.* 55 (6) (1984) 2022–2024. doi:10.1063/1.333552.
- [209] N. M. Nemes, J. E. Fischer, G. Baumgartner, L. Forró, T. Fehér, G. Oszlányi, F. Simon, A. Jánossy, Conduction-electron spin resonance in the superconductor  $k_3c_{60}$ , *Phys. Rev. B* 61 (2000) 7118–7121. doi:10.1103/PhysRevB.61.7118.
- [210] A. Brataas, Y. Tserkovnyak, Spin and charge pumping by ferromagnetic-superconductor order parameters, *Phys. Rev. Lett.* 93 (2004) 087201. doi:10.1103/PhysRevLett.93.087201.
- [211] H. J. Skadsem, A. Brataas, J. Martinek, Y. Tserkovnyak, Ferromagnetic resonance and voltage-induced transport in normal metal-ferromagnet-superconductor trilayers, *Phys. Rev. B* 84 (2011) 104420. doi:10.1103/PhysRevB.84.104420.
- [212] M. Houzet, Ferromagnetic Josephson junction with precessing magnetization, *Phys. Rev. Lett.* 101 (2008) 057009. doi:10.1103/PhysRevLett.101.057009.
- [213] C. Richard, M. Houzet, J. S. Meyer, Andreev current induced by ferromagnetic resonance, *Phys. Rev. Lett.* 109 (2012) 057002. doi:10.1103/PhysRevLett.109.057002.

- [214] M. Trif, Y. Tserkovnyak, Dynamic magnetoelectric effect in ferromagnet/superconductor tunnel junctions, *Phys. Rev. Lett.* 111 (2013) 087602. doi:10.1103/PhysRevLett.111.087602.
- [215] C. Holmqvist, S. Teber, M. Fogelström, Nonequilibrium effects in a Josephson junction coupled to a precessing spin, *Phys. Rev. B* 83 (2011) 104521. doi:10.1103/PhysRevB.83.104521.
- [216] P. J. M. van Bentum, P. Wyder, Far-infrared absorption of thin superconducting aluminum films in the pair-breaking and paramagnetic limits, *Phys. Rev. B* 34 (1986) 1582–1594. doi:10.1103/PhysRevB.34.1582.
- [217] D. C. Mattis, J. Bardeen, Theory of the anomalous skin effect in normal and superconducting metals, *Phys. Rev.* 111 (1958) 412–417. doi:10.1103/PhysRev.111.412.
- [218] A. A. Abrikosov, L. P. Gor'kov, I. M. Khalatnikov, A superconductor in a high frequency field, *Zh. Eksp. Teor. Fiz.* 35 (1) (1959) 265. URL <http://jetp.ac.ru/cgi-bin/e/index/e/8/1/p182?a=list>
- [219] J. Linder, M. Amundsen, J. A. Ouassou, Microwave control of the superconducting proximity effect and minigap in magnetic and normal metals, *Sci. Rep.* 6 (2016) 38739. doi:10.1038/srep38739.
- [220] G. M. Eliashberg, Film superconductivity stimulated by a high-frequency field, *JETP Lett.* 11 (1970) 114. URL [http://www.jetpletters.ac.ru/ps/1716/article\\_26086.shtml](http://www.jetpletters.ac.ru/ps/1716/article_26086.shtml)
- [221] B. I. Ivlev, S. G. Lisitsyn, G. M. Eliashberg, Nonequilibrium excitations in superconductors in high-frequency fields, *J. Low Temp. Phys.* 10 (3) (1973) 449–468. doi:10.1007/BF00654920.
- [222] T. M. Klapwijk, J. N. Van den Bergh, J. E. Mooij, Radiation-stimulated superconductivity, *J. Low Temp. Phys.* 26 (3-4) (1977) 385–405. doi:10.1007/BF00655418.
- [223] S. E. Barnes, Theory of electron spin resonance of magnetic ions in metals, *Adv. Phys.* 30 (6) (1981) 801–938. doi:10.1080/00018738100101447.
- [224] R. H. Taylor, Electron spin resonance of magnetic ions in metals an experimental review, *Adv. Phys.* 24 (6) (1975) 681–791. doi:10.1080/00018737500101501.
- [225] K. Baberschke, Electron spin resonance in superconducting materials, *Z. Phys. B* 24 (1) (1976) 53–63. doi:10.1007/BF01312873.
- [226] I. A. Garifullin, EPR study of superconductors, *J. Low Temp. Phys.* 178 (5) (2015) 243–271. doi:10.1007/s10909-014-1252-z.

- [227] Y. Tserkovnyak, A. Brataas, G. E. W. Bauer, B. I. Halperin, Nonlocal magnetization dynamics in ferromagnetic heterostructures, *Rev. Mod. Phys.* 77 (2005) 1375–1421. doi:10.1103/RevModPhys.77.1375.
- [228] F. Hellman, A. Hoffmann, Y. Tserkovnyak, G. S. D. Beach, E. E. Fullerton, C. Leighton, A. H. MacDonald, D. C. Ralph, D. A. Arena, H. A. Dürr, P. Fischer, J. Grollier, J. P. Heremans, T. Jungwirth, A. V. Kimel, B. Koopmans, I. N. Krivorotov, S. J. May, A. K. Petford-Long, J. M. Rondinelli, N. Samarth, I. K. Schuller, A. N. Slavin, M. D. Stiles, O. Tchernyshyov, A. Thiaville, B. L. Zink, Interface-induced phenomena in magnetism, *Rev. Mod. Phys.* 89 (2017) 025006. doi:10.1103/RevModPhys.89.025006.
- [229] L. P. Gor'kov, N. B. Kopnin, Vortex motion and resistivity of type-II superconductors in a magnetic field, *Sov. Phys. Usp.* 18 (7) (1975) 496. doi:10.1070/PU1975v018n07ABEH004891.
- [230] M. Inoue, M. Ichioka, H. Adachi, Spin pumping into superconductors: A new probe of spin dynamics in a superconducting thin film, *Phys. Rev. B* 96 (2017) 024414. doi:10.1103/PhysRevB.96.024414.
- [231] M. S. Kalenkov, A. D. Zaikin, Diffusive superconductors beyond Usadel approximation: Electron-hole asymmetry and large photoelectric effect, *Phys. Rev. B* 92 (2015) 014507. doi:10.1103/PhysRevB.92.014507.
- [232] A. V. Zaitsev, Photoelectric effect in superconductors, *Zh. Eksp. Teor. Fiz.* 90 (3) (1986) 993.  
URL <http://jetp.ac.ru/cgi-bin/e/index/e/63/3/p579?a=list>
- [233] C. H. L. Quay, C. Dutreix, D. Chevallier, C. Bena, M. Aprili, Frequency-domain measurement of the spin-imbalance lifetime in superconductors, *Phys. Rev. B* 93 (2016) 220501. doi:10.1103/PhysRevB.93.220501.
- [234] N. R. Werthamer, Nonlinear self-coupling of Josephson radiation in superconducting tunnel junctions, *Phys. Rev.* 147 (1) (1966) 255–263. doi:10.1103/PhysRev.147.255.
- [235] A. I. Larkin, Y. N. Ovchinnikov, Tunnel effect between superconductors in an alternating field, *Sov. Phys. JETP* 24 (5) (1967) 1035.  
URL <http://jetp.ac.ru/cgi-bin/e/index/e/24/5/p1035?a=list>
- [236] A. Barone, G. Paterno, *Physics and applications of the Josephson effect*, Wiley, New York, 1982.
- [237] G. Marchegiani, P. Virtanen, F. Giazotto, M. Campisi, Self-oscillating Josephson quantum heat engine, *Phys. Rev. Applied* 6 (2016) 054014. doi:10.1103/PhysRevApplied.6.054014.

- [238] J. R. Tucker, M. J. Feldman, Quantum detection at millimeter wavelengths, *Rev. Mod. Phys.* 57 (1985) 1055. doi:10.1103/RevModPhys.57.1055.
- [239] R. E. Horstman, J. Wolter, Gap enhancement in narrow superconducting tunnel junctions induced by homogeneous microwave currents, *Phys. Lett. A* 82 (1) (1981) 43. doi:10.1016/0375-9601(81)90396-0.
- [240] W. Z. Meissner, Das elektrische Verhalten der Metalle im Temperaturgebiet des flüssigen Heliums, *Z. ges. Kälte-Industrie* 34 (1927) 197.  
URL <http://vhkk.org/page/bibliothek/pdf/Z.Gesamtkaelte/ZgKI1927.pdf>
- [241] V. Ginzburg, On the thermoelectric phenomena in superconductors, *Zh. Eksp. Teor. Fiz.* 14 (1944) 134.
- [242] Yu. M. Galperin, V. L. Gurevich, V. I. Kozub, Thermoelectric effects in superconductors, *Sov. Phys. JETP* 39 (4) (1974) 680.  
URL <http://jetp.ac.ru/cgi-bin/e/index/e/39/4/p680?a=list>
- [243] A. Ozaeta, P. Virtanen, F. S. Bergeret, T. T. Heikkilä, Predicted very large thermoelectric effect in ferromagnet-superconductor junctions in the presence of a spin-splitting magnetic field, *Phys. Rev. Lett.* 112 (5) (2014) 057001. doi:10.1103/PhysRevLett.112.057001.
- [244] P. Machon, M. Eschrig, W. Belzig, Giant thermoelectric effects in a proximity-coupled superconductor-ferromagnet device, *New. J. Phys.* 16 (7) (2014) 073002. doi:10.1088/1367-2630/16/7/073002.
- [245] S. Kolenda, C. Sürgers, G. Fischer, D. Beckmann, Thermoelectric effects in superconductor-ferromagnet tunnel junctions on europium sulfide, *Phys. Rev. B* 95 (2017) 224505. doi:10.1103/PhysRevB.95.224505.
- [246] G. J. Snyder, T. S. Ursell, Thermoelectric efficiency and compatibility, *Phys. Rev. Lett.* 91 (2003) 148301. doi:10.1103/PhysRevLett.91.148301.
- [247] I. I. Novikov, The efficiency of atomic power stations (a review), *Atomnaya Energiya* 3 (11) (1957) 409. doi:10.1016/0891-3919(58)90244-4.
- [248] F. L. Curzon, B. Ahlborn, Efficiency of a Carnot engine at maximum power output, *Amer. J. Phys.* 43 (1) (1975) 22–24. doi:10.1119/1.10023.
- [249] L.-D. Zhao, G. Tan, S. Hao, J. He, Y. Pei, H. Chi, H. Wang, S. Gong, H. Xu, V. P. Dravid, C. Uher, G. J. Snyder, C. Wolverton, M. G. Kanatzidis, Ultrahigh power factor and thermoelectric performance in hole-doped single-crystal SnSe, *Science* 351 (6269) (2016) 141–144. doi:10.1126/science.aad3749.

- [250] S. I. Kim, K. H. Lee, H. A. Mun, H. S. Kim, S. W. Hwang, J. W. Roh, D. J. Yang, W. H. Shin, X. S. Li, Y. H. Lee, G. J. Snyder, S. W. Kim, Dense dislocation arrays embedded in grain boundaries for high-performance bulk thermoelectrics, *Science* 348 (6230) (2015) 109–114. doi:10.1126/science.aaa4166.
- [251] M. V. Katsovnik, V. V. Ryazanov, V. V. Schmidt, Observation of thermoelectric effect in an SNS junction, *JETP Lett.* 33 (7) (1981) 356. URL [http://jetpletters.ac.ru/ps/1507/article\\_23032.shtml](http://jetpletters.ac.ru/ps/1507/article_23032.shtml)
- [252] V. V. Ryazanov, V. V. Schmidt, Magnetic-thermoelectric effect in Josephson SNS junction, *Solid State Commun.* 40 (12) (1981) 1055 – 1058. doi:10.1016/0038-1098(81)90250-7.
- [253] A. G. Aronov, Y. M. Gal’perin, Thermoelectric power and nonstationary Josephson effect in S-N-S structures, *JETP Lett.* 19 (5) (1974) 165. URL [http://jetpletters.ac.ru/ps/1774/article\\_26990.shtml](http://jetpletters.ac.ru/ps/1774/article_26990.shtml)
- [254] D. J. Van Harlingen, D. F. Heidel, J. C. Garland, Experimental study of thermoelectricity in superconducting indium, *Phys. Rev. B* 21 (1980) 1842–1857. doi:10.1103/PhysRevB.21.1842.
- [255] Y. M. Galperin, V. L. Gurevich, V. I. Kozub, A. L. Shelankov, Theory of thermoelectric phenomena in superconductors, *Phys. Rev. B* 65 (2002) 064531. doi:10.1103/PhysRevB.65.064531.
- [256] V. L. Ginzburg, Nobel lecture: On superconductivity and superfluidity (what i have and have not managed to do) as well as on the “physical minimum” at the beginning of the XXI century\*, *Rev. Mod. Phys.* 76 (2004) 981–998. doi:10.1103/RevModPhys.76.981.
- [257] C. D. Shelly, E. A. Matrozova, V. T. Petrashov, Resolving thermoelectric “paradox” in superconductors, *Sci. Adv.* 2 (2) (2016) e1501250. doi:10.1126/sciadv.1501250.
- [258] J. Clarke, M. Tinkham, Theory of quasiparticle charge imbalance induced in a superconductor by a supercurrent in the presence of a thermal gradient, *Phys. Rev. Lett.* 44 (1980) 106–109. doi:10.1103/PhysRevLett.44.106.
- [259] J. Eom, C.-J. Chien, V. Chandrasekhar, Phase dependent thermopower in Andreev interferometers, *Phys. Rev. Lett.* 81 (1998) 437–440. doi:10.1103/PhysRevLett.81.437.
- [260] V. Chandrasekhar, Thermal transport in superconductor/normal-metal structures, *Supercond. Sci. Tech.* 22 (8) (2009) 083001. doi:10.1088/0953-2048/22/8/083001.



- [261] A. Parsons, I. A. Sosnin, V. T. Petrashov, Reversal of thermopower oscillations in the mesoscopic Andreev interferometer, *Phys. Rev. B* 67 (2003) 140502. doi:10.1103/PhysRevB.67.140502.
- [262] P. Virtanen, T. T. Heikkilä, Thermopower induced by a supercurrent in superconductor–normal-metal structures, *Phys. Rev. Lett.* 92 (2004) 177004. doi:10.1103/PhysRevLett.92.177004.
- [263] P. Virtanen, T. Heikkilä, Thermoelectric effects in superconducting proximity structures, *Appl. Phys. A* 89 (3) (2007) 625–637. doi:10.1007/s00339-007-4189-0.
- [264] R. Seviour, A. F. Volkov, Giant thermo-emf in multiterminal superconductor/normal-metal mesoscopic structures, *Phys. Rev. B* 62 (2000) R6116–R6119. doi:10.1103/PhysRevB.62.R6116.
- [265] M. Titov, Thermopower oscillations in mesoscopic Andreev interferometers, *Phys. Rev. B* 78 (22) (2008) 224521. doi:10.1103/PhysRevB.78.224521.
- [266] P. Jacquod, R. S. Whitney, Coherent thermoelectric effects in mesoscopic Andreev interferometers, *EPL* 91 (6) (2010) 67009. doi:10.1209/0295-5075/91/67009.
- [267] M. S. Kalenkov, A. D. Zaikin, Large thermoelectric effect in ballistic Andreev interferometers, *Phys. Rev. B* 95 (2017) 024518. doi:10.1103/PhysRevB.95.024518.
- [268] M. S. Kalenkov, A. D. Zaikin, Electron-hole imbalance and large thermoelectric effect in superconducting hybrids with spin-active interfaces, *Phys. Rev. B* 90 (2014) 134502. doi:10.1103/PhysRevB.90.134502.
- [269] M. S. Kalenkov, A. D. Zaikin, Enhancement of thermoelectric effect in diffusive superconducting bilayers with magnetic interfaces, *Phys. Rev. B* 91 (2015) 064504. doi:10.1103/PhysRevB.91.064504.
- [270] M. S. Kalenkov, A. D. Zaikin, L. S. Kuzmin, Theory of a large thermoelectric effect in superconductors doped with magnetic impurities, *Phys. Rev. Lett.* 109 (2012) 147004. doi:10.1103/PhysRevLett.109.147004.
- [271] C. W. J. Beenakker, A. A. M. Staring, Theory of the thermopower of a quantum dot, *Phys. Rev. B* 46 (1992) 9667–9676. doi:10.1103/PhysRevB.46.9667.
- [272] S.-Y. Hwang, R. López, D. Sánchez, Large thermoelectric power and figure of merit in a ferromagnetic-quantum dot-superconducting device, *Phys. Rev. B* 94 (2016) 054506. doi:10.1103/PhysRevB.94.054506.
- [273] S.-Y. Hwang, D. Sánchez, R. López, A hybrid superconducting quantum dot acting as an efficient charge and spin Seebeck diode, *New J. Phys.* 18 (9) (2016) 093024. doi:10.1088/1367-2630/18/9/093024.

- [274] H. Pothier, S. Guéron, N. O. Birge, D. Esteve, M. H. Devoret, Energy distribution function of quasiparticles in mesoscopic wires, *Phys. Rev. Lett.* 79 (1997) 3490–3493. doi:10.1103/PhysRevLett.79.3490.
- [275] M. Nahum, T. M. Eiles, J. M. Martinis, Electronic microrefrigerator based on a normal–insulator–superconductor tunnel junction, *Appl. Phys. Lett.* 65 (24) (1994) 3123–3125. doi:10.1063/1.112456.
- [276] M. M. Leivo, J. P. Pekola, D. V. Averin, Efficient Peltier refrigeration by a pair of normal metal/insulator/superconductor junctions, *Appl. Phys. Lett.* 68 (14) (1996) 1996–1998. doi:10.1063/1.115651.
- [277] J. P. Pekola, T. T. Heikkilä, A. M. Savin, J. T. Flyktman, F. Giazotto, F. W. J. Hekking, Limitations in cooling electrons using normal-metal-superconductor tunnel junctions, *Phys. Rev. Lett.* 92 (2004) 056804. doi:10.1103/PhysRevLett.92.056804.
- [278] M. Rouco, T. T. Heikkilä, F. S. Bergeret, Electron refrigeration in hybrid structures with spin-split superconductors, *Phys. Rev. B* 97 (2018) 014529. doi:10.1103/PhysRevB.97.014529.
- [279] V. J. Kauppila, H. Q. Nguyen, T. T. Heikkilä, Nonequilibrium and proximity effects in superconductor–normal metal junctions, *Phys. Rev. B* 88 (2013) 075428. doi:10.1103/PhysRevB.88.075428.
- [280] H. Q. Nguyen, M. Meschke, H. Courtois, J. P. Pekola, Sub-50-mK electronic cooling with large-area superconducting tunnel junctions, *Phys. Rev. Applied* 2 (2014) 054001. doi:10.1103/PhysRevApplied.2.054001.
- [281] S. Kawabata, A. Ozaeta, A. S. Vasenko, F. W. Hekking, F. Sebastián Bergeret, Efficient electron refrigeration using superconductor/spin-filter devices, *Appl. Phys. Lett.* 103 (3) (2013) 032602. doi:10.1063/1.4813599.
- [282] R. C. Dynes, J. P. Garno, G. B. Hertel, T. P. Orlando, Tunneling study of superconductivity near the metal-insulator transition, *Phys. Rev. Lett.* 53 (1984) 2437–2440. doi:10.1103/PhysRevLett.53.2437.
- [283] S. Chakraborty, T. T. Heikkilä, Thermoelectric radiation detector based on a superconductor-ferromagnet junction: Calorimetric regime, *J. Appl. Phys.* 124 (12) (2018) 123902. doi:10.1063/1.5037405.
- [284] F. Menges, P. Mensch, H. Schmid, H. Riel, A. Stemmer, B. Gotsmann, Temperature mapping of operating nanoscale devices by scanning probe thermometry, *Nat. Commun.* 7 (2016) 10874. doi:10.1038/ncomms10874.
- [285] A. Rezaei, A. Kamra, P. Machon, W. Belzig, Spin-flip enhanced thermoelectricity in superconductor-ferromagnet bilayers, *New J. Phys.* 20 (7) (2018) 073034. doi:10.1088/1367-2630/aad2a3.

- [286] J. Linder, M. E. Bathen, Spin caloritronics with superconductors: Enhanced thermoelectric effects, generalized Onsager response-matrix, and thermal spin currents, *Phys. Rev. B* 93 (2016) 224509. doi:10.1103/PhysRevB.93.224509.
- [287] M. E. Bathen, J. Linder, Spin Seebeck effect and thermoelectric phenomena in superconducting hybrids with magnetic textures or spin-orbit coupling, *Sci. Rep.* 7 (2017) 41409. doi:10.1038/srep41409.
- [288] I. V. Bobkova, A. M. Bobkov, Thermospin effects in superconducting heterostructures, *Phys. Rev. B* 96 (2017) 104515. doi:10.1103/PhysRevB.96.104515.
- [289] K. Uchida, M. Ishida, T. Kikkawa, A. Kirihara, T. Murakami, E. Saitoh, Longitudinal spin Seebeck effect: from fundamentals to applications, *J. Phys.: Condens. Matter* 26 (34) (2014) 343202. doi:10.1088/0953-8984/26/34/343202.
- [290] S. Hoffman, K. Sato, Y. Tserkovnyak, Landau–Lifshitz theory of the longitudinal spin Seebeck effect, *Phys. Rev. B* 88 (2013) 064408. doi:10.1103/PhysRevB.88.064408.
- [291] F. S. Bergeret, I. V. Tokatly, Singlet-triplet conversion and the long-range proximity effect in superconductor-ferromagnet structures with generic spin dependent fields, *Phys. Rev. Lett.* 110 (11) (2013) 117003. doi:10.1103/PhysRevLett.110.117003.
- [292] F. S. Bergeret, I. V. Tokatly, Spin-orbit coupling as a source of long-range triplet proximity effect in superconductor-ferromagnet hybrid structures, *Phys. Rev. B* 89 (13) (2014) 134517. doi:10.1103/PhysRevB.89.134517.
- [293] C. Espedal, P. Lange, S. Sadjina, A. G. Mal’shukov, A. Brataas, Spin hall effect and spin swapping in diffusive superconductors, *Phys. Rev. B* 95 (2017) 054509. doi:10.1103/PhysRevB.95.054509.

## Appendix A. Conservation of spin and charge by the electron-phonon scattering

The inelastic electron-phonon scattering solely cannot relax charge the spin polarization and therefore it should keep  $\mu$  and  $\mu_z$  constant. The electron-phonon collision integral (CI) reads

$$I_{qp-ph}(\varepsilon) = \frac{g_{ph}}{4} \int_{-\infty}^{\infty} d\omega |\omega| \omega \hat{K}(\varepsilon, \varepsilon') \quad (\text{A.1})$$

$$\hat{K} = \left[ \hat{\Sigma}_{ph}^R \hat{g}^K(\varepsilon) - \hat{g}^K(\varepsilon) \hat{\Sigma}_{ph}^A - \hat{g}^R(\varepsilon) \hat{\Sigma}_{ph}^K + \hat{\Sigma}_{ph}^K \hat{g}^A(\varepsilon) \right]$$

where  $\omega = \varepsilon' - \varepsilon$  and the self energies are

$$\hat{\Sigma}_{ph}^K(\varepsilon, \varepsilon') = \coth(\omega/2T) \hat{g}^K(\varepsilon') - (\hat{g}^R(\varepsilon') - \hat{g}^A(\varepsilon'))$$

$$\hat{\Sigma}_{ph}^A(\varepsilon, \varepsilon') = \coth(\omega/2T) \hat{g}^A(\varepsilon') + \hat{g}^K(\varepsilon')/2$$

$$\hat{\Sigma}_{ph}^R(\varepsilon, \varepsilon') = \coth(\omega/2T) \hat{g}^R(\varepsilon') - \hat{g}^K(\varepsilon')/2.$$

We are interested in conservation laws for the charge and spin

$$\dot{\mu} = \int_{-\infty}^{\infty} d\varepsilon \text{Tr} \left[ \tau_3 \hat{I}_{qp-ph} \right] = 0 \quad (\text{A.2})$$

$$\dot{\mu}_z = \int_{-\infty}^{\infty} d\varepsilon \text{Tr} \left[ \sigma_3 \hat{I}_{qp-ph} \right] = 0 \quad (\text{A.3})$$

For this purpose we write the kernel of CI (A.1) as follows:

$$\begin{aligned} \hat{K} = & \coth(\omega/2T) [\hat{g}^R(\varepsilon') \hat{g}^K(\varepsilon) - \hat{g}^R(\varepsilon) \hat{g}^K(\varepsilon')] + \\ & \coth(\omega/2T) [\hat{g}^K(\varepsilon') \hat{g}^A(\varepsilon) - \hat{g}^K(\varepsilon) \hat{g}^A(\varepsilon')] \\ & - [\hat{g}^K(\varepsilon') \hat{g}^K(\varepsilon) + \hat{g}^K(\varepsilon) \hat{g}^K(\varepsilon')] / 2 \\ & - \hat{g}^R(\varepsilon) \hat{g}^A(\varepsilon') - \hat{g}^R(\varepsilon') \hat{g}^A(\varepsilon) \\ & + \hat{g}^R(\varepsilon) \hat{g}^R(\varepsilon') + \hat{g}^A(\varepsilon') \hat{g}^A(\varepsilon) \end{aligned} \quad (\text{A.4})$$

To prove the conservation laws it is enough to show that

$$\int_{-\infty}^{\infty} d\varepsilon \text{Tr} \hat{\gamma} \left[ \hat{K}(\varepsilon, \varepsilon + \omega) - \hat{K}(\varepsilon, \varepsilon - \omega) \right] = 0 \quad (\text{A.5})$$

where  $\hat{\gamma} = \sigma_3$  for spin and  $\hat{\gamma} = \tau_3$  for charge. If the relation (A.5) holds then integral in (A.1) is identically zero.

At first we note that the CI (A.1) vanishes if the distribution function is the equilibrium one,  $\hat{f} = \tanh(\varepsilon/2T)$ . Hence we can rewrite the kernel in the form

$$\begin{aligned} \hat{K} = & \coth(\omega/2T) [\hat{g}^R(\varepsilon') \hat{g}_1^K(\varepsilon) - \hat{g}^R(\varepsilon) \hat{g}_1^K(\varepsilon')] + \\ & \coth(\omega/2T) [\hat{g}_1^K(\varepsilon') \hat{g}^A(\varepsilon) - \hat{g}_1^K(\varepsilon) \hat{g}^A(\varepsilon')] \\ & - [\hat{g}_1^K(\varepsilon') \hat{g}_1^K(\varepsilon) + \hat{g}_1^K(\varepsilon) \hat{g}_1^K(\varepsilon')] / 2, \end{aligned} \quad (\text{A.6})$$

where the new Keldysh function is  $\hat{g}_1^K = \hat{g}^K - \tanh(\varepsilon/2T) \hat{g}^{RA}$ . Then the relation (A.5) follows from the fact that all terms in the kernel (A.6) are symmetric with respect to the interchange of  $\varepsilon$  and  $\varepsilon'$  and the simultaneous sign change of  $\omega$ .

## Appendix B. Pauli matrices in Nambu–spin space

In this review, we study the properties of the Green's function that is a matrix in the  $4 \times 4$  space spanned by the outer product of  $2 \times 2$  Nambu (electron-hole) and spin spaces. We represent matrices in these spaces in terms of the

identity operator and the three Pauli matrices  $\tau_i$  and  $\sigma_j$  ( $i, j = 1, 2, 3$ ) for the Nambu and spin space separately. Therefore, products of such matrices  $\tau_i\sigma_j$  should be understood as outer products. There are hence in total 16 such matrices: the  $4 \times 4$  identity matrix  $\hat{1}$ , the nine combinations of the pairs of Pauli matrices, and the six Pauli matrices acting on either space alone. In the latter matrices we do not explicitly write the outer product with the  $2 \times 2$  identity matrix as it would make equations unnecessarily cumbersome. In these cases the individual Pauli matrices show up alone. The exact matrix representation of these operators is often not very relevant, but for completeness we show a few examples:

$$\begin{aligned} \tau_1 &= \begin{pmatrix} 0 & 0 & 1 & 0 \\ 0 & 0 & 0 & 1 \\ 1 & 0 & 0 & 0 \\ 0 & 1 & 0 & 0 \end{pmatrix}, & \sigma_1 &= \begin{pmatrix} 0 & 1 & 0 & 0 \\ 1 & 0 & 0 & 0 \\ 0 & 0 & 0 & 1 \\ 0 & 0 & 1 & 0 \end{pmatrix} \\ \tau_3 &= \begin{pmatrix} 1 & 0 & 0 & 0 \\ 0 & 1 & 0 & 0 \\ 0 & 0 & -1 & 0 \\ 0 & 0 & 0 & -1 \end{pmatrix}, & \sigma_3 &= \begin{pmatrix} 1 & 0 & 0 & 0 \\ 0 & -1 & 0 & 0 \\ 0 & 0 & 1 & 0 \\ 0 & 0 & 0 & -1 \end{pmatrix} \\ \tau_3\sigma_3 &= \begin{pmatrix} 1 & 0 & 0 & 0 \\ 0 & -1 & 0 & 0 \\ 0 & 0 & -1 & 0 \\ 0 & 0 & 0 & 1 \end{pmatrix}, & \tau_1\sigma_1 &= \begin{pmatrix} 0 & 0 & 0 & 1 \\ 0 & 0 & 1 & 0 \\ 0 & 1 & 0 & 0 \\ 1 & 0 & 0 & 0 \end{pmatrix} \end{aligned}$$

In this representation, the rows thus correspond to the order “spin up electron”, “spin down electron”, “spin up hole” and “spin down hole”, respectively.